EPRI

2024 TECHNICAL REPORT

Materials Reliability Program: Probabilistic Fracture Mechanics Evaluation of PWR Cast Austenitic Stainless Steel Piping Components (MRP-479)

PORTIONS TRANSLATED

Materials Reliability Program: Probabilistic Fracture Mechanics Evaluation of PWR Cast Austenitic Stainless Steel Piping Components (MRP-479)

3002023893

Final Report, June 2024

EPRI Project Manager
D. Shim

All or a portion of the requirements of the EPRI Nuclear Quality Assurance Program apply to this product.	YES NO

EPRI
3420 Hillview Avenue, Palo Alto, California 94304-1338 USA
800.313.3774 ▪ 650.855.2121 ▪ askepri@epri.com ▪ www.epri.com

DISCLAIMER OF WARRANTIES AND LIMITATION OF LIABILITIES

THE FOLLOWING ORGANIZATION(S), UNDER CONTRACT TO EPRI, PREPARED THIS REPORT:

Dominion Engineering, Inc.

THE TECHNICAL CONTENTS OF THIS PRODUCT WERE **NOT** PREPARED IN ACCORDANCE WITH THE EPRI QUALITY PROGRAM MANUAL THAT FULFILLS THE REQUIREMENTS OF 10 CFR 50, APPENDIX B. THIS PRODUCT IS **NOT** SUBJECT TO THE REQUIREMENTS OF 10 CFR PART 21.

NOTE

For further information about EPRI, call the EPRI Customer Assistance Center at 800.313.3774 or e-mail askepri@epri.com.

Together…Shaping the Future of Energy®

ACKNOWLEDGMENTS

The following organizations, under contract to EPRI, prepared this report:

Dominion Engineering, Inc.
12100 Sunrise Valley Drive, Suite 220
Reston, VA 20191

Principal Investigators
K. Fuhr
M. Wolfson
G. White
M. Burkardt

This report describes research sponsored by EPRI.

This publication is a corporate document that should be cited in the literature in the following manner: *Materials Reliability Program: Probabilistic Fracture Mechanics Evaluation of PWR Cast Austenitic Stainless Steel Piping Components (MRP-479).* EPRI, Palo Alto, CA: 2024. 3002023893.

ABSTRACT

The material microstructure of cast austenitic stainless steel (CASS) materials challenges the reliability of ultrasonic examination techniques. As such, the qualification requirements for ultrasonic testing (UT) procedures, personnel, and equipment used for examination of CASS piping in accordance with the American Society of Mechanical Engineers (ASME) Boiler and Pressure Vessel Code, Section XI, Mandatory Appendix VIII have not been developed. Based on current research, the most difficult challenges for examination of CASS piping components are detection of axial cracks and depth sizing of circumferential cracks.

In addition to the limitations of UT examination, CASS material is subject to thermal aging, which causes degradation of fracture toughness over time. The extent of toughness degradation depends on the delta ferrite (δ-*Fe*) content of the particular component. The failure mode of concern for CASS material is growth of a crack (e.g., from a preexisting fabrication flaw) to a size that could challenge the integrity of the component, given the reduced critical crack size at the lower fracture toughness. The main crack growth mechanism of interest in CASS material exposed to pressurized water reactor (PWR) coolant is fatigue cracking. Plant experience and testing show that austenitic stainless steel material in the PWR environment is generally resistant to stress corrosion cracking, while the delta ferrite content of CASS material is expected to have a beneficial effect for the susceptibility to stress corrosion cracking.

This report describes the probabilistic fracture mechanics (PFM) approach and results obtained to address the challenges in qualification of UT examinations for CASS piping. PFM analyses assess the structural implication of axial flaws being present in CASS piping and propagating as cracks without crediting inservice examination. Additional PFM analyses assess the structural margin provided by an alternative flaw evaluation methodology that does not require depth sizing information upon detection of circumferential cracking. The PFM evaluations were performed using a software code developed specifically for this project called PIPER-CASS (Piping Integrity Probabilistic Evaluation for Reactors – Cast Austenitic Stainless Steel). PIPER-CASS focuses on modeling of fatigue crack growth and stability of CASS piping components, including thermally aged material with low toughness.

This work is intended to support development of Mandatory Appendix VIII, Supplement 9 for CASS and alternatives to the current Section XI examination and flaw acceptance requirements for CASS piping components.

Keywords

ASME Boiler and Pressure Vessel Code (BPVC)
Cast austenitic stainless steel (CASS)
Fatigue crack growth
Probabilistic fracture mechanics (PFM)
Nondestructive examination (NDE)

EXECUTIVE SUMMARY

Deliverable Number: 3002023893

Product Type: Technical Report

Product Title: Materials Reliability Program: Probabilistic Fracture Mechanics Evaluation of PWR Cast Austenitic Stainless Steel Piping Components (MRP-479)

Primary Audience: Developers of Codes and Standards related to cast austenitic stainless steel (CASS) piping components

Secondary Audience: Technical staff at pressurized water reactor (PWR) licensees and regulators

KEY RESEARCH QUESTION

What analytical solutions are available to supplement the current nondestructive examination (NDE) capabilities for CASS piping components, specifically for detection of axial cracking and depth sizing of circumferential cracking?

RESEARCH OVERVIEW

This report describes the probabilistic fracture mechanics (PFM) approach and results intended to support alternative examination requirements for CASS components. This work is intended to support development of ASME Boiler and Pressure Vessel Code, Section XI, Mandatory Appendix VIII, Supplement 9 for CASS and refinement of Section XI, Subarticle IWB-2500 (Examination Categories B-F and B-J) examination requirements specific to CASS piping. For axial cracking, the effect on nuclear safety (rupture probability) and defense-in-depth (leak tightness) was investigated assuming no benefit of periodic NDE. For circumferential cracking, an alternative flaw evaluation procedure is proposed for acceptance of detected cracking without relying on a qualified depth sizing capability.

KEY FINDINGS

- For this effort, a Python-based PFM code called PIPER-CASS (Piping Integrity Probabilistic Evaluation for Reactors – Cast Austenitic Stainless Steel) was developed. This PFM code applies many of the same models as the xLPR program but focuses on modeling fatigue crack growth and elastic-plastic fracture mechanics (EPFM) crack stability.
- The PFM modeling results show that periodic examination to detect axially oriented cracking in main loop CASS piping (including both base load PWRs and PWRs operating under flexible power operation (FPO)) and in surge line CASS piping (including base load but not FPO) is unnecessary to ensure pipe structural and leak tight integrity. Surge lines in CE plants operating under FPO have an increased concern for fatigue crack growth due to the potential for a large number of surge transients to be triggered by FPO power shifts.

- The PFM modeling results show that, for a detected crack with an angular full-length up to 32°, the proposed alternative flaw evaluation method ensures structural integrity of CASS main loop piping components for one fuel cycle of continued operation following the detection of a circumferentially oriented crack.

WHY THIS MATTERS

The heterogenous microstructure of CASS materials is an impediment to qualification of certain aspects of ultrasonic examination (UT). A technical basis demonstrating that detection of axial cracking in CASS piping is unnecessary addresses the challenge of UT procedures reliably meeting the performance demonstration qualification standards. The lack of qualified depth sizing capability for circumferential cracks or crack-like flaws in CASS piping prevents application of standard flaw evaluation procedures, so an alternative procedure is needed to permit continued operation and limit unnecessary emergent repairs.

HOW TO APPLY RESULTS

This work is expected to provide technical bases for ASME Code committee actions to address examination of CASS components. This includes new ASME Code Cases and development of Section XI, Mandatory Appendix VIII, Supplement 9 for qualified CASS examination and potential alternatives to Section XI, Subarticle IWB-2500 (Examination Categories B-F and B-J) examination requirements specific to CASS piping.

LEARNING AND ENGAGEMENT OPPORTUNITIES

- The Extremely Low Probability of Rupture (xLPR) Probabilistic Fracture Mechanics Code, Version 2.2 (EPRI 3002023872) was released by EPRI in January 2023. Several of the xLPR code modules were adapted for use in PIPER-CASS.
- MRP-362, Rev. 1 (EPRI 3002007383) presents the technical justification for the flaw tolerance evaluation of CASS piping to support ASME Code Case N-838. A PFM model for fully aged CASS piping was used to develop flaw size acceptance limits satisfying a set of failure probability acceptance criteria addressing each loading Service Level.
- EPRI 3002010314 documents a round-robin study to determine the performance of NDE techniques on a set of flawed CASS specimens that contained realistic surface and geometric conditions.
- MRP-424 (EPRI 3002010517) includes a draft of the examination requirements for CASS piping welds, providing a framework from which the final version of Section XI, Mandatory Appendix VIII, Supplement 9 can be drafted.

EPRI CONTACTS: Do Jun Shim, Technical Executive, dshim@epri.com

PROGRAM: Nuclear Power, P41; PWR Materials Reliability Program (MRP), P41.01.04

IMPLEMENTATION CATEGORY: Reference – Technical Basis

NOMENCLATURE

Acronyms

ASME [Code]	American Society of Mechanical Engineers [Boiler and Pressure Vessel Code]
B&W	Babcock & Wilcox
BWR	Boiling water reactor
CASS	Cast austenitic stainless steel
CCS	Commercial Custom Software
CE	Combustion Engineering
CGR	Crack growth rate
CMTR	Certified material test report
CSPP	Custom Software Project Plan
DEI	Dominion Engineering, Inc.
DHS	Downhill simplex solver
EFPY	Effective full power year
EPFM	Elastic-plastic fracture mechanics
EPRI	Electric Power Research Institute
FCG[R]	Fatigue crack growth [rate]
FPO	Flexible power operations
GE	General Electric
ID	Inner diameter
J-R	J-integral material resistance [curve]
MRP	EPRI PWR Materials Reliability Program
NDE	Nondestructive examination
NRC	U.S. Nuclear Regulatory Commission

NSC	Net-section collapse
NUREG[/CR]	Designation of report authored by [contractor to] U.S. NRC
OD	Outside diameter
PDI	Performance Demonstration Initiative
PFM	Probabilistic fracture mechanics
PIPER-CASS	Piping Integrity Probabilistic Evaluation for Reactors – Cast Austenitic Stainless Steel
PWR	Pressurized water reactors
PWSCC	Primary water stress corrosion cracking
RCP	Reactor coolant pump
RCS	Reactor coolant system
RG	U.S. NRC Regulatory Guide
RGTS	Radial gradient thermal stress
RO	Ramberg-Osgood
RPV	Reactor pressure vessel
RTM	Requirements Traceability Matrix
SC	Surface crack (part through-wall)
SDD	Software Design Description
SESC	Semi-elliptical surface crack
SIF	Software Implementation Files
SL	[ASME Code, Section XI] Service Level
SQA	Software quality assurance
SRS	Software Requirements Specification
STP	Software Test Plan
STR	Software Test Report

TRN	Trapezoidal (transitioning) through-wall crack
TW	Through-wall (idealized, rectangular crack)
UI	User Instructions
UT	Ultrasonic testing
V&V	Verification and validation
WEC	Westinghouse Electric Company
WRS	Weld residual stress
xLPR	Extremely Low Probability of Rupture

Variables

Variables are listed below, with Latin characters followed by Greek. If a variable's definition is contextual, the context is provided in [brackets].

a	Crack depth
c	Crack half-length
C_r	Coefficient of the power-law J-R curve
C_{Kth}	Crack growth ΔK_I threshold scaling factor
C_{SS}	Fatigue crack growth rate scaling parameter for stainless steel
C_{vsat}	Room temperature Charpy impact energy at saturated thermal aging
J	J-integral characterizing the local stress-strain field at the crack tip indicating the applied driving energy for propagation of the crack tip
J_{ic}	Ductile crack initiation toughness
J_R	Material resistance to tearing, as indicated by the J-integral
K_I	Crack tip stress intensity factor (Mode I)
ΔK_I	Crack tip stress intensity factor range
$\Delta K_{I,th}$	Threshold crack tip stress intensity factor range
m	Exponent of the power-law J-R curve

n	Ramberg-Osgood equation plasticity exponent
n_{ss}	Exponent on ΔK for fatigue crack growth rate of stainless steel
P	[General] Internal pressure (gauge, unless otherwise specified) [Fracture toughness] Thermal aging parameter (see NUREG/CR-4513 Rev. 2) [Section 6.4.2] Probability of an event
$P(x;N,p)$	Probability of x events occurring across N independent samples, given that each event has a p probability of occurrence in a given sample (see Section 6.4.2)
R_i	Inner radius
R_m	Mean radius
t	Wall thickness
α	Ramberg-Osgood equation yield offset parameter
δ-Fe	Delta ferrite content of the material
ϵ_o	Ramberg-Osgood equation reference strain
μ	Mean of the normal distribution
ρ	Material density
σ	[Statistical distributions] Standard deviation of the normal distribution [Loads] Stress
σ_f	Flow strength (average of yield and ultimate), at operating temperature
σ_y	Yield strength, at operating temperature
σ_u	Ultimate strength, at operating temperature
ϕ	Parameter for correlation between material composition and Charpy impact energy (see NUREG/CR-4513 Rev. 2)
Θ	[General] Circumferential crack half-angle [Fracture toughness] Normalized aging parameter (see NUREG/CR-4513 Rev. 2)

UNIT CONVERSION FACTORS

1 inch = 25.4 mm

1°F = 1.8°C + 32

1 Δ°F = 1.8 Δ°C

1 ksi = 1000 psi = 6.895 MPa

1 ksi$\sqrt{\text{inch}}$ = 1.099 MPa$\sqrt{\text{m}}$

1 lbf/inch = 0.1751 N/mm = 0.1751 kJ/m^2 = 0.1751 MPa·mm

CONTENTS

LIST OF FIGURES

LIST OF TABLES

1 INTRODUCTION

1.1 Background

Cast austenitic stainless steels (CASS) are used for some pressurized water reactor (PWR) piping components. Ultrasonic testing (UT) technology applied to CASS components is challenged by the microstructural heterogeneity of CASS components. Thus, current UT examination techniques applied to CASS components are not capable of meeting typical qualification standards used for qualification of procedures, equipment, and personnel defined for non-cast piping. As such, the requirements have not been developed for qualifying ultrasonic examination of CASS piping in American Society of Mechanical Engineers (ASME) Boiler and Pressure Vessel Code (ASME Code), Section XI [1], Mandatory Appendix VIII[1]. Recent research related to the examination of CASS piping components identified that the detection of axial cracking and depth sizing of circumferential cracking are some of the key challenges [2].

In addition to the limitations of UT examination, CASS material is subject to thermal aging, which causes a degradation of fracture toughness over time. This behavior may result in a reduction in the critical crack size that would produce unstable rupture of the CASS component. The extent of toughness degradation of a particular component depends on the chemical composition (high Mo and high Ni are more susceptible), casting method (static cast is more susceptible than centrifugally cast), and delta ferrite content (δ-*Fe*; higher δ-*Fe* is more susceptible). NUREG/CR-4513, Rev. 2 [3] provides a methodology to estimate the fracture toughness degradation of CASS due to thermal aging and proposes an update to the standard screening criteria for CASS thermal aging effects—summarized in Table 1-1 of this report—reflecting additional data from the two decades since the criteria were published by NRC [4]. The ASME Code considers susceptibility of CASS (specifically alloys CF3, CF8, and CF8M or their chemical equivalents) to thermal aging by requiring a Z-factor in stability evaluations for CASS alloys when the δ-*Fe* is >14% and a larger Z-factor specifically for CF8M with δ-*Fe* >25%.

Inspection requirements for CASS material exposed to PWR coolant are established to address the concern for fatigue cracking, as plant experience and testing show that austenitic stainless steel material is generally resistant to stress corrosion cracking (SCC) in the PWR environment. Environmental crack growth by SCC tends to be reduced for aged CASS versus unaged CASS and for higher levels of δ-ferrite [5]. In other words, these conditions that promote susceptibility of CASS to toughness degradation tend to reduce susceptibility to SCC.

An overview of common reactor coolant system (RCS) locations for CASS in Westinghouse Electric Company (WEC) PWRs and Combustion Engineering (CE) PWRs located in the United States is shown in Figure 1-1 and Figure 1-2, respectively. The main loop piping and elbows

[1] Supplement 9 to Mandatory Appendix VIII of Section XI [1] has been reserved as "In the course of preparation" for a future section on "Qualification Requirements for Cast Austenitic Piping Welds."

along with reactor coolant pump casings in many WEC PWRs are CASS. For CE PWRs, surge line piping components, reactor coolant pump (RCP) casings, and some main loop piping safe ends are CASS.[2] The only CASS material in the main loop of Babcock and Wilcox (B&W) PWRs and AP-1000 plants is the RCP casing.

Table 1-1
Screening Criteria for Susceptibility to Thermal Aging for CASS Material (CF-3, CF-8, and CF-8M), Given by NUREG/CR-4513, Rev. 2 [3]

Molybdenum Content (Mo; wt. %)	Nickel Content (Ni; wt. %)	Casting Method	Screening Criterion[3]
High (2.0% – 3.0%)	≥ 10%	Static	Ferrite > 11%
		Centrifugal	Ferrite > 13%
	< 10%	Static	Ferrite > 14%
		Centrifugal	Ferrite > 19%
Low (0.5% max.)	Any	Static	Ferrite > 20%
		Centrifugal	None (Screened-out)

[2] Two plants that have shut down also used CASS for the pump suction elbows (Palisades) or for the main loop piping (Fort Calhoun).

[3] The ferrite content is calculated using Hull's equivalent factors.

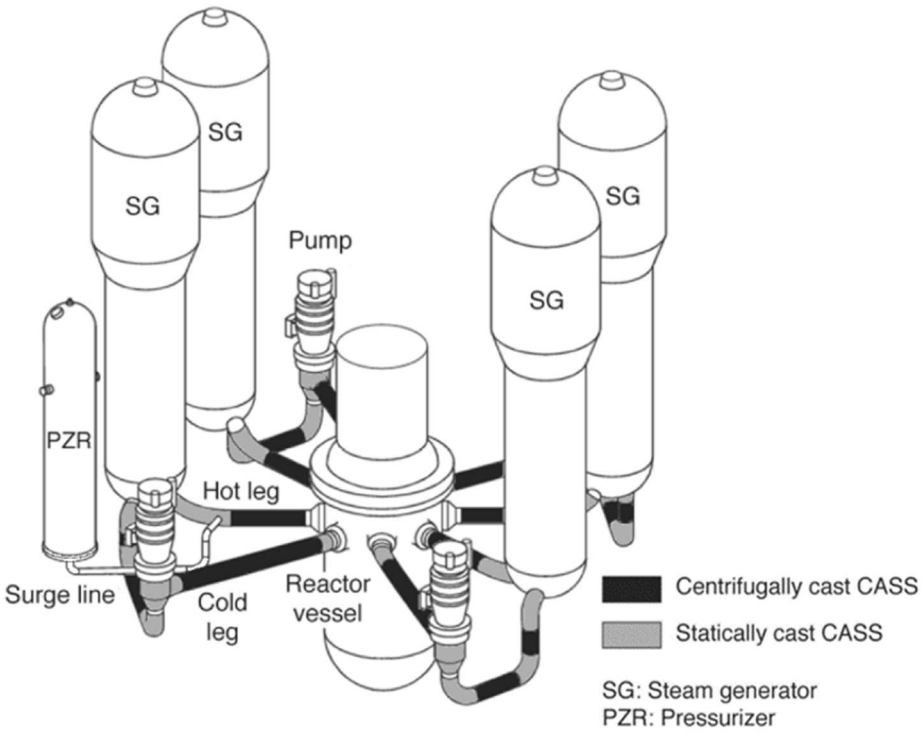

Figure 1-1
Common Locations of CASS Piping in RCS of Westinghouse-Designed Plants [6]

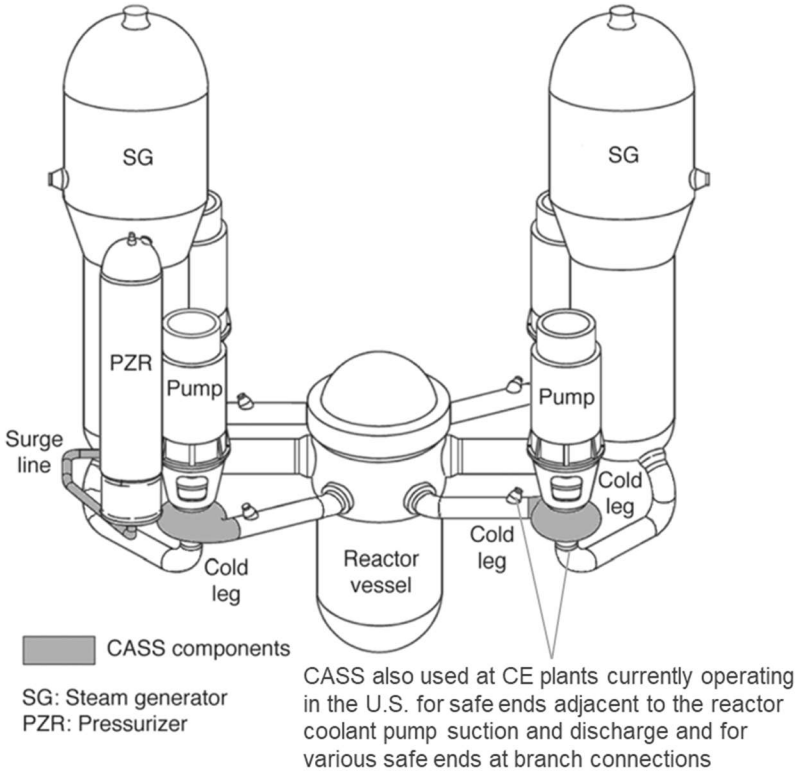

Figure 1-2
Common Locations of CASS Piping in RCS of Operating CE-Designed Plants (Adapted from [6])

1.2 Objectives

In this project, analytical evaluations using probabilistic fracture mechanics (PFM) software were applied to address the current limitations in qualification of nondestructive examination (NDE) techniques for CASS piping components. The specific objectives are discussed in Section 1.2.1 for examinations to detect axially oriented cracking and in Section 1.2.2 for examinations to detect circumferentially oriented cracking. For both crack orientations, the report objectives include describing the full PFM analysis justifying changes to inspection requirements in ASME Code, Section XI, including supporting analyses, sensitivity analyses, and verification and validation (V&V).

This work is intended to provide a technical basis for modifications to the ASME Code to provide appropriate examination requirements for CASS piping, given the NDE examination challenges. This includes development of ASME Code, Section XI, Mandatory Appendix VIII, Supplement 9 for CASS, as well as potential changes or ASME Code Case alternatives to Section XI Subarticle IWB-2500 (Examination Categories B-F and B-J) examination requirements specific to CASS piping and to the standard Section XI Subarticle IWB-3640 flaw evaluation methodology.

1.2.1 Axial Cracking

The objectives of this work with respect to examinations to detect axially oriented cracking are as follows:

- Investigate the effect on nuclear safety (rupture probability) and defense-in-depth (leak tightness) of axial fatigue cracking assuming no benefit of periodic NDE nor online leak detection.
- Assess whether the results support that detection of axial cracks is not necessary to maintain structural and leak tight integrity such that periodic Mandatory Appendix VIII-qualified volumetric examinations are not needed.

1.2.2 Circumferential Cracking

The objectives of this work with respect to examinations to detect and size circumferentially oriented cracking are as follows:

- Investigate the effect on nuclear safety of circumferential fatigue cracking assuming periodic NDE, but without qualified depth sizing capability.
- Assess whether the results support an alternative flaw evaluation procedure, relative to the current Section XI IWB-3640 procedure, for which Mandatory Appendix VIII-qualified depth sizing of circumferential cracks is not necessary.

1.3 Scope

This investigation focuses on CASS piping components in the main loop of WEC PWRs and CASS surge line piping components in CE PWRs. The cases developed cover the plants located in the United States. The results are equally applicable to these components in international plants of the same designs, materials, and loadings, subject to any differences in regulatory requirements for flaw evaluations. PFM analysis of other piping systems with CASS piping components are not in the scope of this analysis. As described in Section 9.3, the results for WEC main loop piping components are extended to justify their applicability to comparable locations having CASS in other plant designs. Piping welds and components that have been mitigated using a process that changes the thickness or materials (e.g., inlay or overlay) are not covered by this analysis. The dissimilar metal welds at all the CASS safe ends in CE surge lines have been mitigated with weld overlays.

This report describes the methods, results, and conclusions of PFM analyses investigating: (1) the need for periodic nondestructive examination to detect axial cracking in CASS piping components and (2) an alternative flaw evaluation procedure for circumferential cracks or crack-like flaws in which the stability margins of ASME Code, Section XI are applied conservatively assuming that the flaw is an idealized through-wall crack.

The examination of CASS piping components is not a concern for boiling water reactors (BWRs), which do not make significant use of CASS for piping.

1.4 Approach

For this effort, a Python-based PFM code is developed. This PFM code, which is called PIPER-CASS (Piping Integrity Probabilistic Evaluation for Reactors – Cast Austenitic Stainless Steel), includes stress intensity factor (K_I) solutions for normal operating and transient conditions, crack growth, crack coalescence, crack transition, inservice inspection, and crack stability modules.

This report presents final results from PFM analyses for both axial and circumferential cracking orientations.[4] These results constitute a technical basis for revising inspection requirements in ASME Code.

1.4.1 Axial Cracking

For axially oriented cracking, the PFM evaluates the potential for fatigue crack growth over the entire plant life and assesses the probabilities of leakage and rupture. Fatigue crack initiation is not credited in these analyses. Instead, the presence of multiple coplanar manufacturing flaws at the time of initial plant startup is conservatively assumed. Given the challenges in qualifying

[4] Interim results were presented in previous technical updates ([7], [8]) and a conference paper [9].

examination procedures to detect axially oriented cracking, inspections are not included in the PFM analysis.

1.4.2 Circumferential Cracking

For circumferentially oriented cracking, the PFM evaluates the probability of rupture associated with an alternate flaw evaluation process which assumes a through-wall crack. The initial flaw is set to the maximum length of an acceptable flaw to demonstrate the proposed limit of applicability for the process meets the acceptance criteria for structural stability. Similarly, the applied piping loads represent limiting loads for an allowable flaw at the proposed limit of applicability. Fatigue crack growth is performed for one fuel cycle of continued operation for the flawed component, and the probability of rupture during the period of continued operation is assessed. Additional details on this approach are provided in Section 3.

1.5 Report Organization

This report is organized into the following sections:

1. *Introduction* – Section 1 describes the background, objectives, scope, and approach, and provides an overview of the organization of this report. It also describes the classification of the present work in the context of Regulatory Guide (RG) 1.245 [10].
2. *PIPER-CASS PFM Code Overview* – Section 2 describes the models implemented in PIPER-CASS and their technical bases.
3. *Alternative Flaw Evaluation Approach for Circumferentially Oriented Flaws in CASS* – Section 3 details the alternative flaw evaluation approach that would not rely on depth sizing capability when determining the acceptability of circumferentially oriented flaws in CASS piping components for continued operation.
4. *Inputs and Cases Evaluated* – Section 4 describes the analysis inputs for component geometry, fracture toughness, material properties, loading, and initial crack geometry. The matrix of base cases and sensitivity cases is also provided.
5. *Acceptance Criteria* – Section 5 discusses the acceptance criteria for the maximum allowable rupture probability for each Service Level condition. In this section, definitions for failure as applied to axial and circumferential cracks are also provided.
6. *Axial Cracking Results and Discussion* – Section 6 presents and discusses the results of the axial cracking analyses assessing the effect of omitting periodic NDE capable of detecting such cracking on nuclear safety and leak tightness criteria. The results include input importance assessments, convergence, and sensitivity studies.
7. *Circumferential Cracking Results and Discussion* – Section 7 presents and discusses the results of the circumferential cracking analyses assessing the effect on nuclear safety criteria of a modified flaw evaluation methodology that does not credit qualified depth

sizing capability. The results also include input importance assessments, convergence, and sensitivity studies.

8. *Uncertainties* – Section 8 provides a discussion of key input or modeling uncertainties that apply to PIPER-CASS.
9. *Conclusions* – Section 9 provides the conclusions of this report and implications for inservice inspections of CASS components for the fleet of WEC and CE PWRs.
10. *References* – Section 10 lists the references cited in this report.

Additionally, the report contains the following appendices:

A. *Material Data* – Appendix A provides material strength and toughness data.
B. *Description of PIPER-CASS PFM Code* – Appendix B provides a high-level table comparing PIPER-CASS versus xLPR modules.
C. *Benchmarking Versus xLPR* – Appendix C provides details of benchmarking efforts that compare PIPER-CASS with the xLPR program, which NRC has approved for use within a specific range of applications ([10], [11]).

1.6 RG 1.245 Classification

In RG 1.245 [10], the U.S. Nuclear Regulatory Commission (NRC) developed a framework to develop contents of a licensing submittal when performing PFM analyses. The companion document, NUREG/CR-7278 [12], provides a technical basis for the framework of RG 1.245. These two NRC documents provide guidance and best practices for PFM analyses and documentation that are incorporated into this EPRI report directly or by reference, including supporting analyses, sensitivity analyses, and V&V. Table 1-2 provides an overview of the classification of PIPER-CASS in the context of RG 1.245, along with an overview of the report sections which include content related to each of the tables in RG 1.245.

Table 1-2
Classification of PIPER-CASS in the Context of RG 1.245

RG 1.245 Table	PIPER-CASS Classification	Description	Report Section
C-2: SQA and V&V Categories	QV-3	Custom code	SQA and V&V description: Section B.11 Benchmarking versus xLPR: Appendix C
C-3: Submittal Guidelines for Models	M-3 M-4	Model derived from a category M-1 or M-2 model Well-established model not previously part of an NRC-approved code	Discussion of the models included in PIPER-CASS: Sections 2 and B Additional discussion of "M-4" models: Section B.2 and parts of Section B.8 Discussion of uncertainties: Section 8
C-4: Categorization Based on Knowledge and the Importance of Inputs Used in the Analysis	Classification varies and is input dependent		Documentation of inputs: Section 4 Additional sensitivity studies for high-importance inputs: Section 4.7
C-5: Submittal Guidelines for Inputs			
C-6: Summary Guidelines for Uncertainty Propagation	UP-1	Analysis does not employ a surrogate model	Discussion of Monte Carlo sampling scheme: Section B.1 Discussion of number of realizations: Sections 6.4.2 and 7.4
C-7: Submittal Guidelines for Statistical Convergence	SC-1	[Acceptance criteria met with at least one order of magnitude margin] AND [no importance sampling AND no surrogate models used]	Assessment of convergence: Sections 6.4 and 7.4
C-8: Submittal Guidelines for Sensitivity Analysis	SA-6	First-of-a-kind code (QV-2, QV-3) with many independent variables (e.g., >5, determined on a case-by-case basis)	Input importance studies: Sections 6.2 and 7.2
C-9: Submittal Guidelines for Outputs Uncertainty Characterization	O-1	Acceptance criteria met with at least one order of magnitude margin	Discussion of uncertainties: Section 8
C-10: Submittal Guidelines for Sensitivity Studies	SS-6	Category QV-2 or QV-3 code with many independent variables (e.g., >5, determined on a case-by-case basis)	Input definition for sensitivity studies: Section 4.7 Sensitivity study results and discussion: Sections 6.3 and 7.3

2 PIPER-CASS PFM CODE OVERVIEW

The PIPER-CASS (Piping Integrity Probabilistic Evaluation for Reactors – Cast Austenitic Stainless Steel) code is a probabilistic fracture mechanics simulation for fatigue crack growth in nuclear piping. Each realization of the single-loop Monte Carlo simulation represents a single piping segment or piping weld. PIPER-CASS may also be run in deterministic mode (i.e., a single realization with only deterministic inputs). A given run of PIPER-CASS models either axial or circumferential cracking. In axial cracking mode, PIPER-CASS models an axial slice of the pipe thickness where cracks may grow and interact. In circumferential cracking mode, PIPER-CASS models the cross section of the pipe where cracks may similarly grow and interact. The overall structure of the PIPER-CASS code and the steps involved in an analysis are provided as a flow chart in Figure 2-1. Details on the calculation steps in the time loop are provided in Figure 2-2, including the actual modeling of fatigue crack growth.

While a crack initiation module is present for extensibility, for the analyses presented herein, all cracks are assumed to be present from the start of the simulation (i.e., the initiation module is disabled). Part-through-wall cracks are modeled as semi-elliptical surface cracks (SESC), except that, consistent with xLPR, the crack stability models generally are derived for a constant-depth (i.e., rectangular) crack shape (see Section B.8). Through-wall cracks may be trapezoidal through-wall (TRN) cracks when they initially grow through-wall, or they may be idealized rectangular through-wall (TW) cracks. Cracks grow by fatigue caused by the modeled transients that are superimposed upon normal operating conditions. For axial cracks, the driving hoop stress fluctuations are generated by pressure transients and radial thermal gradients caused by RCS transients. For circumferential cracks, the driving hoop stress fluctuations may be driven by these same sources as well as mechanical axial and global bending loads (such as seismic events). The stability of each crack is evaluated under the loading conditions for each Service Level (A/normal, B/off-normal, C/emergency, and D/faulted). An inservice inspection module is present which is capable of modeling volumetric and visual examinations.

Appendix B provides details on the key analysis steps, and Section B.11 describes the V&V performed along with the software baseline documentation package. To facilitate validation of the PIPER-CASS simulation, the modules are based on those of xLPR. Differences, where present, are noted.

PIPER-CASS is written in the Python programming language and makes extensive use of array data structures that maintain the flexibility of Python while providing enhanced computational performance through the back-end pre-compiled C code. Array data structures permit vectorized code that also facilitates operations on a subset of the data structure through Boolean masks or integer index arrays. For time invariant parameters, the distributions are sampled for all realizations prior to entering the time loop. Additionally, PIPER-CASS makes use of multiprocessing and permits the execution of the code on commercial cloud computing nodes, facilitating the scaling of individual runs to millions of realizations.

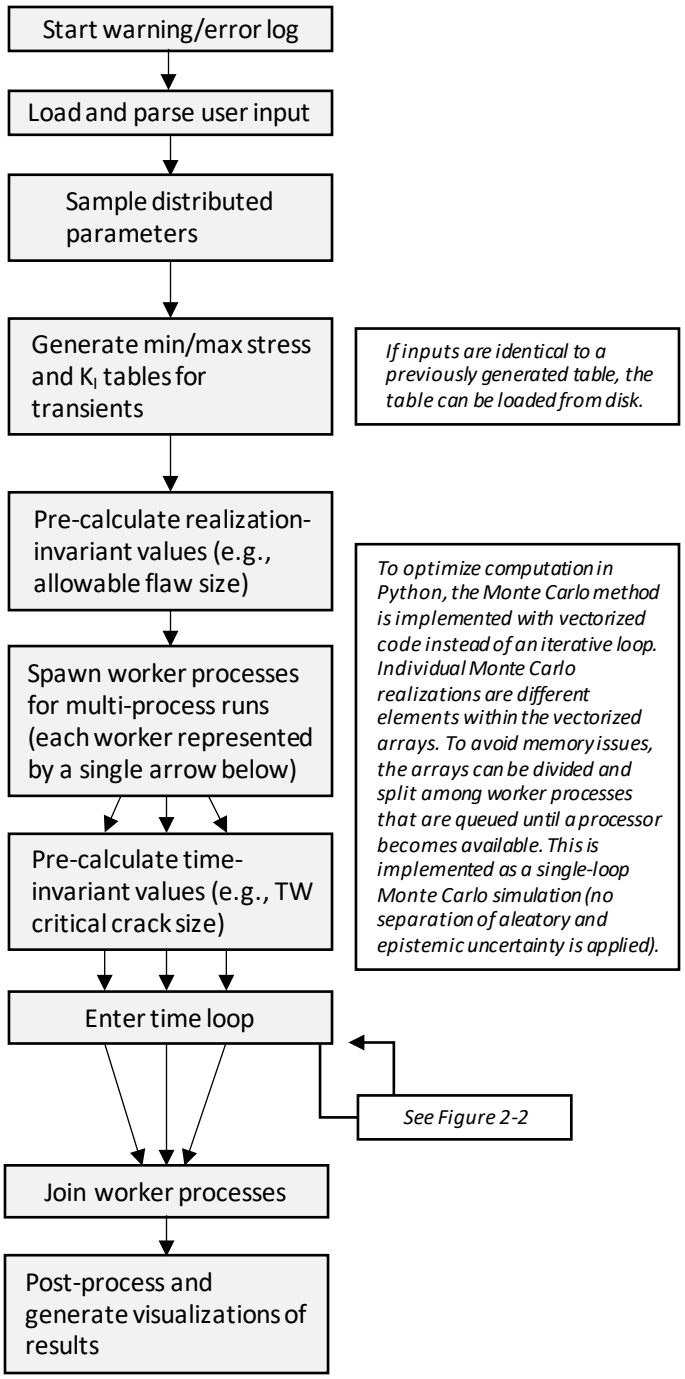

Figure 2-1
PIPER-CASS Probabilistic Model Code Structure Flow Chart

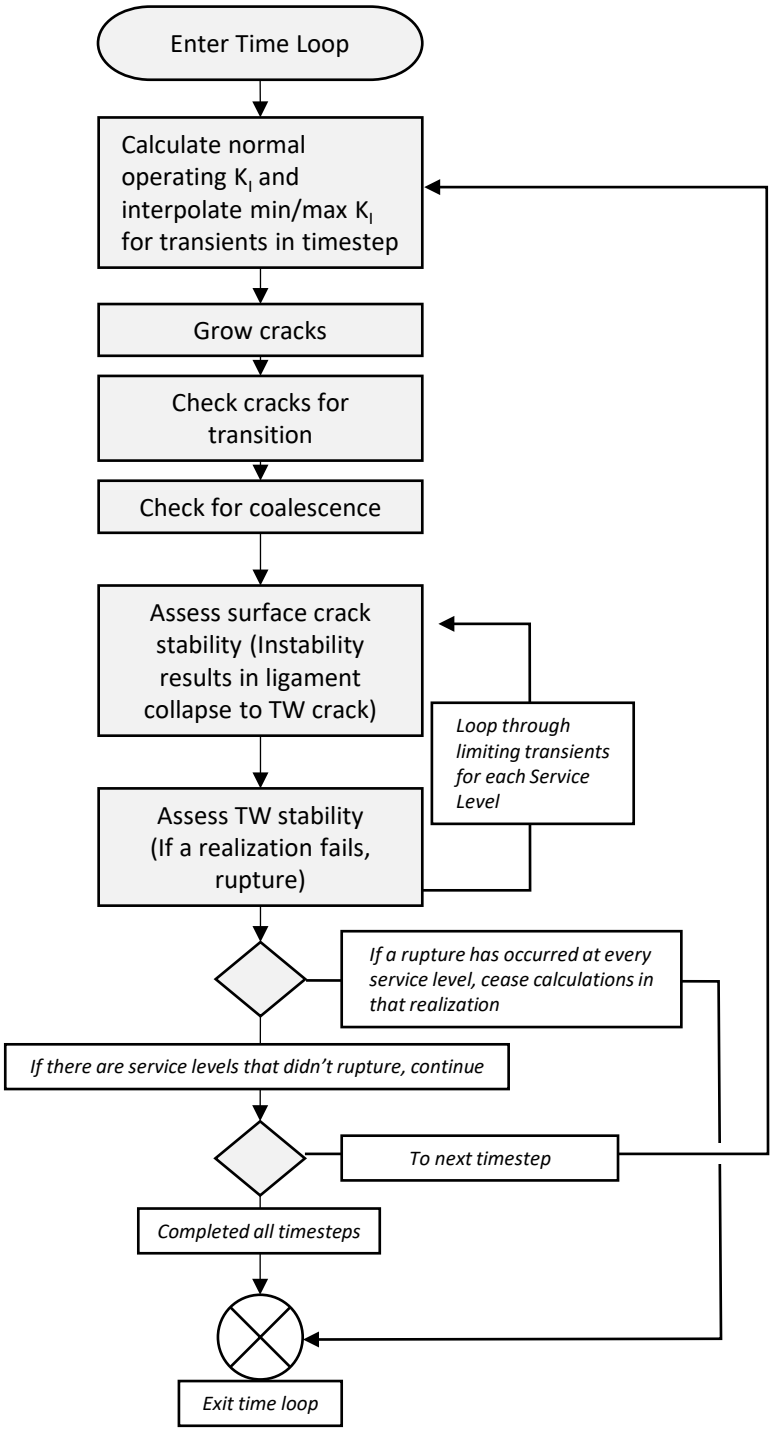

Figure 2-2
PIPER-CASS Probabilistic Model Code Structure Flow Chart: Detail of Time Loop

3 ALTERNATIVE FLAW EVALUATION APPROACH FOR CIRCUMFERENTIALLY ORIENTED FLAWS IN CASS

This section presents the proposed alternative flaw evaluation process for circumferentially oriented flaws in CASS piping components, for which qualified depth sizing information is not available. This evaluation process is applicable to flaws in main loop piping.

3.1 Standard Section XI Piping Flaw Evaluation

The flaw evaluation procedure for detected circumferential cracking specified by IWB-3640 of ASME Code, Section XI requires the following key steps:

1. *Initial Flaw Size*. Obtain the flaw length and depth using a UT sizing procedure qualified per Section XI, Mandatory Appendix VIII. Set the initial crack size in the flaw evaluation accordingly.
2. *Subcritical Growth*. Per IWB-3641(d), increment the crack size per a deterministic fatigue crack growth calculation (e.g., using ASME Code Case N-809) for the assumed evaluation time period.
3. *IWB-3640 Depth Limit*. The maximum allowable flaw depth per IWB-3640 is 75% through-wall. If the flaw depth at the end of the assumed evaluation period is greater than 75% through-wall, the flaw is unacceptable for the assumed evaluation period, regardless of the results of step 4.
4. *Allowable Flaw Size and Stress Checks*. Per IWB-3641(e), using the crack length and depth at the end of the assumed evaluation period and the applicable Service Level loadings, determine whether the end-of-evaluation period flaw size is allowable (as required by C-2600 of Section XI) and whether each Service Level loading is less than the allowable stress.

3.2 Alternative Flaw Evaluation Approach

In the absence of a qualified depth sizing process for CASS piping components, an alternative flaw evaluation process is considered in which the flaw is conservatively assumed in the evaluation to be a 100% through-wall crack. In this alternative approach, the 75% through-wall limit of IWB-3640 would not be enforced, but the allowable flaw length would be determined that ensures sufficient margin for flaw stability. Because the Z-factor approach in Section XI, Nonmandatory Appendix C provides greater margin on flaw stability for shorter flaws, this proposed approach has a maximum limit of applicability, which is the largest allowable flaw length for which this methodology is validated by the PFM. The steps of the alternative flaw procedure are depicted in Figure 3-1 and described below:

1. *Initial Flaw Size.* Set the initial flaw length as the length reported per the qualified UT length sizing. Recognizing the lack of a qualified depth-sizing method, conservatively assume that the depth is 100% through-wall.
2. *Subcritical Growth.* Increment the crack length using a deterministic fatigue crack growth calculation for the assumed evaluation period, under the conservative assumption that the flaw is an idealized through-wall crack with equal angular extent on the ID and OD.
3. *Allowable Flaw Size and Stress Checks.* If the end-of-evaluation-period length is shorter than both the limit of applicability and the limiting allowable length, the detected flaw is acceptable for the assumed evaluation period.
   - Compare the end-of-evaluation-period length against the limit of applicability given in this report.
   - Perform an elastic-plastic fracture mechanics (EPFM) allowable flaw size calculation for the assumed through-wall flaw with the end-of-evaluation-period length calculated by the preceding step. Determine the appropriate Z-factor for the predicted δ-ferrite content as given by C-6330(a) of Nonmandatory Appendix C of ASME Code, Section XI 2019 Edition [1]. Using C-6320, calculate the length for which a flaw with a/t = 1.0 has an allowable stress equal to each of the Service Level loadings to determine the limiting allowable length.

Lacking a reliable depth sizing capability, analytically ensuring leak tightness is not practical. However, defense-in-depth is maintained given that the PFM results show acceptable margin for flaw stability, that stainless steel components are resistant to boric acid corrosion, and that unidentified leak rate monitoring programs in plant technical specifications require timely actions to maintain safe operability for recovery, including a shutdown, in the unlikely case of leakage.

3.3 PFM Validation of Alternative Flaw Evaluation

EPFM stability assessments relying on the Z-factor approach, like allowable flaw size calculations, contain more margin on flaw stability for shorter flaws. PFM analyses are thus performed to determine a limit of applicability for the alternative flaw evaluation process that maintains acceptable margin on flaw stability. An idealized through-wall crack is again applied, given the higher stress intensity factors of that flaw shape and the unknown depth of flaws for which the alterative process is applied. The steps of the PFM validation analyses are depicted in Figure 3-2 and described below:

1. *Set Limit of Applicability.* Set the initial crack length as the limit of applicability to be evaluated. The piping loads are set as the maximum allowable under the alternative flaw evaluation process, with the following approach to set the relative levels of membrane, primary bending, and secondary bending:
   - The primary membrane stress is given by the pressure endcap force. In reviewing a sample of plant submittals, axial piping forces tend to be small relative to the pressure

endcap force. A sensitivity was considered with a higher membrane stress loading based on the upper limit of reviewed plant data.

- The secondary to primary bending load ratio is 99:1. Secondary bending stress is not subject to the structural factor for bending when comparing against the bending stress at incipient plastic collapse in Equation 9 of C-6321. Assuming 99% of bending stress as secondary is conservative but appropriate because of large thermal expansion global bending loads in piping.

2. *Subcritical Growth from Allowable to Acceptable Size.* Shrink the crack length per a deterministic fatigue crack growth calculation for the assumed evaluation period to obtain the acceptable flaw length from the allowable length. Where the amount of deterministic growth is small, this step may be omitted to simplify inputs and their verification (i.e., the initial crack size is set to the allowable size).
3. *Probabilistic Growth*. Use the PFM code to grow the crack over the duration of the evaluation period, considering multiple sources of uncertainty and variability. The flaws are evaluated for stability under net-section collapse (NSC) and EPFM criteria for the range of sampled material properties, and the resultant probability of rupture is compared against the acceptance criteria.

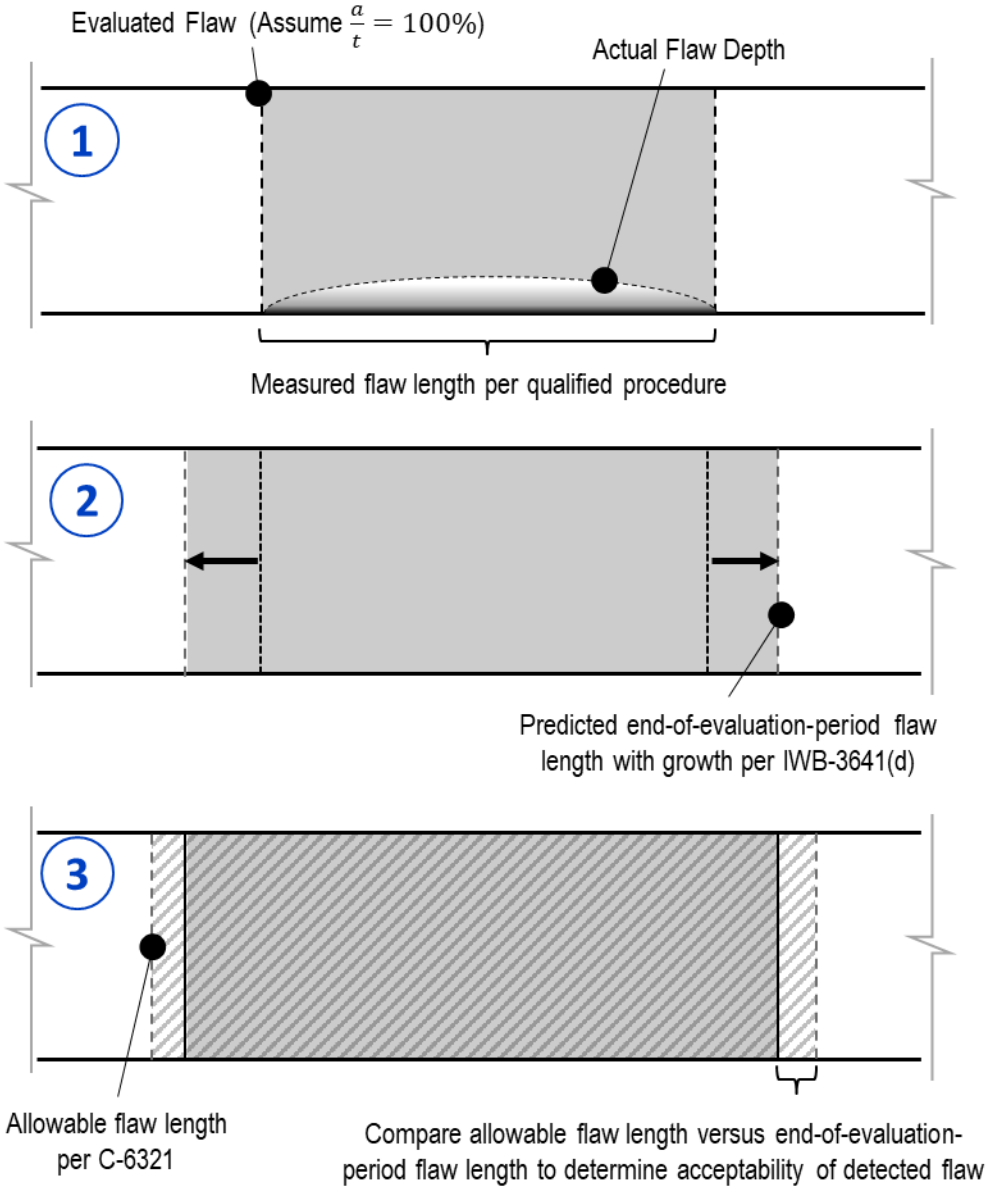

Figure 3-1
Proposed Flaw Evaluation Method for Circumferential Flaws in CASS Piping Components[5]

[5] In Figure 3-1 and Figure 3-2, the curvature of the pipe is ignored for simplicity.

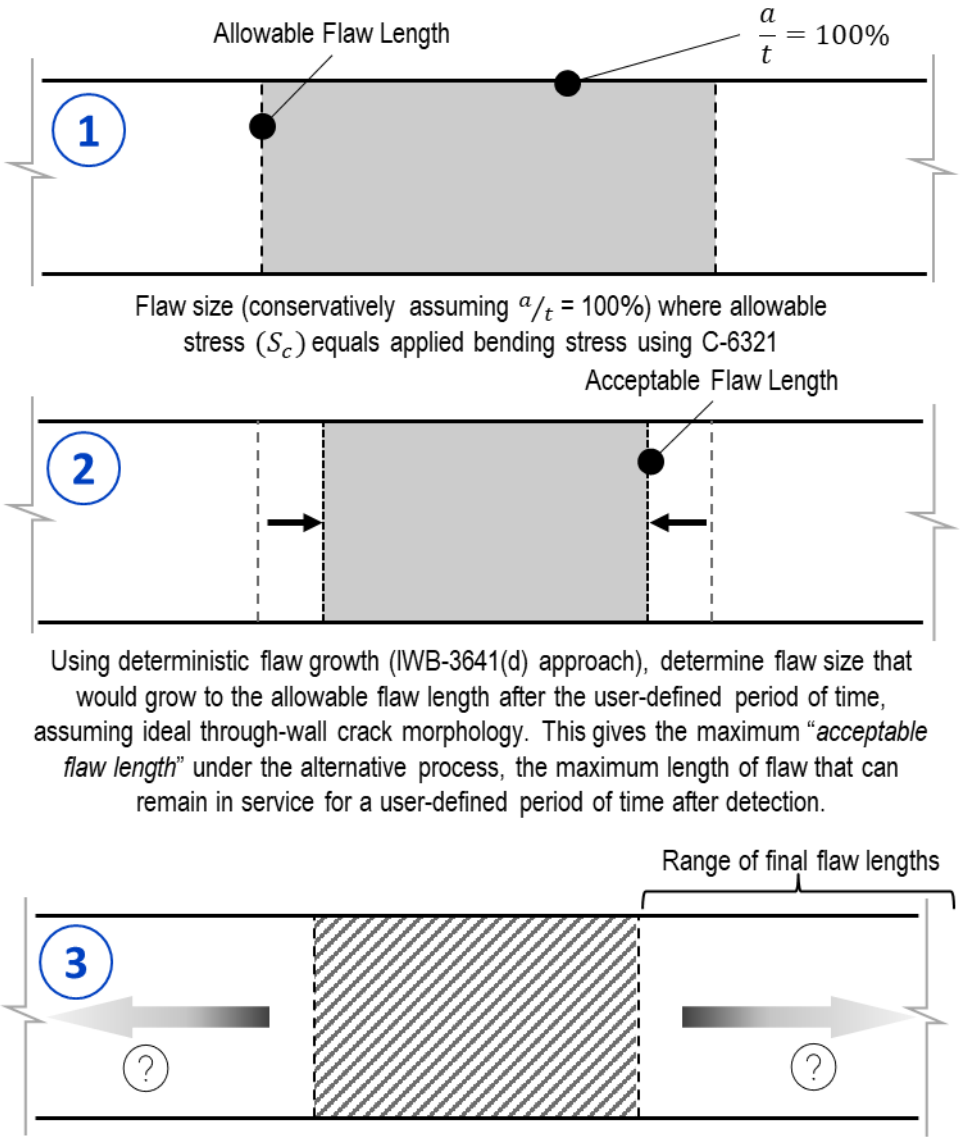

Figure 3-2
Method for using PFM to Evaluate the Margin Provided by Proposed Flaw Evaluation Method

4 INPUTS AND CASES EVALUATED

4.1 Geometry Cases

Two geometry cases each are considered for WEC and CE PWRs to cover the range of main loop CASS piping sizes in WEC U.S. PWRs and the variability in wall thickness for the CASS surge lines in CE U.S. PWRs.

The examination coverage required by Subarticle IWB-2500 (Examination Categories B-F and B-J) includes the weld and a short section of base metal on either side of the weld. Per the requirements of IWB-3641, the procedures in Nonmandatory Appendices C and H of Section XI, which are based on equations applicable to a section of straight pipe, are applicable to a flaw in the initial portion of an elbow closest to the adjoining weld. Hence, in this study, a section of straight piping of uniform thickness was modeled for the purpose of calculating the cumulative probability of rupture and of leakage. The same approach is also applied in MRP-362 R1 [13], which evaluates the flaw tolerance of portions of Class 1 and 2 piping comprised of SA-351 statically- or centrifugally-cast base metal and provides the technical basis for Code Case N-838 [14]. Of course, if an actual crack was detected in an elbow beyond the distance from the adjoining weld for which Nonmandatory Appendices C and H apply, any evaluation of that flaw would need to consider the stresses specific to the elbow geometry.

To cover the range of piping diameters and thicknesses in WEC main loop piping, the following geometry cases are considered within this study:

- *WEC 1 Geometry*: 27.5 inch (699 mm) outside diameter (OD), 2.32 inch (58.9 mm) wall thickness (t), and inner radius to thickness ratio (R_i/t) of 4.93.
- *WEC 2 Geometry*: OD = 37.59 inch (955 mm), t = 3.09 inch (78.5 mm), and R_i/t = 5.08.

For CE PWRs operating in the U.S. other than System 80 [15], the surge line includes piping components (elbows, piping, and safe ends) fabricated from CASS [16]. The surge line piping at all CE PWRs operating in the U.S. has a nominal size and thickness of NPS 12 SCH 160 [16], for which the nominal wall thickness is 1.312 inches. While surge line piping at all operating CE PWRs is the same nominal size, there is spatial variation within the surge line. Per the available information, the similar metal weld locations are machined to a reduced thickness: 1.01 inch or 1.17 inch (25.7 mm or 29.7 mm), depending on the plant. Consequently, the range of geometries present can be covered by performing analyses at the extremes of the thicknesses present, reflected by the two selected geometry configurations:

- *CE 1 Geometry*: OD = 12.75 inch (324 mm), t = 1.01 inch (25.7 mm), and R_i/t = 5.31.
- *CE 2 Geometry*: OD = 12.75 inch (324 mm), t = 1.31 inch (33.3 mm), and R_i/t = 3.87.

Differences in wall thickness represent competing effects for crack growth and stability. In general, thicker wall components are more flaw tolerant and less likely to rupture at a given set of loads because of the increased cross section of material to transmit the load. Conversely,

thicker wall components may experience faster crack growth due to steeper stress gradients from thermal transients. Therefore, both extremes of component wall thickness must be examined. In the case of the CE surge lines, the two geometry cases address both the spatial variability in wall thickness in the axial direction for a single plant configuration and the variation in reduced wall thickness at the welds among the two plant configurations.

4.2 Material Inputs

The WEC PWR main loop CASS piping components are constructed of one of two alloys: CF8A and CF8M, which are the cast equivalents of wrought 304 and 316 grades, respectively. The CE PWR surge line CASS piping components and safe ends are constructed of CF8M. This analysis applies CF8M to all base cases as this CASS alloy is the most susceptible to thermal aging and therefore represents the bounding material input. Sensitivity cases using CF8, which has higher aged toughness but lower strength, were also performed for circumferential cracking, to demonstrate that the CF8M material is bounding. Since the PIPER-CASS runs represent plant operation for up to 80 years and since ruptures, if any, are predicted to occur toward the end of the modeled operational period, the CASS material is modeled as having reached the saturation point of the aging effect. Thermal aging of CASS material tends to increase the material strength and reduce the material toughness, so sensitivity cases are considered for unaged CASS material to demonstrate the aged condition is bounding. Key CF8M material inputs are discussed below.

The critical crack size is highly dependent on the fracture toughness and flow strength of aged CASS material, so it is important to reflect the potential variability in these inputs. The material strength and toughness distributions are developed based on the fully aged material data in Appendix E of MRP-362, Rev. 1 [13], which are excerpted in Appendix A of this report. Correlations between these inputs are also applied, as described in the following subsections.

4.2.1 Toughness

CASS is susceptible to thermal embrittlement, and therefore, the critical crack size for unstable rupture is expected to be limited by the reduced fracture toughness properties caused by thermal aging. In other words, the low fracture toughness results in the EPFM stability criterion being limiting compared to the NSC stability criterion. As noted previously, PIPER-CASS models the CASS material as being fully aged.

The two key inputs to degree of fracture toughness reduction for a particular cast component are the δ-*Fe* formed during casting and the precise chemical composition of the alloy. This analysis considers a nominal δ-*Fe* content of 40%, modeled as a normal distribution to account for epistemic uncertainty in measured δ-*Fe* content. Most cast components have δ-*Fe* content well below 30%, so a value of 40% δ-*Fe* is bounding.

The δ-*Fe* content and the material composition parameter (ϕ) are used to calculate a series of derived J-R curve inputs as described in Section B.2. The variability factor on C_{vsat} and the

composition factor multiplier (ϕ/δ-*Fe* of 1.78) are developed by calibration to yield distribution of $J_{0.08}$ (J-integral at 0.08 inch [2 mm] crack extension) values that meet the following criteria:

- Match the variability of $J_{0.08}$ data in MRP-362 Rev. 1, Appendix E [13] normalized to δ-*Fe* of 25% using the NUREG/CR-4513, Rev. 2 [3] relations.

  MRP-362 Rev. 1, Appendix E provides J-R curve parameters from test data for CF8M with a wide range of δ-*Fe* and toughness. The low toughness data are noted in MRP-362 Rev. 1 to all be from foreign plants or be generated from material with specifications and fabrication processes that may be different than employed for U.S. plants. Using such data would result in smaller critical crack sizes than would be expected for materials in U.S. PWRs.

- The 1st percentile of the distribution of non-normalized $J_{0.08}$ in PIPER-CASS should approximately equal the "lower bound" value for static cast CF8M with 30-40% δ-*Fe* in NUREG/CR-4513, Rev. 2.[6]

  Due to the high variability obtained from the prior bullet, this calibration ensures some realizations at the extreme low end of the variability in toughness without yielding unrealistically small values of toughness.

The distribution of $J_{0.08}$ values are presented in Figure 4-1, with the lower bound line at the 1.4th percentile. These values are compared with NUREG/CR-4513, Rev. 2 "lower bound" values, data applied in MRP-362, Rev. 1 Figure C-1 normalized for δ-*Fe*, and data presented in MRP-362, Rev. 1 Appendix E normalized for δ-*Fe*. The resultant range of J-R curves is shown in Figure 4-2. The deterministic "screening criteria" used in NUREG/CR-4513, Rev. 2 to determine susceptibility to thermal aging effects are not used by PIPER-CASS.

The material composition factor normalized by δ-*Fe* (ϕ / δ-*Fe)* affects the curvature of the distribution in Figure 4-1. The chosen value of 1.78 is a reasonable input (60th percentile) based on the composition of CF8M heats listed in Table A1 of NUREG/CR-4513, Rev. 2. Furthermore, this mean value of ϕ (1.78×40=71.2) bounds all of the CF8M heats listed in Table A1 of NUREG/CR-4513, Rev. 2; the highest value is 61.4.

It is noted that xLPR utilizes the more general expression for the J_R resistance curve that allows separate quantification of the ductile crack initiation toughness, J_{ic}, where $J_R = C_r\Delta a^m + J_{ic}$. PIPER-CASS also optionally has the ability to apply this more general expression for the J_R resistance curve. As the fits of C_r and m in NUREG/CR-4513, Rev. 2 [3] implicitly include the effect of crack blunting and initiation of tearing, J_{ic} was appropriately set to zero as input to the code for this effort.

[6] NUREG/CR-4513, Rev. 2 [3] states that its methodology is applicable up to the equivalent of 10k hours at 400°C, corresponding to 15 EFPY for CF8M components at 320°C (608°F). However, application of these correlations to a service life beyond this limit is considered appropriate following a review of underlying data. Appendix C of NUREG/CR-4513 Rev. 2 shows the Charpy-toughness data for samples collected with aging times at 400°C (750°F) substantially greater than 10,000 hours. This data includes samples for CF8M aged for 50,000 hours. These data show explicitly the expected plateau behavior for toughness as the aging time is increased.

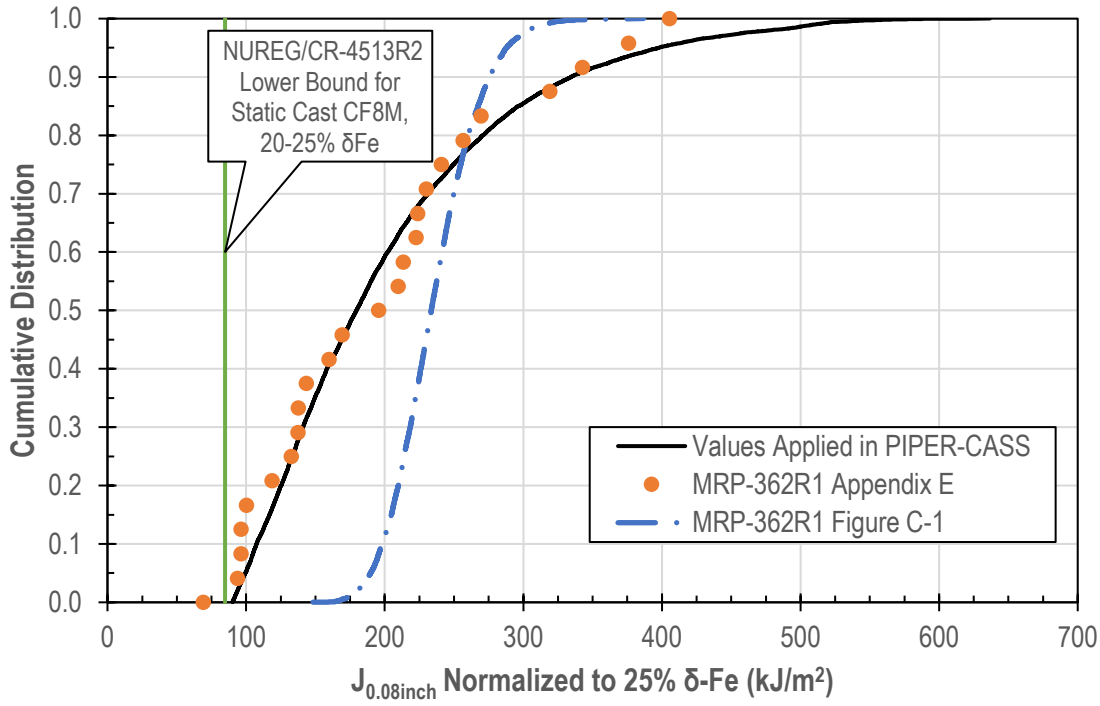

Figure 4-1
Calibration of CF8M Fracture Toughness Distribution Normalized to 25% δ-*Fe*

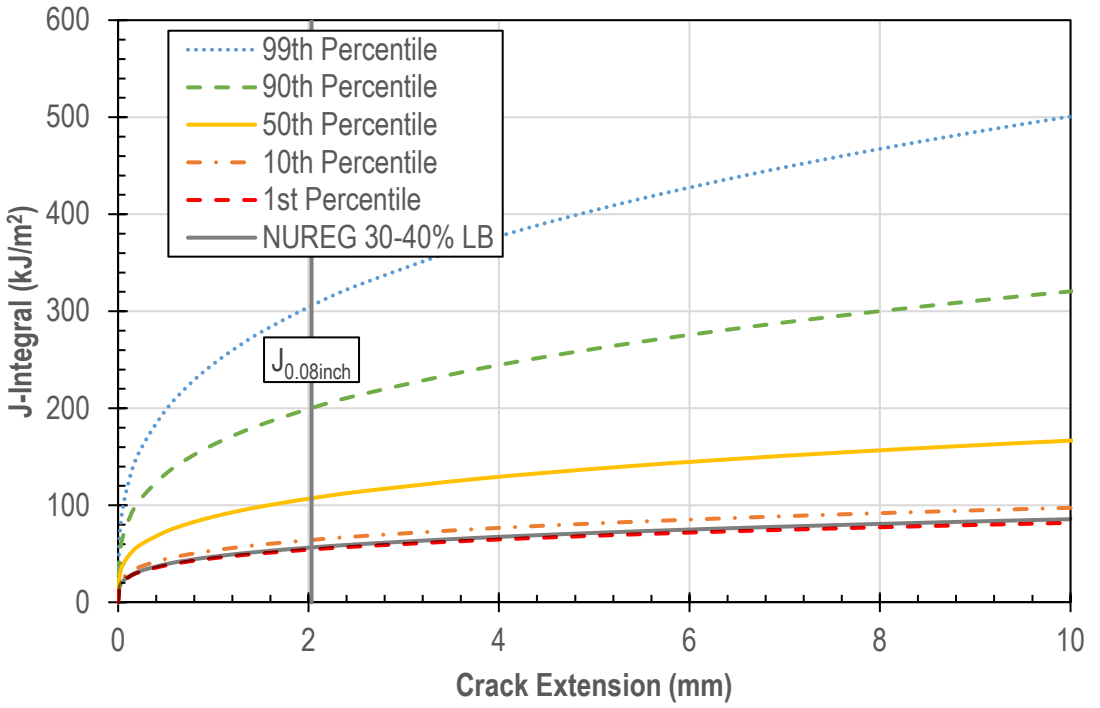

Figure 4-2
Variability in Material Toughness with Ductile Crack Extension for Static Cast CF8M with Distributed δ-*Fe* and Variability Added to C_{vsat}

4.2.2 Strength

The aged yield strength and ultimate strength are applied as normal distributions. Metal strength data is often normally distributed, and the normal distribution provides a larger tail at lower strengths than, for example, the lognormal distribution. Normal distributions are fitted to the data for fully aged material strength in Appendix E of MRP-362, Rev. 1 [13] that is repeated in Appendix A of this report. The normal distributions were fit using the maximum likelihood estimators, resulting in the values in Table 4-1. A lower limit is applied on the distributions such that the sampled strengths are at least 90% of the ASME Code, Section II-D minimum, as seen in Figure 4-3. The material yield and ultimate strengths for a given material are correlated, so the variance in the normal distribution is adjusted to yield a correlated sample, as described in Section 4.2.3. The resultant at-temperature flow strength (average of σ_y and σ_u) for fully aged CF8M is compared against that in Appendix A of MRP-362 Rev. 1 in Figure 4-4, which samples an unaged flow strength and a flow strength aging factor. The PIPER-CASS approach results in lower flow strength except for the extreme tail of the distribution, where the truncation maintains strengths at more realistic values.

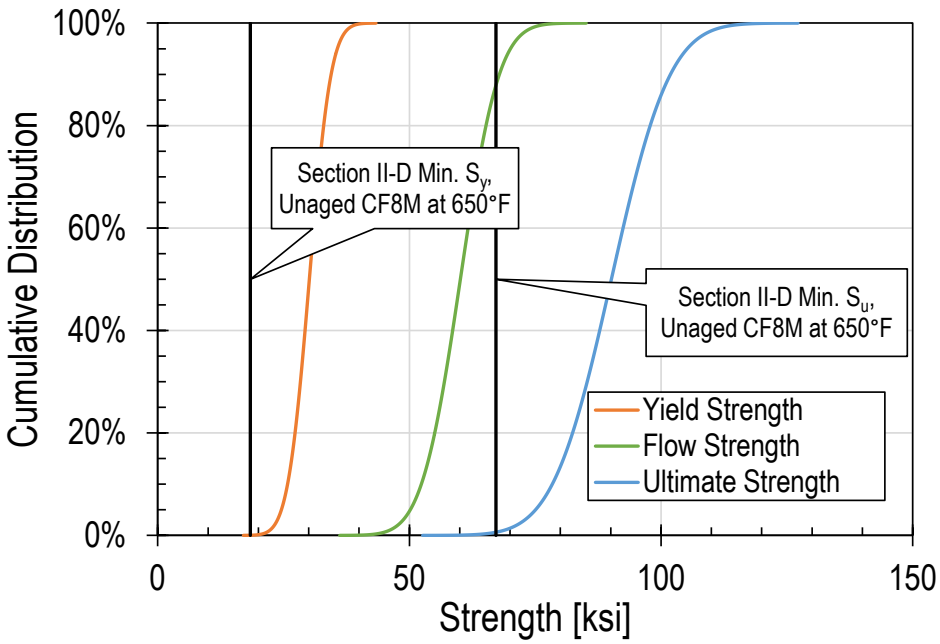

Figure 4-3
Distribution of Yield, Flow, and Ultimate Tensile Strength Inputs for CF8M at Fully Saturated Aging Condition Applied by PIPER-CASS

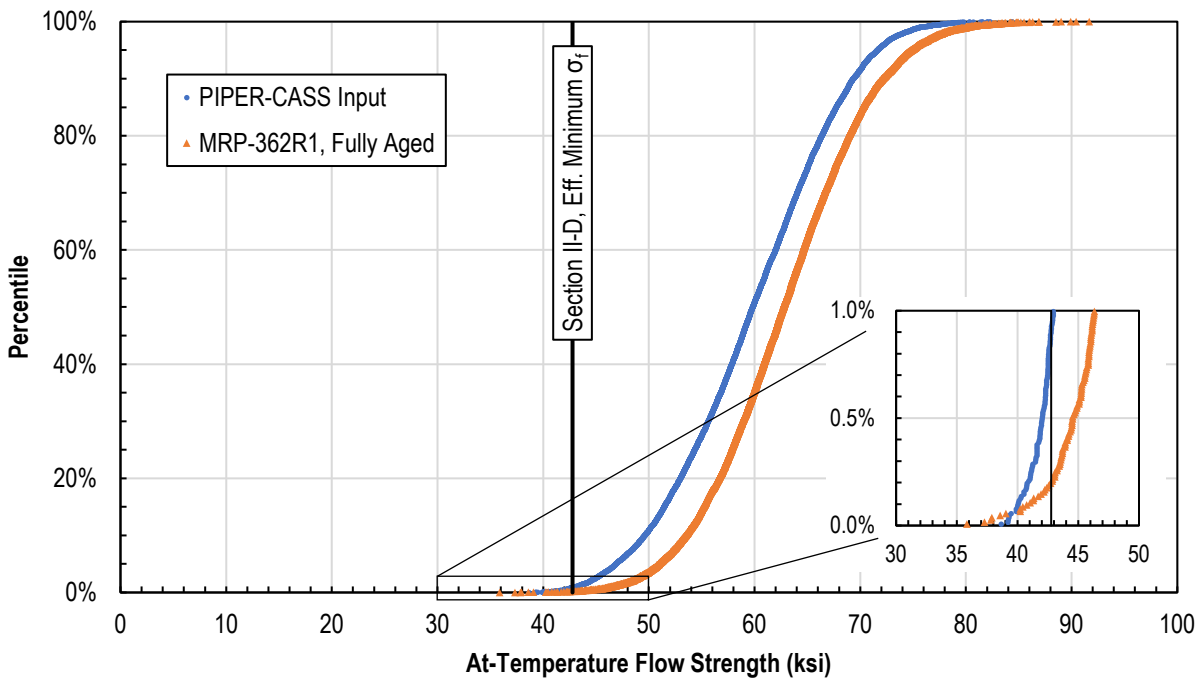

Figure 4-4
Comparison of the Fully Aged Flow Strength Applied by PIPER-CASS with that in Appendix A of MRP-362 Rev. 1 (for 10,000 samples)

4.2.3 Parameter Correlation

Strength and toughness tend to be correlated for aged CF8M data, with strength increasing with aging and toughness decreasing with aging (negative correlation). Additionally, yield strength and ultimate strength tend to be positively correlated. The matrix of correlation coefficients was determined for the data in Appendix A. Correlation coefficient magnitudes in the 0.6 to 0.9 range are observed in the data, with higher strength to toughness correlations with the unnormalized $J_{0.08}$ than with $J_{0.08}$ normalized to δ-*Fe* of 25%. The achieved correlations of sampled data were within 1% of the yield to ultimate strength correlation. For the strength to toughness correlation, the correlation was moderated to achieve an effect between the observed correlation to the normalized and unnormalized $J_{0.08}$ data.

The calibrated toughness distributions were adjusted to remain valid following the imposition of correlation coefficients.

4.2.4 Other

For the analyses presented herein, the rise time upper limit of 2,000 sec applied in xLPR is also maintained[7]. This choice was made within xLPR because of the concern for large extrapolation error outside the range of loading rise times available in the laboratory data used to develop the crack growth rate (CGR) model [17]. However, this choice might introduce a non-conservatism into the calculation of CGR[8]. Section 6.3 includes a sensitivity case investigating the effects of these two modeling choices by removing the cap on the rise time and by removing the $f_{SS,alloy}$ multiplier of 0.8.

The Ramberg-Osgood α parameter is derived by PIPER-CASS using in the same fashion as MRP-362, Rev. 1. When performing the calculation of the α parameter (Section B.2), the flow strength is truncated to a minimum of 32 ksi to prevent negative values of the Ramberg-Osgood α parameter. The α parameter is calculated using the flow strength as the reference stress, but the parameter is baselined to the yield strength for further calculations per NUREG/CR-6142 Eqn. 7 [18].

Other material properties for CF8M required for calculations of temperature and stress during transients (Young's modulus, Poisson ratio, thermal expansion coefficient, density, specific heat, and conductivity) are taken from Section II-D of the ASME Code [19]. The temperature-dependence of conductivity is handled by the code using the full table of values from 68°F to 1,382°F (20°C to 750°C).

4.3 Loading Inputs

The loading inputs are categorized into three sets: constant loads, transient loads applicable to crack growth, and loads applied to evaluate stability for each Service Level.

4.3.1 Constant Loading

Normal operating temperatures representative for U.S. pressurizer temperature (653°F (345°C) for the CE pressurizer surge line) and representative of U.S. PWR hot legs (609°F (320.5°C) for the WEC main loop piping) are applied. Because the fatigue crack growth equation yields higher

[7] Section 5(c)(3) of Code Case N-809 [31] includes the option to apply a value of S_{ENV} = 20 as an alternative to tabulating a rise time value from the stress history of a transient. A value of S_{ENV} = 20 corresponds to a rise time of 21,715 sec, which is bounding of nearly all transients [17]. This alternative is a conservative option if one prefers not to develop rise time information. As rise time information is calculated by PIPER-CASS, this conservative modeling simplification is not applied.

[8] The sensitivity investigation of the effect of the limit on rise time as applied in the CGR equation is included in Section 6.3.1 and Section 7.3.1. Very few transients accumulate rise times exceeding 2,000 sec. Specifically, only very lengthy transients, such as Cooldown, have a sustained positive stress rate of 1,000 psi/hr (6.9 MPa/hr) exceeding a rise time of 2,000 sec. The effect of increasing the rise time by an order of magnitude (to 20,000 sec) increases the crack growth rate due to that transient by a factor of two. Because most transients have a rise time less than 2,000 sec, the net overall effect on crack growth is shown to be small.

growth rates at higher temperatures, applying the hot leg normal operating temperature bounds any flaws in CASS at cold leg temperatures.

Constant welding residual stress (WRS) profiles are also applied. For fatigue crack growth, the steady-state WRS only impacts the load ratio, with increased tensile WRS magnitude yielding a modestly higher crack growth rate. The axial and hoop WRS profiles are taken from NP-4690-SR Figure 3-3 [20] for CE cases and from the pre-mitigation mean data of Table 13 and Table 14 of xLPR-MSGR-WRS V1 [21] for WEC cases. These WRS profiles are shown in Figure 4-5 and Figure 4-6. The reactor pressure vessel (RPV) inlet and outlet nozzles are dissimilar metal welded nozzles where WRS is expected to be generally higher than similar metal welds in CASS piping. Therefore, the WRS profiles for the RPV nozzles are considered appropriate for this analysis.

For circumferential cracks, the static loads are set from the maximum allowable loadings calculated using the approach in Section 3.3 Step 1. The lowest of the loadings is applied with primary membrane, primary bending, and secondary bending as dead-weight (DW) force, DW bending, and normal thermal expansion (NTE) bending, respectively. The other allowable loadings are superimposed on this load state as "Stability Loading."

4.3.2 Transient Loading

Transients of the reactor coolant system leading to changes in pressure and temperature are compiled from proprietary transient data. For WEC main loop cases, the general transients described in MRP-393 [22] are applied at the best-estimate frequencies for each transient listed in the text description in MRP-393 (as shown in Table 4-5). The flow rate for these transients is taken as 25.1 m/s.

For CE cases, the transients described in the design specification for the pressurizer of one CE plant with a CASS surge line are applied at the more realistic frequencies from a licensee's surge line Section XI Nonmandatory Appendix L evaluation in Reference [23] (as shown in Table 4-6 and Table 4-7).[9] Stratification transients are modeled as being established and disrupted by a step change in fluid temperature, with the global bending moment applied as a "Type II" stress. As in MRP-464 [24], the "Hot Standby Stratification at △90°F" transient is reduced to a ΔT of 20°F to better match the stresses calculated modeling the detailed thermocouple data in CEN-387 R1-NP [16]. Unlike the main loop, for which the flow rate is quantified and well characterized, the flow rate in the surge line can vary significantly in the course of a transient. For abrupt temperature changes like insurge and outsurge events, the magnitude of radial gradient thermal stress (RGTS) is affected by the heat transfer coefficient calculated from the input flow rate. A representative value is chosen in the range 0.05 m/s to 1.3 m/s based on the

[9] The "normal variations" transient included in the specification models +/-100 psig cycles at 16,666 cycles per year, or about 50 times per day. This is not a realistic pressure variation on such a high frequency and therefore is excluded from Reference [23] and this evaluation.

design specification flow rates for plant transients and 0.03 m/s or 0.12 m/s for stratification transients to match expected flow conditions and heat transfer rates.

4.3.2.1 Flexible Power Operations

For cases that include consideration of flexible power operations (FPO), additional plant loading and unloading transient pairs (i.e., ramp down then ramp up) are included that represent three categories of power reductions similar to the categories considered in EPRI 3002010416 [25]:

- Pre-planned reduction from 100% to 80% power lasting less than a day and having a ramp rate of 1% change in power per minute (power change over the course of 20 minutes)[10]
- Pre-planned reduction from 100% to 50% power lasting a week or more and having a ramp rate of 1% change in power per minute (power change over the course of 50 minutes)
- Uncommon reduction from 100% to 30% power for an indeterminate duration and having a ramp rate of 2% change in power per minute (power change over the course of 35 minutes)

The temperature and pressure histories for these transients are defined by adjusting the loading and unloading transients from base load operation. For WEC, the base case (85% power change at 0.2% per minute) transient is truncated to the desired power range, then the time points are scaled to the desired ramp rate. For CE, only the portion of the curve where the surge line is near the hot leg temperature is scaled (originally an 85% power change at 5% per minute); the number of surges is kept constant. The frequency of these FPO transients is defined to obtain a total of 330 loading and unloading events per year, which is equal to the typical Westinghouse plant original design basis including load following (13,200 transients over 40 years, approximately one cycle per day) as discussed in MRP-459 [26].

The FPO transients in Table 4-8 are considered in the base case for circumferential cracking and as a sensitivity for axial cracking.

4.3.3 Stability Loading – Axial Cracking

Axially oriented cracks only have a single loading that drives crack instability: the operating pressure. A maximum operating pressure is defined to evaluate crack stability at each of the four main Service Levels: A, B, C, and D. Every timestep, all active cracks (which have not coalesced or previously failed as stability check) are assessed for stability at each Service Level.

4.3.4 Stability Loading – Circumferential Cracking

The stability loads for circumferential cracks are set as described in Section 3.3 Step 1. For each Service Level, the applicable pressure loading contributes endcap force, and the remainder of

[10] A slower ramp rate of 0.5% power per minute (40 minute unloading or loading duration) is considered as a sensitivity.

the membrane loading and bending are applied as loads affecting crack stability. The stability loads are recalculated for each input set that could result in a different allowable stress (e.g., differences in geometry, material strength, or Z-factor).

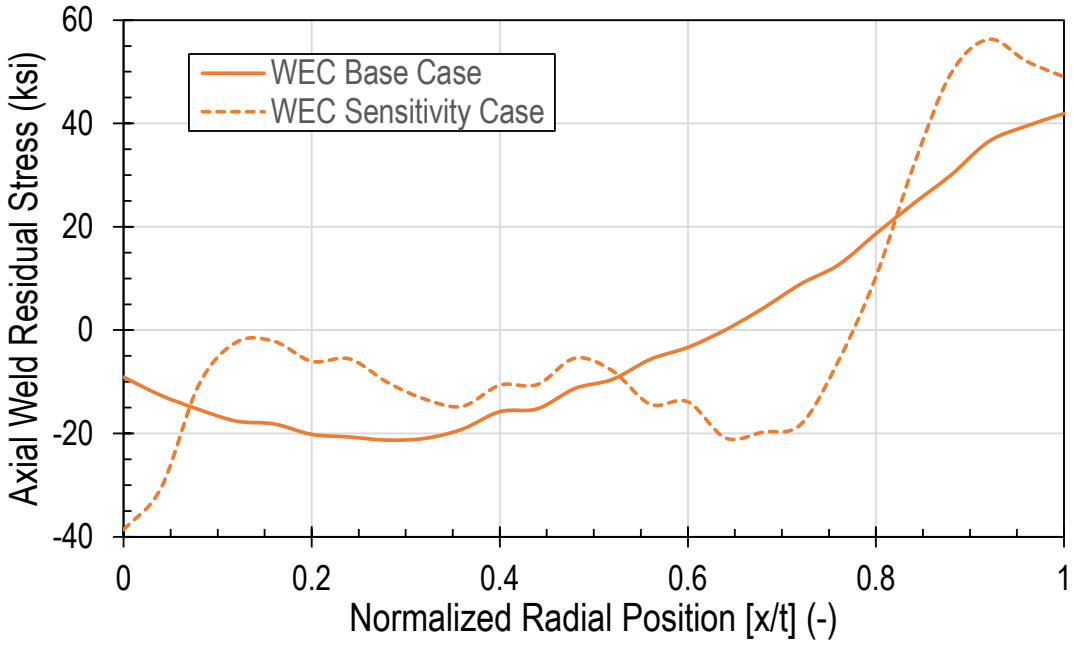

Figure 4-5
Axial WRS Profiles

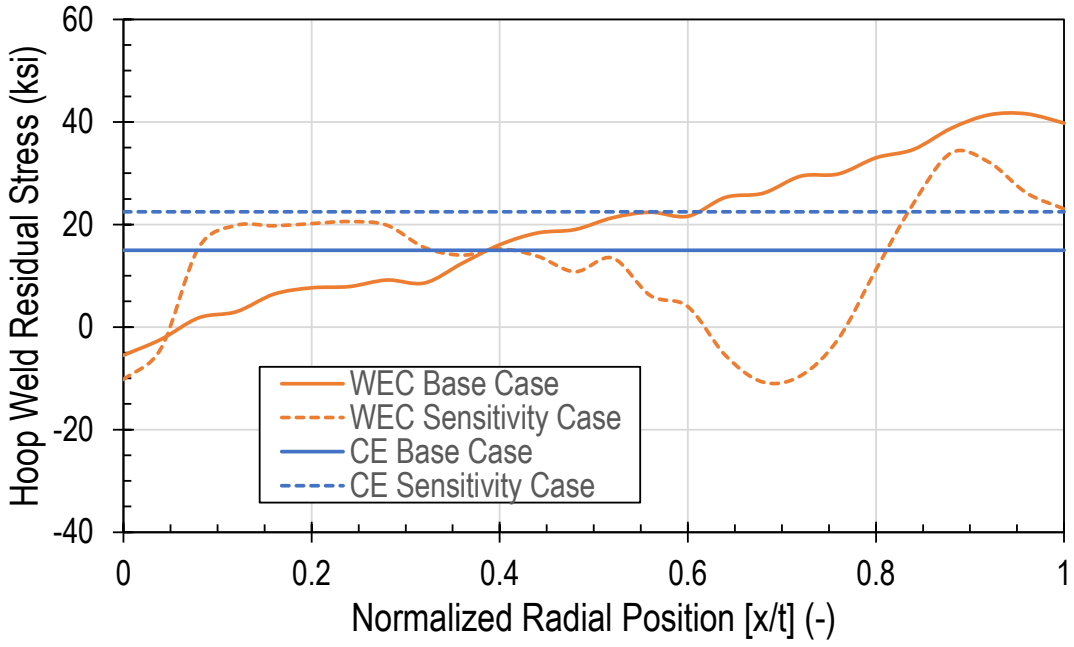

Figure 4-6
Hoop WRS Profiles

4.4 Initial Crack Size

4.4.1 Axial Cracking

Cracks actively growing via fatigue are conservatively assumed to be present at the start of the simulation time period. Fatigue crack growth for 80 full years is modeled to bound the concerns for both fatigue crack initiation and manufacturing flaws. Furthermore, the potential for coalescence of multiple pre-existing initial flaws on the same axial growth plane are explicitly considered in the analyses.

The base case models initial axial surface cracks on the ID with a semi-elliptical shape, as illustrated in Figure 4-7, having a depth of 25% through-wall (a/t = 0.25). Based on data for CASS material crediting preservice radiographic testing, this depth was selected to reasonably bound any manufacturing flaws actually present. An assessment of manufacturing flaws in large-diameter CASS piping elbows ([27], [28]) concluded that the maximum initial flaw depth should be taken as 15% through-wall when performance of pre-service radiography is credited. Based on the data collected, this study assigned a probability of 1% for the flaw depth to be greater than 15% of the wall thickness. The 25% through-wall initial crack applied in this study is conservatively greater than this 15% recommendation and the same as recommended in Section 4.1 of MRP-362, Rev. 1 [13], which considered the study recommending the 15% depth, as well as pre-service inspection practices for CASS components and industry precedent successfully used in other applications in the industry.

The length is set such that the aspect ratio ($2c/a$) is 6, resulting in a half-length of 0.75t. As discussed in Section 4.1 of MRP-362, Rev. 1 [13], the value of $2c/a$ of 6 has been successfully used in other applications in the industry. The analysis in MRP-362, Rev. 1 assumes a 25% through-wall (a/t = 0.25) crack with a total length six times the depth as a reasonable bound on any potential manufacturing flaws, consistent with the approach taken in this report. Five (5) cracks are simulated to be randomly located on a single plane in the piping such that cracks cover about 20% of the piping length. As cracks are randomly placed, some may overlap and meet the criteria for coalescence at the start of the simulation.

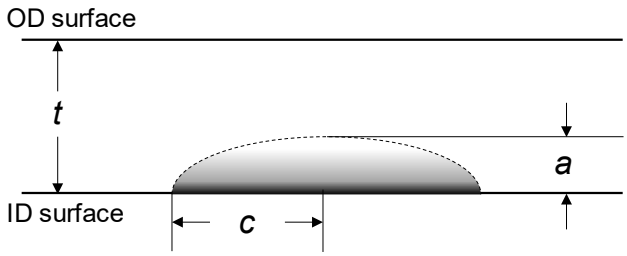

Figure 4-7
Illustration of Axial Surface Crack and Key Dimensions

4.4.2 Circumferential Cracking

As described in Section 3.3, the circumferential cracking PFM analyses evaluate the period of continued operation following acceptance of a detected flaw. Consequently, a crack actively growing via fatigue is assumed to be present at the start of the simulation. Fatigue crack growth for one operating cycle (2 years) is simulated. Cracks are modeled as circumferential, idealized through-wall cracks with a half-length equal to the acceptable size for the crack to remain in service for an additional cycle of operation based on the methodology in Section 3.2. Such a circumferential crack is illustrated in Figure 4-8. For the base cases, an angular half-length (Θ) of 16° is modeled. Exploratory cases evaluating a range of allowable flaw sizes were also performed in determining the appropriate flaw lengths for the base cases.

Because the methodology in Section 3 still relies on the UT length sizing measurement, the uncertainty on length sizing is included as a normal distribution centered on the nominal flaw length. For such a distribution, the root mean square error (RMSE) and standard deviation are equivalent. For the PFM, the RMSE value on the flaw total length ($2c$) is 0.75 inch, which is consistent with the current performance demonstration requirement for UT length sizing in piping welds for wrought austenitic stainless steel and dissimilar metals (Section XI, Mandatory Appendix VIII, Supplement 2 and 10, respectively).

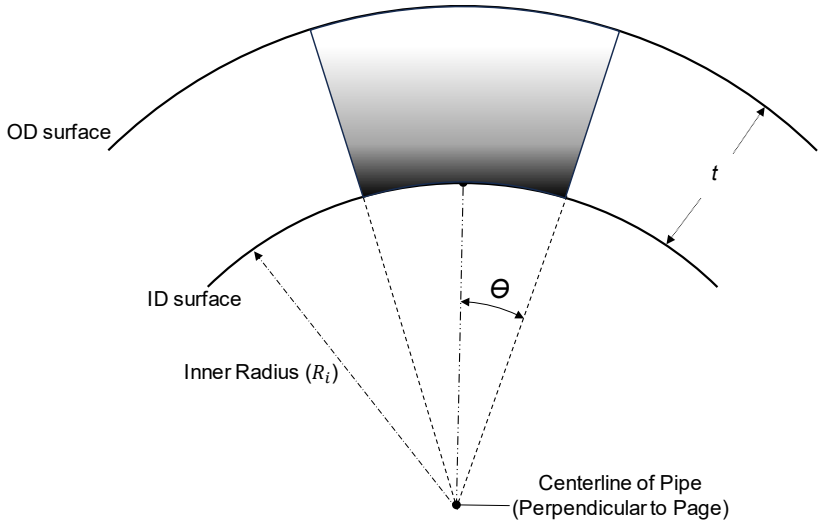

Figure 4-8
Illustration of Idealized Through-Wall Circumferential Crack and Key Dimensions

4.5 Table of Inputs

Inputs that are common across all the base cases are listed in Table 4-1. Table 4-2 lists inputs that are shared between axial and circumferential cracking cases but vary between WEC and CE, while Table 4-3 and Table 4-4 list other inputs for axial and circumferential cases, respectively. Table 4-5 through Table 4-8 list the average frequency of the pressure and temperature transients.

Table 4-1
PIPER-CASS Base Case Inputs (Common to All Base Cases)

Input Name	Value (Notes 1, 2)	Units	Basis
Timestep	1	Month	Convergence study (see Section 6.4.1)
Start Time	0	Year	Start of simulation at beginning of plant operation
Operating Pressure	2,250 (15.5)	psi (MPa)	Representative of U.S. PWRs
Material	CF8M	-	Most susceptible CASS alloy to thermal aging in WEC main loop and CE surge line piping
Yield Strength	Normal distribution μ: 35.52 (244.9) σ: 8.363 (57.66) Min: 16.56 (114.2)	ksi (MPa)	MRP-362, Rev. 1 [13] data at 650°F, aging factor from NUREG/CR-4513, Rev. 2 [3]. Minimum corresponds to 90% of minimum yields strength per ASME Code Section II-D Table Y-1 at 650°F, 2019 Edition
Ultimate Tensile Strength	Normal distribution μ: 86.90 (599.2) σ: 11.39 (78.53) Min: 60.30 (415.8)	ksi (MPa)	MRP-362, Rev. 1 [13] data at 650°F, aging factor from NUREG/CR-4513, Rev. 2 [3]. Minimum corresponds to 90% of minimum ultimate strength per ASME Code Section II-D Table U at 650°F, 1992 Edition
Pearson Correlation Coefficient: Yield and Ultimate Strength	0.7	-	Calibrated to match CF8M material data from MRP-362, Rev. 1 [13]
Pearson Correlation Coefficient: Yield Strength and C_{vsat} Variability	-0.7	-	Calibrated to match CF8M material data from MRP-362, Rev. 1 [13]
Pearson Correlation Coefficient: Ultimate Strength and C_{vsat} Variability	-0.83	-	Calibrated to match CF8M material data from MRP-362, Rev. 1 [13]
Young's Modulus	25,300 (174,000)	ksi (MPa)	ASME Code Section II-D [19]
Specific Heat	0.130 (545.8)	Btu/(lb-R) (J/(kg-K))	ASME Code Section II-D [19]
Density	501 (8030)	lb/ft^3 (kg/m^3)	ASME Code Section II-D [19]
Variability Factor on Charpy Impact Energy	Lognormal distribution Log-μ: 0.6 Log-σ: 0.55 Min: 1.0 Max: 10.0	-	Calculated as discussed in Section 4.2.1
δ-*Fe*	Normal distribution μ: 40% σ: 2%	-	Upper bound based on available material data [3]

Input Name	Value (Notes 1, 2)	Units	Basis
Material Composition Factor (ϕ / δ-*Fe*)	1.78	-	Calculated as discussed in Section 4.2.1
NUREG/CR-4513 Revision for Material Toughness Correlations	2	-	Latest data applicable in the range of δ-*Fe*
Cast Method for Material Toughness Correlations	Static	-	More bounding casting condition with respect to thermal aging
Ramberg-Osgood Exponent (n)	6.6	-	PVP2015-45191, Table 2 [29]
Poisson's Ratio	0.31	-	ASME Code Section II-D [19]
General Crack Growth Rate Scaling Parameter (C_{ss})	Lognormal distribution Log-μ: -0.22314 Log-σ: 0.42	-	xLPR-CGR [30] (Note 3)
Paris Law Exponent	2.25	-	xLPR-CGR [30] and N-809 [31]
Crack Growth ΔK_I Threshold Scaling Factor (C_{Kth})	Lognormal distribution Log-μ: 0 Log-σ: 0.139 Max: 1.517	-	xLPR-CGR [30]
Coefficient of Thermal Expansion	9.8E-06 (1.77E-05)	1/°F (1/°C)	ASME Code Section II-D [19]
Coalescence Proximity Factor	0.5	-	IWA-3330(a) [1]
Rise Time Cap	2,000	Seconds	xLPR-CGR [30]
Operating Cycle Length	2	Year	Bounding cycle length for U.S. PWR

Notes:

1. For the normal distribution, μ and σ are the mean and standard deviation of the distribution, respectively.
2. For the lognormal distribution, log-μ and log-σ are the mean and standard deviation, respectively, of the normal distribution obtained by a log-transform of the lognormal distribution.
3. xLPR alloy factor for CF8M (7.28×10^{-6}) is obtained by inputting a C_{SS} distribution with a median of 0.8, which is multiplied by the coefficient of 9.10×10^{-6} within PIPER-CASS.

Table 4-2
PIPER-CASS Base Case Inputs Common to Axial and Circumferential Cases (Where Base Cases Differ)

Input Name	WEC				CE			
	Value, WEC 1	Value, WEC 2	Units	Basis	Value, CE 1	Value, CE 2	Units	Basis
Pipe Outer Radius	13.75 (349.25)	18.79 (477.4)	inch (mm)	Representative of range of WEC main loop piping geom.	6.375 (161.9)		inch (mm)	Representative of CASS CE surge line piping geometry
Pipe Wall Thickness	2.32 (58.9)	3.09 (78.5)	inch (mm)	Representative of range of WEC main loop piping geom.	1.01 (25.7)	1.312 (33.3)	inch (mm)	Minimum and maximum pipe and weld thickness for CE surge line
Operating Temperature	609 (320.5)		°F (°C)	Representative of U.S. PWR hot legs	653 (345)		°F (°C)	Representative of U.S. PWR surge lines
Service Level A Stability Pressure	2,250 (15.5)		psi (MPa)	Set to normal operating pressure	2,250 (15.5)		psi (MPa)	Set to normal operating pressure
Service Level B Stability Pressure	2,315.4 (15.96)		psi (MPa)	MRP-393 [22]	2,400 (16.54)		psi (MPa)	Representative of range of SL B Pressure of U.S. CE PWR
Service Level C/D Stability Pressure	2,550 (17.58)		psi (MPa)	Representative of range of SL C/D pressure of U.S. WEC PWR	2,576 (17.76)		psi (MPa)	Representative of range of SL C/D pressure of U.S. CE PWR

Table 4-3
PIPER-CASS Axial Cracking Base Case Inputs

Input Name	Value, WEC		Value, CE		Units	Basis
	WEC 1	WEC 2	CE 1	CE 2		
End Time	80				Year	Represents plant operating duration for subsequent license renewal
Cracked Region Length	87.0 (2209)	116 (2943)	37.9 (962)	49.2 (1250)	inch (mm)	Cracks cover 20% of piping
Initial Crack Half-Length (c)	1.74 (44.2)	2.32 (58.9)	0.758 (19.2)	0.984 (25.0)	inch (mm)	Crack with depth of 25% thickness and 2c/a=6
Initial Crack Shape	Semi-elliptical surface crack (SESC)				-	Covers reasonable manufacturing flaws
Initial Crack Aspect Ratio (a/c)	0.3333				-	Covers reasonable manufacturing flaws
Initial Crack Quantity	5				-	Flaws cover 20% of piping
Weld Residual Stress	Orange line in Figure 4-6		Blue line in Figure 4-6		ksi	WEC: xLPR-WRS [21] CE: NP-4690-SR [20]

Table 4-4
PIPER-CASS Circumferential Cracking Base Case Inputs

Input Name	Value, WEC 1	Value, WEC 2	Units	Basis
End Time	2		Year	Representative of a single plant operating cycle
Initial Crack Half-Length	16		°	Base case length chosen per Section 3 to limit acceptable flaw sizes
Initial Crack Half-Length Uncertainty	Normal distribution σ: 0.375 (9.5)		inch (mm)	Equivalent to a length sizing uncertainty of RMSE = 0.375 inch
Initial Crack Quantity	1		-	A single bounding crack is modeled, as described in Section 3.3
Initial Crack Shape	Idealized through-wall (TW) crack		-	A single bounding crack is modeled, as described in Section 3.3
Weld Residual Stress	Solid orange line in Figure 4-5		ksi	xLPR-WRS [21]
Normal Operating Piping Axial Stress	0 (0)	0 (0)	ksi (MPa)	Primary axial pipe forces are generally negligible relative to endcap pressure; this input is superimposed on pressure stress
Normal Operating Bending Stress	0.148 (1.02)	0.117 (0.81)	ksi (MPa)	Allowable bending stress under Service Level A with 1% as primary and 99% as secondary, as described in Section 3.3.
NTE Bending Stress	14.6 (101)	11.6 (80.0)	ksi (MPa)	
Additional Bending Stress for Crack Stability under Service Level A-D	A: 0.0 (0.0) B: 1.22 (8.41) C: 2.73 (18.8) D: 4.48 (30.9)	A: 0.0 (0.0) B: 1.25 (8.62) C: 2.77 (19.1) D: 4.51 (31.1)	ksi (MPa)	Additional stress superimposed on normal operation stresses to reach allowable stresses calculated as described in Section 3.3.

Table 4-5
PIPER-CASS WEC Base Case Transient Listing

Transient Name	Frequency [per year]
Heatup	3.33
Cooldown	3.33
Loading 5	16.67
Unloading 5	16.67
Large Step Decrease	0.33
Loading 15	3.33
Unloading 15	3.33
Trip A	3.83
Trip B	2.67
Trip C	0.17
Primary Side Leak Test	0.166
Secondary Side Leak Test	0.166
OBE (Circumferential only)	0.67

Table 4-6
PIPER-CASS CE Base Case Plant Transient Listing

Transient Name	Frequency [per year]
Heatup	2.38
Cooldown	2.38
Loading	15
Unloading	15
Step Load Increase	6.5
Step Load Decrease	6.5
Reactor Trip	1.917
Leak Test Up	1.93
Leak Test Down	1.93
Loss of Flow	0.01667
Loss of T-G Load	0.1333
Loss of Secondary Pressure	0.08

Table 4-7
PIPER-CASS CE Base Case Heatup/Cooldown Surge Transient Listing

ΔT [°C (°F)]	Plant P & T Condition	Frequency [per year]
178 (320)	Low	0.70
178 (320)	High	0.70
139 (250)	Low	3.57
139 (250)	High	3.57
111 (200)	Low	3.80
111 (200)	High	3.80
83 (150)	Low	4.77
83 (150)	High	4.77
11 (20)	High	836

Table 4-8
PIPER-CASS Base Case FPO Transient Listing (for WEC Circumferential Cracking)[11]

Power Change	Rate of Change	Frequency [per year]
30% to 100% (Loading)	2% per minute	4/year
100% to 30% (Unloading)	2% per minute	4/year
50% to 100% (Loading)	1% per minute	50/year
100% to 50% (Unloading)	1% per minute	50/year
80% to 100% (Loading)	1% per minute	276/year
100% to 80% (Unloading)	1% per minute	276/year

4.6 Base Case Matrix

A separate base case is run for each orientation and each in-scope geometry.

The axial base cases are run with a simulation duration of 80 years, representing flaw growth over 80 years of plant operation since the start of commercial operation. Each base case includes five SESC cracks with 25% depth (a/t) and $2c/a = 6$ ($c = 0.75t$); these cracks cover about 20% of the evaluated pipe length.

The circumferential base cases are run with a simulation duration of 2 years, representing one fuel cycle of continued operation following flaw acceptance. Each base case includes a single

[11] For axial cracking cases, inclusion of this FPO transient set is evaluated by Sensitivity Case I (see Table 4-10).

TW crack with a nominal half-length of 16° centered at the location of maximum bending. As discussed in Section 7.6, circumferential cracking cases are not included for the CE surge line geometry cases because the proposed flaw evaluation methodology is not applicable for these components.

The case designation, geometry, initial crack, short notes, and applicable sensitivity cases (defined in subsequent tables) are shown in Table 4-9. Each of the base cases is evaluated for 9.6×10^6 realizations. Refer to the Section 6.4.2 and Section 7.4 for discussion on statistical convergence of results.

Table 4-9
PIPER-CASS Base Case Matrix

Component	Geometry	Crack Orientation	Case	Applicable Sensitivity Cases
CE Surge Line Piping	CE 1	Axial	CE_AX_1	A, B, C, D, G, H, I, J, K, L, M, t1, t2, t3
	CE 2	Axial	CE_AX_2	A, B, C, D, H, I, J, K, L, M
WEC Main Loop Piping	WEC 1	Axial	WEC_AX_1	A, B, C, D, E, F, G, H, I, K, L, N, O
		Circumferential	WEC_CIRC_1	A, B, C, E, F, G, H, L, P, Q, R, S, t1, t2, t3
	WEC 2	Axial	WEC_AX_2	A, B, C, D, E, F, G, H, I, K, L
		Circumferential	WEC_CIRC_2	A, B, C, E, F, G, H, L, P, Q, R, S

4.7 Sensitivity Cases

Numerous sensitivity cases are implemented to determine the overall impact of various inputs. Table 4-10 describes each sensitivity case and shows the specific inputs changed in each case. Unless otherwise specified, sensitivity case runs are performed for 1.92×10^6 realizations.

4.7.1 Crack Growth Rate Sensitivities

Sensitivity Cases A and B investigated two differences between the PIPER-CASS base case inputs (identical to the crack growth rate in xLPR [30]) and ASME Code Case N-809 [31]. Sensitivity Case A removes the alloy-specific factor of 0.8 for CF8M versus CF8 FCG included in the xLPR model. This factor of 0.8 was not applied in ASME Code Case N-809 as a conservative simplification [17].

Sensitivity Case B considers the effect of including only the upper half of the distribution of FCG variability. N-809 is intended for deterministic crack growth calculation and therefore does not include any term for random variability. However, N-809 crack growth curves represent median values, so the second sensitivity addresses the impact of weighting the random variability of crack growth to the upper 50^{th} percentile of sampled values. The result is that most cracks

modeled in this sensitivity will have crack growth rates which exceed the N-809 crack growth rates. The input changes in Sensitivity Cases A and B both result in a modest increase in crack growth rates.

4.7.2 WRS Sensitivities

Sensitivity Cases C and D examine the impact of WRS by increasing and decreasing its severity, respectively. For the WEC geometry Sensitivity Case C, a 50% weld repair profile is applied. While repaired welds are beyond the scope of this analysis, a weld repair WRS profile is a more appropriate input for this sensitivity case. For the CE geometry, the magnitude of the constant stress is increased by 50%, which is appropriate for the constant through-wall WRS profile. Sensitivity Case D sets WRS to a constant zero stress through the thickness, representing a location in piping away from a weld.

For circumferential cases, the WRS sensitivity is applied with a part-through-wall initial crack. This is because the depth-averaged WRS acting on a through-wall crack is effectively zero since the net forces across the cross-section balance to zero.

4.7.3 Transient Sensitivities

The WEC base case uses the pressure and temperature histories of Heatup and Cooldown transients in MRP-393 [22], which follow a "best estimate" of actual operating practices (up to about 40°F/hr or -70°F/hr). Sensitivity Case E instead applies bounding Heatup and Cooldown transients with a continuous thermal ramp rate at the Technical Specification limit of 100°F/hr with a corresponding pressure history.[12]

Similarly, base cases use the best estimate frequency of transient occurrences, so Sensitivity Case F increases the quantity of these transients to design basis values to identify the effect of additional transient cycles.

The impact of starting flexible power operation (FPO) during the plant service life is assessed in Sensitivity Cases H and I. These transients apply FPO transients described in Section 4.3.2.1 at the frequency listed in Table 4-8, with different power ramp rates for the 100%-80% power unloading and 80%-100% power loading transients: either 1% per minute (20 minute transient) or 0.5% per minute (40 minute transient). The circumferential WEC base cases include the FPO transients as defined in axial Sensitivity I. The onset of FPO is assumed to occur after 60 years for the CE surge line cases, considering the significant extent of simulated fatigue crack growth with the insurge and outsurge events conservatively assumed to occur with each power shift.

[12] CE base cases already include heatup and cooldown at Technical Specification limits, so Sensitivity E is not evaluated for CE.

Transients for the CE cases are based on pressurizer design specification for a specific plant with a CASS surge line. Theis design specification includes a pair of "normal variations" transients, which, as discussed in Section 4.3, are not realistic for this analysis. Sensitivity Case J assumes a more realistic estimate of normal pressure variations. Sensitivity Case M considers the effect of increasing the minimum flow rate applied to the surge event transients in Table 4-7 from 0.3 m/s to 0.5 m/s, thereby increasing the heating rate and the RGTS.

4.7.4 Initial Crack Size Sensitivities

Sensitivity Cases G and N investigates the impact of initial crack depth on rupture probability, and Sensitivity Cases K and P investigates the impact of initial cracked length in the piping.

4.7.4.1 CE Axial Sensitivities

For CE, Sensitivity Case G modifies the depth of initial cracks to match a distribution of manufacturing flaws reported for large-bore CASS elbows when crediting radiographic examination (see Section 4.4). The distribution is shifted to result in an initial crack depth of 15% through-wall (a/t = 0.15) at the 99th percentile. The sampled crack depth is combined with a constant 6:1 aspect ratio ($2c/a$) to produce a variable crack length. The resultant distribution of crack depths in CE Sensitivity Case G is shown in Figure 4-9.

Sensitivity Case K investigates the impact of the initial cracked length of the piping by increasing the number of initial cracks from five (5) to eight (8).

4.7.4.2 WEC Axial Sensitivities

Especially large initial cracks are assumed for the WEC sensitivity cases given the relatively small fatigue crack growth rates and large wall thicknesses for the main loop piping.

Sensitivity Case K for WEC cases uses a single part-through-wall crack that is so long that its growth rate and stability are similar to those for an infinitely long crack of the same depth. The crack length is set to approximately 8 times the 0.01 percentile of critical through-wall crack size (i.e., 2c = at least 84 inches (2.1 m)). The depth of this crack is also increased to 33% through-wall (a/t = 0.33).

Sensitivity Case G in WEC cases further increases the depth of this very long initial crack to 50% through-wall (a/t = 0.5), to show that PIPER-CASS would predict ruptures in a scenario with an extremely severe initial crack.

Sensitivity Case N models a single idealized through-wall crack with a half-length equal to that of a single initial crack from the base case (i.e., 0.75t). This case investigates how the probability of rupture is impacted by conservative initial crack assumptions.

4.7.4.3 WEC Circumferential Sensitivities

Sensitivity Case G for WEC circumferential cracking considers an initial semi-elliptical surface crack with 50% depth (a/t) instead of the through-wall crack of the base case. Idealized though-

wall cracks are modeled to not propagate due to stresses that balance radially through-wall, such as WRS and RGTS. This sensitivity demonstrates that the assumption of an initial through-wall crack is limiting versus a part-through-wall crack.

Sensitivity Case P for WEC circumferential cracking assesses the uncertainty on crack length. The MRP-424 [32] proposes text for Section XI, Mandatory Appendix VIII, Supplement 9 that includes an RMSE of 1.0 inch for length sizing of circumferential flaws in CASS piping, which is applied for this sensitivity.

4.7.5 Material Sensitivity

Sensitivity Case L represents unaged CASS material, with higher toughness and lower strength than the base case of fully aged CASS material. Sensitivity L is evaluated because these trends have competing effects on crack stability (i.e., higher toughness increases EPFM stability and lower strength decreases EPFM and NSC stability.

Eleven (11) strength data for different heats of unaged CF8M material tested at elevated temperature (550°F to 650°F (288°C to 343°C)) were identified: four from EPRI 1019128 Table B-4 [6] and seven from NUREG/CR-4513 Rev. 2 Table B-1 [3]. The other 20 apparent data in EPRI 1019128 (from heats C-####-#) are room temperature data scaled to 650°F (343°C) assuming the temperature derating factor implied by the tensile strength values in ASME Code, Section II-D. Furthermore, nine of these heat C-####-# strength data appear to be the same mechanical test repeated for two chemical checks listed in a certified material test report (CMTR).

The average and standard deviation of these 11 data are applied; the distributions are truncated to sample no lower than the 1st percentile of the distribution, which results in a minimum at 90% of the Section II-D minimum for yield strength and at 82% for ultimate strength. The observed correlation between yield and ultimate strengths is similar to the base case, so the input is not changed.

The median C_v for unaged at-temperature CF8M data (without duplicates) in NUREG/CR-4513 Rev. 2 Table B-1 [3] is 250 J/cm^2, ranging from about 165 to 365 J/cm^2. Therefore, the material toughness inputs were chosen to result in a median of approximately 200 J/cm^2 for C_v, somewhat below the observed median, with values ranging from about 100 J/cm^2 to 460 J/cm^2. A correlation coefficient was not fit and imposed between strength and C_v. This conservative choice is appropriate considering that C_v data are only available for five (5) heats also with strength data.

4.7.6 Circumferential Material and Loading Sensitivities

Whereas the bounding material state is relatively clear for the PFM approach utilized for evaluation of axial cracking, the approach of Section 3 for circumferential cracking justifies additional sensitivities. These sensitivities assess material inputs with higher toughness than the

base case but where the Z-factor may be lower, resulting in higher allowable stresses for application in the PFM.

Sensitivity Case Q lowers the mean of the δ-ferrite distribution to 25% and applies the lower Z-factor per C-6330(a) of Section XI, 2019 Edition [1] for CF8M with 14% to 25% δ-ferrite when calculating the allowable stresses.

Sensitivity Case R for circumferential cracking was considered using inputs appropriate for aged CF8, which has a reduced aging effect relative to CF8M, leading to higher toughness and lower strength. For a given flaw size, the allowable loads are also greater for CF8 because of the lower Z-factor per C-6330(a) relative to CF8M with δ-*Fe* of 40%. In this sensitivity case, the strength inputs are based off those for unaged CF8M, scaled down by the ratio of values for CF8 versus CF8M in Section II-D; the aging factor is set to be the saturation limit in NUREG/CR-4513, Rev. 2 [3] for CF3, which is slightly less than CF8. The toughness parameters are given by the CF8 relations in NUREG/CR-4513, Rev. 2, with the same added variability in $C_{v,sat}$ as for the CF8M base case. Other parameters are also updated to be applicable to values for CF8.

As a final sensitivity, a case was considered with the base case material but with increased piping axial forces. Sensitivity Case S adds a membrane stress equal (+10% of the normal pressure stresses for Service Levels A, B, and C and +100% for Service Level D).

4.7.7 Temporal Convergence Sensitivities

Three Sensitivity Cases, t1, t2, and t3, demonstrate the temporal convergence of PIPER-CASS. By completing the same analysis with three different timesteps, the timestep selection used in base cases can be verified as appropriate. To perform the detailed comparison of outputs, the number of realizations is reduced, and more comprehensive output options are enabled.

4.7.8 Targeted Final Size Sensitivity

Sensitivity Case O utilizes a special mode of PIPER-CASS to model the distribution of crack sizes at plant startup that could yield a critical crack by the end of plant operation. In this case, all realizations start with an idealized through-wall crack at the minimum critical through-wall crack length for the full range of material properties sampled across all realizations and all Service Level stability loadings. The crack is then grown smaller (backwards in time) for the period of assumed plant operation.

Table 4-10
Description of Sensitivity Cases and Modified Inputs

Sensitivity Case	Description	Applicability	Parameter	Base Case Value	Sensitivity Case Value
A	Remove factor of 0.8 on growth	CE Axial, WEC Axial, WEC Circ.	C_{ss}	Lognormal distribution Log-μ: -0.22314 Log-σ: 0.42	Lognormal distribution **Log-μ: 0.0** Log-σ: 0.42
B	Only include upper 50th percentile of C_{ss} distribution	CE Axial, WEC Axial, WEC Circ.	C_{ss}	Lognormal distribution Log-μ: -0.22314 Log-σ: 0.42	Lognormal distribution Log-μ: -0.22314 Log-σ: 0.42 **Min: 0.799**
C	Elevated WRS	CE Axial, WEC Axial	WRS_{Hoop}	Solid Lines in Figure 4-6	Dashed lines in Figure 4-6
		WEC Circ.	Initial Crack	TW Crack	SESC with 50% depth (a/t)
			WRS_{Axial}	Solid Line in Figure 4-5	Dashed Line in Figure 4-5
D	Remove WRS	CE Axial, WEC Axial	WRS_{Hoop}	Figure 4-6	0 ksi (0 MPa) constant
E	Increase rate of Heatup and Cooldown transient to 100°F/hr and disable rise time limit	WEC Axial, WEC Circ.	Heatup and Cooldown P and T History	MRP-393 Figures 2-1 and 2-2	100°F/hr ramp rate
			Rise time cap	2,000 sec	Infinite (no cap)
F	Apply transients at design basis frequency	WEC Axial, WEC Circ.	Heatup	3.33/year	5/year
			Cooldown	3.33/year	5/year
			Loading by 5%	16.67/year	170/year
			Unloading by 5%	16.67/year	170/year
			Large Step Decrease	0.33/year	1/year
			Loading by 15%	3.33/year	12.5/year
			Unloading by 15%	3.33/year	12.5/year
			Trip A	3.83/year	5/year
			Trip B	2.67/year	4/year
			Trip C	0.17/year	0.5/year
			Primary side leak test	0.166/year	0.6667/year

Sensitivity Case	Description	Applicability	Parameter	Base Case Value	Sensitivity Case Value
			Secondary side leak test	0.166/year	0.6667/year
G	Variation of Initial Crack Depth	WEC Axial	Initial Crack Aspect Ratio (a/c)	0.3333	WEC 1 geometry: 0.0276 WEC 2 geometry: 0.0309 (Initial crack depth of 50% through-wall)
			Number of Cracks	5	1
			Initial Crack Half-Length (c)	WEC 1: 1.74 inch (44.2 mm) WEC 2: 2.32 inch (58.9 mm)	WEC 1: 42 inch (1067 mm) WEC 2: 50 inch (1270 mm)
		CE 1 Axial	Initial Crack Half-length (c)	0.7575 inch	Lognormal distribution Log-μ: -1.4106 Log-σ: 0.2674 Max: 3.0
		WEC Circ.	Initial Crack	TW Crack	SESC with 50% depth (a/t)
H	Use of flexible power operations (begins part-way through operation for CE)	CE Axial, WEC Axial, WEC Circ.	FPO transient Frequency	Axial: None Circ.: Table 4-8	Table 4-8
			Ramp Rate for 80-100% and 100-80% Transients	Axial: None Circ.: 1%/min	0.5%/min
			For CE axial, time at which base case Loading and Unloading halt and FPO transients begin	Only base load transients used in CE Axial base cases	60 years (0 years for WEC)
I	Additional flexible power operations, with 1%/minute power ramp for 80%-100% and 100%-80% loading	CE Axial, WEC Axial (Equiv. to WEC Circ. base case)	FPO transient Frequency	None	Table 4-8
			Ramp Rate for 80-100% and 100-80% Transients	None	1.0%/min
			For CE axial, time at which base case Loading and Unloading halt and FPO transients begin	Only base load transients used in CE Axial base cases	60 years (0 years for WEC)

Sensitivity Case	Description	Applicability	Parameter	Base Case Value	Sensitivity Case Value
J	Apply normal variations in pressure and temperature with a reasonable magnitude	CE Axial	Transient Normal Variations – Pressure	None	15 psi (0.1 MPa) pressure spike occurring over 2 minute duration occurring 16,667 times per year
			Transient Normal Variations – Temperature	None	6°F (3.3°C) temperature spike occurring over 2 minute duration occurring 16,667 times per year
K	Increased initial length of cracking	CE Axial	Number of Cracks	5	8
		WEC Axial	Number of Cracks	5	1
			Initial Crack Half-Length (*c*)	WEC 1: 1.74 inch (44.2 mm) WEC 2: 2.32 inch (58.9 mm)	WEC 1: 42 inch (1067 mm) WEC 2: 50 inch (1270 mm)
			Initial Crack Aspect Ratio (*a*/*c*)	0.3333	WEC 1: 0.0184 WEC 2: 0.0206 (Initial crack depth of 33% through-wall)
L	Unaged material	CE Axial, WEC Axial, WEC Circ.	Yield strength	Normal distribution μ: 35.52 (244.9) σ: 8.363 (57.66) Min: 16.56 (114.2) Units: ksi (MPa)	Normal distribution μ: 24.7 (170) σ: 3.47 (23.9) Min: 16.6 (115) Units: ksi (MPa)
			Ultimate tensile strength	Normal distribution μ: 86.90 (599.2) σ: 11.39 (78.53) Min: 60.30 (415.8) Units: ksi (MPa)	Normal distribution μ: 64.5 (445) σ: 3.98 (27.4) Min: 55.3 (381) Units: ksi (MPa)
			Variability Factor on Charpy Impact Energy	Lognormal distribution Log-μ: 0.6 Log-σ: 0.55 Min: 1.0 Max: 10.0	Normal distribution μ: 1.0 σ: 0.3 Min: 0.5 Max: 3.0

Sensitivity Case	Description	Applicability	Parameter	Base Case Value	Sensitivity Case Value
			δ-*Fe*	Normal distribution μ: 40% σ: 2%	3.0%
			Pearson correlation coefficient: yield strength and C_{vsat} variability	-0.7	0.0
			Pearson correlation coefficient: ultimate strength and C_{vsat} variability	-0.83	0.0
M	Surge event flow rate	CE Axial	Flow Rate for: △250°F High △250°F Low △200°F High △200°F Low △20°F High	0.03 m/s	0.05 m/s
N	Initial TW crack, half-length (*c*) of 0.75*t*	WEC 1 Axial	Number of Cracks	5	1
			Initial Crack Type	SESC	TW
O	Targeted final through-wall crack size	WEC 1 Axial	Number of Cracks	5	1
			Initial Crack Type	SESC	TW
			Initial Crack Half-Length (c)	1.739 inch	Equal to half-length of smallest critical crack in run
			Direction of Time	Forward (Cracks grow bigger)	Backward (Cracks grow smaller)
P	Increase length sizing RMSE	WEC Circ.	Initial Crack Half-Length Uncertainty	Normal distribution σ: 0.375 inch	Normal distribution σ: 0.50 inch
Q	CF8 Material	WEC Circ.	Material	CF8M	CF8
			Yield strength	Normal distr. μ: 35.52 (244.9) σ: 8.363 (57.66) Min: 16.6 (114.2) Units: ksi (MPa)	Normal distr. μ: 25.41 (175.2) σ: 3.64 (25.1) Min: 17.01 (117.3) Units: ksi (MPa)

Sensitivity Case	Description	Applicability	Parameter	Base Case Value	Sensitivity Case Value
			Ultimate tensile strength	Normal distr. μ: 86.90 (599.2) σ: 11.39 (78.53) Min: 60.3 (415.8) Units: ksi (MPa)	Normal distr. μ: 61.56 (424.4) σ: 4.30 (29.6) Min: 52.60 (362.6) Units: ksi (MPa)
			Pearson correlation coefficient: yield and ultimate strength	0.7	0
			Pearson correlation coefficient: yield strength and C_{vsat} variability	-0.7	0
			Pearson correlation coefficient: ultimate strength and C_{vsat} variability	-0.83	0
			Specific heat	545.8 J/(kg-K)	547.1 J/(kg-K)
			Variability Factor on Charpy Impact Energy	Lognormal distr. Log-μ: 0.6 Log-σ: 0.55 Min: 1.0 Max: 10.0	Normal distribution μ: 1.0 σ: 0.3 Min: 0.5 Max: 3.0
			Material Composition Factor (ϕ / δ-Fe)	1.78	1.6
			Ramberg-Osgood Coefficient (α)	Per MRP-362R1 [13]	Per xLPR-SRD-FW [33]
			Ramberg-Osgood Exponent (n)	6.6	7.1
			General crack growth rate scaling parameter (C_{ss})	Lognormal distr. Log-μ: -0.22314 Log-σ: 0.42	Lognormal distr. Log-μ: 0.0 Log-σ: 0.42
			Normal Operating Bending Stress, NTE Bending Stress, and Additional Bending Stress for Crack Stability under Service Level A-D	Set to maximum allowable stresses using Z-factor in Category 2 of Table C-6330-1 (per Section XI C-6330(a))	Set to maximum allowable stresses using Z-factor per equations in Section XI C-6330(a)

Sensitivity Case	Description	Applicability	Parameter	Base Case Value	Sensitivity Case Value
R	25% δ-ferrite	WEC Circ.	δ-*Fe*	Normal distribution μ: 40% σ: 2%	Normal distribution μ: 25% σ: 2%
			Normal Operating Bending Stress, NTE Bending Stress, and Additional Bending Stress for Crack Stability under Service Level A-D	Set to maximum allowable stresses using Z-factor in Category 2 of Table C-6330-1 (per Section XI C-6330(a))	Set to maximum allowable stresses using Z-factor per equations in Section XI C-6330(a)
S	Increased membrane stress	WEC Circ.	Normal Operating Piping Axial Stress	0.0	10% of endcap stress from normal pressure
			Additional Bending Stress for Crack Stability under Service Level D	0.0	90% of endcap stress from normal pressure
			Normal Operating Bending Stress, NTE Bending Stress, and Additional Bending Stress for Crack Stability under Service Level A-D	Set to maximum allowable stresses	Set to updated maximum allowable stresses
t1	Temporal convergence, 5 day timestep	CE Axial, WEC Circ.	Timestep	1 month	5 days
			Number of Realizations	1.92×10^6	10^4
t2	Temporal convergence, 25 day timestep	CE Axial, WEC Circ.	Timestep	1 month	25 days
			Number of Realizations	1.92×10^6	10^4
t3	Temporal convergence, 50 day timestep	CE Axial, WEC Circ.	Timestep	1 month	50 days
			Number of Realizations	1.92×10^6	10^4

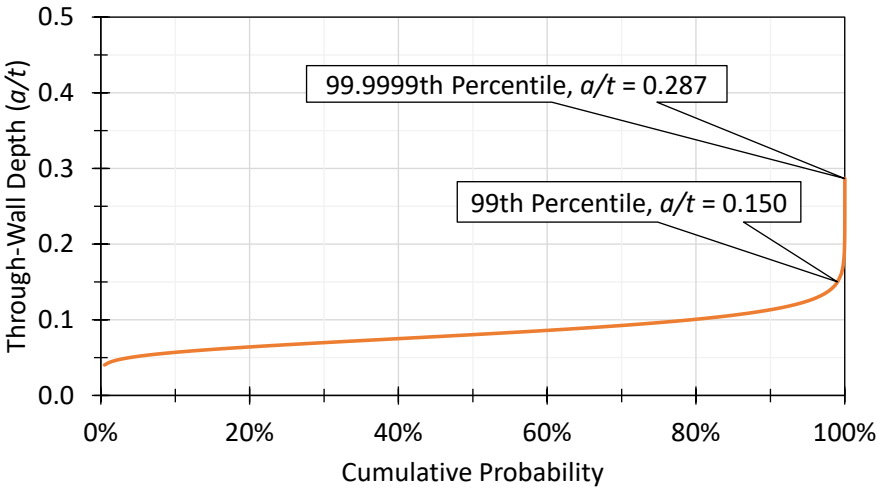

Figure 4-9
Crack Depth Distribution in Sensitivity Case G

5 ACCEPTANCE CRITERIA

For cases with axially oriented cracking, the same acceptance criteria as in MRP-362, Rev. 1 [13] are applied to the calculated cumulative probability of a rupture for an individual weld location over 80 years without assuming the benefit of any examinations or leak detection. For cases with axially oriented cracking, these same acceptance criteria are applied to the calculated cumulative probability of a rupture for an individual weld location over a 2-year operating cycle. These acceptance criteria, shown in Table 5-1, are applicable to a single weld location. Separate acceptance criteria are applied for the probability of rupture under the separate loadings for Service Levels A, B, C, and D. As explained in Section 3.1 of MRP-362, Rev. 1, the acceptance criteria in Table 5-1 are conditional probabilities that reflect the allowable rupture probability given that an event of that Service Level occurs. Multiplying the conditional rupture probability for a given Service Level and the corresponding probability of occurrence results in an overall marginal probability of failure (rupture) of 10^{-6} or lower. MRP-362, Rev. 1 recommended the allowable conditional failure probabilities in Table 5-1 on the basis of an assessment of the failure probabilities implied by the tables in Nonmandatory Appendix C of Section XI for allowable circumferential flaw size by Service Level for the case of limit load failure given the statistical distribution for material flow strength.[13] Hence, this approach ensures a rupture risk comparable or below that implied for ASME Code Section XI for acceptance of flaws when material behavior is fully ductile and fracture toughness is not limiting. MRP-362, Rev. 1 provides the technical basis for ASME Code Case N-838 [14], which has been found conditionally acceptable by the NRC provided that Code Case N-838 is not used to evaluate flaws in CASS piping with δ-*Fe* content exceeding 25%. The leakage cumulative probability was also assessed using PIPER-CASS as a secondary parameter.

PIPER-CASS calculates the stability of each realization under exposure to specific Service Level loadings and reports the fraction of realizations that rupture over time.[14] Consequently, the results from PIPER-CASS are cumulative conditional probabilities that assume occurrence of the loading corresponding to each Service Level. As an example, a Service Level D transient expected to happen once in 100 operating years (10^{-2}/year) with a result of 10^{-4} cumulative rupture probability represents approximately the same risk ($10^{-2}\times10^{-4}=10^{-6}$) as a Service Level A transient expected to occur once or more per year with a result of 10^{-6} cumulative rupture probability.[15] The frequency of occurrence of each transient is not reflected in the reported

[13] These risk results were obtained for the rules for evaluating circumferentially oriented flaws in Article C-5000 of Section XI, Nonmandatory Appendix C. These results show the risk inherent in leaving a circumferential flaw in service in fully ductile material. They provide a reference risk level for an individual piping weld that can be applied regardless of flaw orientation or failure mode.

[14] xLPR results are instead reported as the marginal probability of rupture, in which a rupture only occurs if the transient is modeled to occur during that timestep [34].

[15] Because the probability of occurrence can never be greater than 1.0, transients that occur more than once per year do not increase the marginal probability of rupture above the conditional probability of rupture.

cumulative probability of rupture, and instead separate acceptance criteria are applied for each Service Level.

Table 5-1
PIPER-CASS Acceptance Criteria (Same as Recommended by MRP-362 R1 [13])

Service Level	Probability of Occurrence	Conditional Rupture Probability
A	1.0	10^{-6}
B	0.1	10^{-5}
C	$< 10^{-2}$	10^{-4}
D	$< 10^{-2}$	10^{-4}

6 AXIAL CRACKING RESULTS AND DISCUSSION

6.1 Axial Cracking Base Case Results

The base cases, one for each of the four geometries, are described in Section 4.6 with case numbering nomenclature defined in Table 4-9. The acceptance criteria are based on the allowable rupture probability, as discussed in Section 5. Rupture probability results from PIPER-CASS are the cumulative conditional probability of rupture after an 80 year service life given the occurrence of the transient generating the limiting loading for that Service Level.

Results for the base cases are shown for each Service Level in Table 6-1. Without crediting periodic nondestructive examinations, the rupture and leakage frequencies are expected to increase with time. Only the CE 2 base case experiences ruptures or leakage in any realization, and these were permissible by the acceptance criteria. No other base case experiences any ruptures or leakage (no part-through-wall crack grows to be through-wall).

The random initial crack placement of the five part-through-wall cracks results in about 61% of all realizations having at least one pair of semi-elliptical cracks that coalesce at the start of the simulation. Coalescence at the beginning of the run results in a longer initial crack that tends to grow more quickly than the individual cracks. Additional details on the relative amounts of crack growth in each case is provided in Figure 6-1, which characterizes the amount of growth through the wall thickness averaged across the set of postulated cracks. Informed by further details in Section 6.2.2, the competing factors that drive crack growth in this PFM simulation can be assessed. The larger radius to thickness ratio[16] in the WEC 2 geometry results in higher pressure stresses versus the WEC 1 geometry, which result in increased growth rates. Conversely, the larger thickness of the WEC 2 geometry results in increased distance to grow through-wall. The higher pressure stresses of the WEC 2 geometry increase the growth rate to a greater degree than the larger thickness of WEC 2 increases the time needed to grow through-wall. Similarly, the thicker wall of the CE 2 geometry increases the RGTS such that the relative growth through the wall thickness increases by a factor that outweighs the effect of the relative increase in wall thickness versus the CE 1 geometry.

[16] WEC 2 geometry has a higher R_i/t ratio than WEC 1, and CE 1 geometry has a higher R_i/t ratio than CE 2.

Table 6-1
Base Case Cumulative Probabilities of Occurrence over 80 Years

Case Name	Service Levels with Ruptures	Cumulative Probability of Rupture			Leakage
		Service Level A	Service Level B	Service Level C/D	
WEC_AX_1	None	< 1E-7	< 1E-7	< 1E-7	< 1E-7
WEC_AX_2	None	< 1E-7	< 1E-7	< 1E-7	< 1E-7
CE_AX_1	None	< 1E-7	< 1E-7	< 1E-7	< 1E-7
CE_AX_2	None	< 1E-7	1.0E-7	1.0E-7	2.1E-7

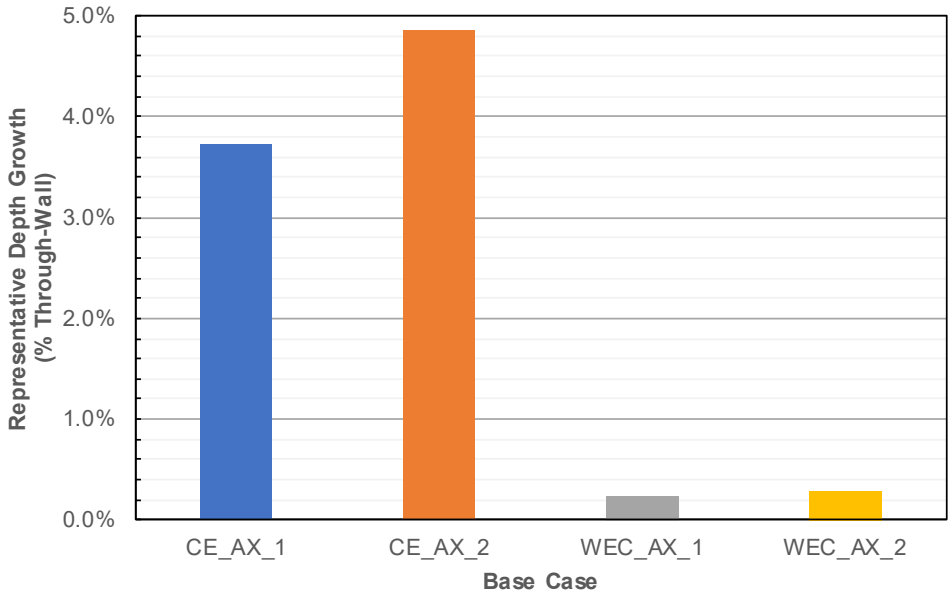

Figure 6-1
SESC Depth Growth Representative of Each Base Case

6.2 Input and Transient Importance

6.2.1 Inputs Contributing to Through-Wall Crack Critical Half-Length

Several sampled parameters are compared to the critical through-wall crack size of each realization to determine the correlation between the sampled parameter and the critical crack size. This correlation is shown in Figure 6-2 for WEC_AX_1 and Figure 6-3 for CE_AX_1. Brighter color points show multiple realizations resulting in the same set of values, whereas darker points are shown for values only occurring in individual or very few realizations. Note that these figures depict the correlation at Service Level A. Due to the modest difference in loading across all Service Levels and the stringent acceptance criteria for Service Level A, this Service Level is

the bounding condition, so it is the focus of this section. However, the trends discussed in this section hold for Service Levels B, C, and D.

The toughness coefficient, C_r, shows a strong positive correlation with the critical crack size. This is expected given the formulation of the J_R resistance curve, $J_R = C_r \Delta a^m$, and because EPFM stability (toughness focused) is generally limiting to NSC stability (strength focused) for the input material properties. A weaker negative correlation can be seen in the three strength parameters. The negative correlation between strength and critical crack size, while non-intuitive at face value, is due to the negative correlation coefficient applied between toughness and the strength parameters when sampling material properties. Both yield and ultimate strength are negatively correlated to Charpy-impact toughness variability factor to more closely match the material properties in PIPER-CASS to the known CASS material properties. The strength and toughness correlations, taken together, suggest that the critical though-wall crack size is controlled by toughness parameters over strength parameters.

There is almost no correlation between δ-*Fe* content and the critical crack size despite the well-defined relationship between the δ-*Fe* content and the severity of reduction in toughness with thermal aging. This is an effect of the small variability in δ-*Fe* compared to the larger variability factor applied on C_{vsat}.[17] If the variability on C_{vsat} were removed or if a wider range of δ-*Fe* were considered, a clear correlation between δ-*Fe* content and critical crack size is apparent. In other words, the variability factor on C_{vsat} masks the negative correlation of δ-*Fe* content to critical crack size for the current input set.

Finally, there is a slight positive correlation between the critical crack size and the α parameter of the Ramberg-Osgood equation. The observed positive correlation is due to the α parameter being calculated as a function of the inverse of the material strength and being proportionate to the plastic applied J-integral. Additional asymmetry in the point locus for the α parameter is caused by the truncation of the yield strength to a lower limit of 32 ksi (221 MPa) when calculating the α parameter to prevent physically invalid values.

[17] The 90th percentile of the distribution is 2.0 times the median for C_{vsat} whereas it is about 1.06 times the median for δ-*Fe*.

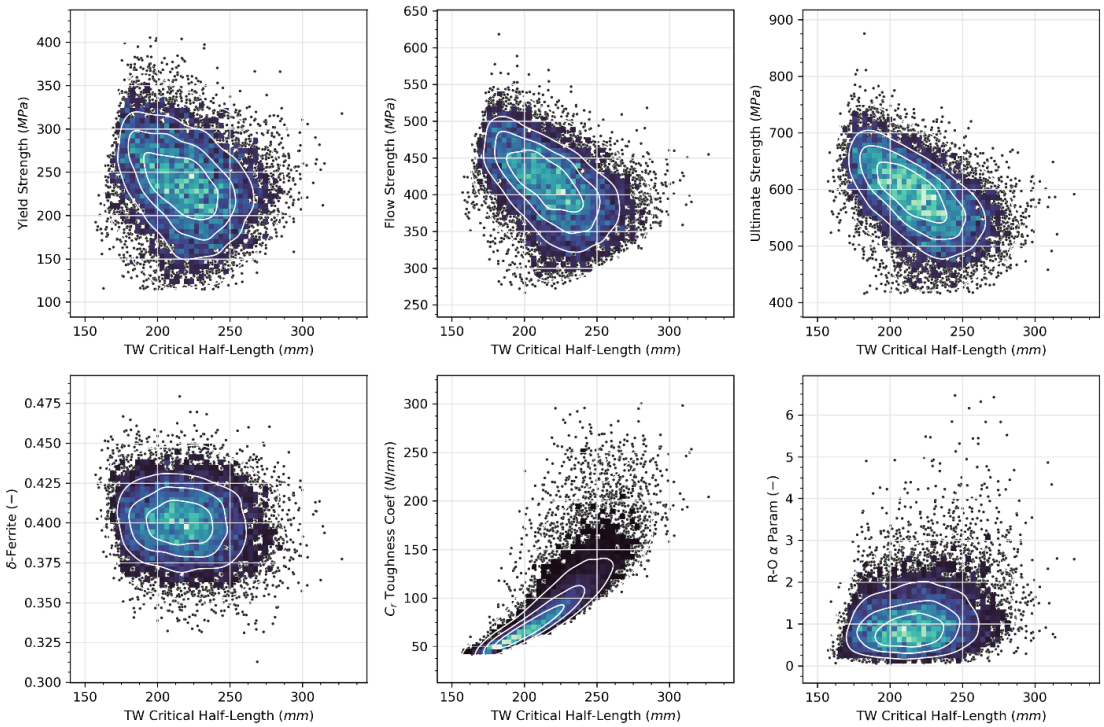

Figure 6-2
Impact of Sampled Values on Critical Crack Length at Service Level A for Case WEC_AX_1

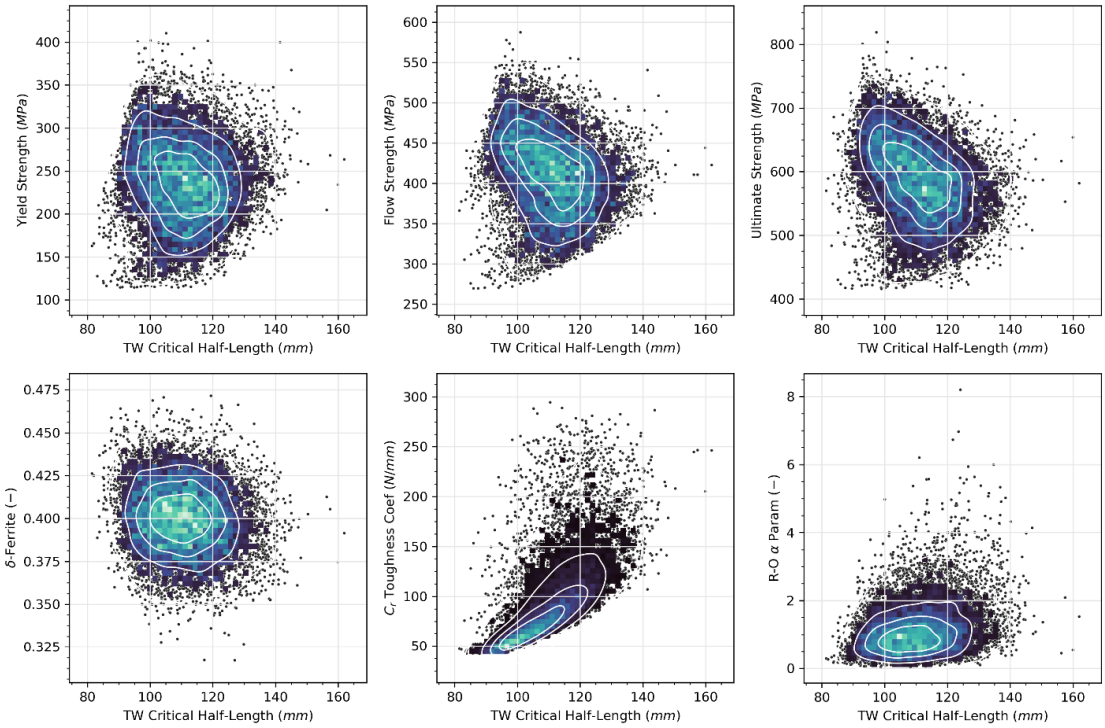

Figure 6-3
Impact of Sampled Values on Critical Crack Length at Service Level A for Case CE_AX_1

6.2.2 Transient Contribution to Growth

As discussed in Section 4.3, each of the base case runs includes multiple transients that drive fatigue crack growth in the execution of PIPER-CASS. Figure 6-4 and Figure 6-5 show the relative contribution of each transient to growth for cracks in the length and depth directions. The relative contribution of the transients to crack growth is similar between WEC 1 and WEC 2 as well as between CE 1 and CE 2, so only one case is shown for each component type. Any transients not shown in these figures are minor contributors to crack growth and are lumped into "Other." Some transients do not contribute to crack growth because stresses are always compressive ($K_{I,max} < 0$), the stress rate never exceeds the rise time threshold (1 ksi/hr (6.9 MPa/hr)), or ΔK_I is always below the threshold for growth ($\Delta K_{I,th}$).

For the WEC base case (Figure 6-4), Trip A, Trip B, Heatup, and Cooldown contribute approximately equally to and dominate growth both in the depth direction and in the length direction. These transients are most severe due to the elevated RGTS at the ID during reactor trip transients and the large rise times and pressure change during heatup and cooldown.

For the CE base case (Figure 6-5), the greatest contribution to the part-through-wall crack growth (both depth-wise and length-wise, respectively) is due to the surge transients representing insurge and outsurge events during heatup, cooldown, and hot standby. The various loading and unloading transients, which also include insurge and outsurge events, drive a further third of the growth.

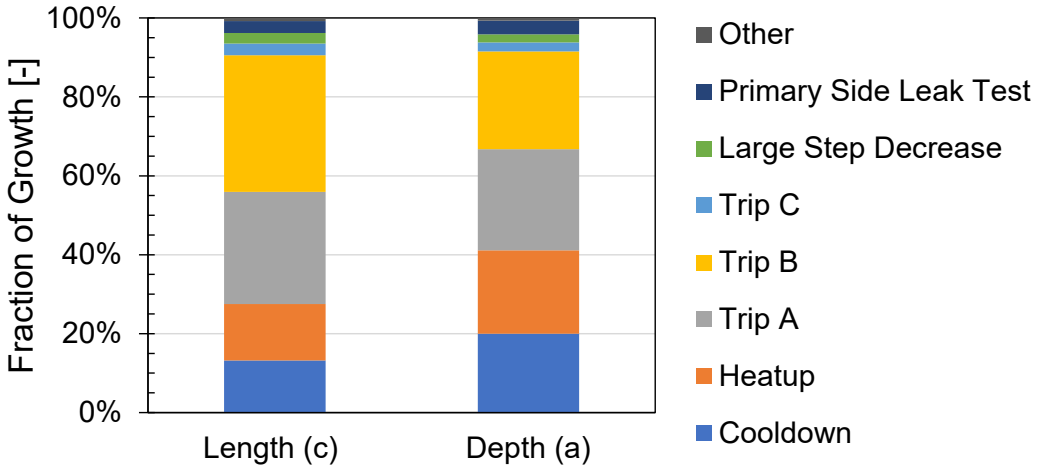

Figure 6-4
Fraction of Growth by Transient for Axial Part-Through-Wall Cracks in Case WEC_AX_1

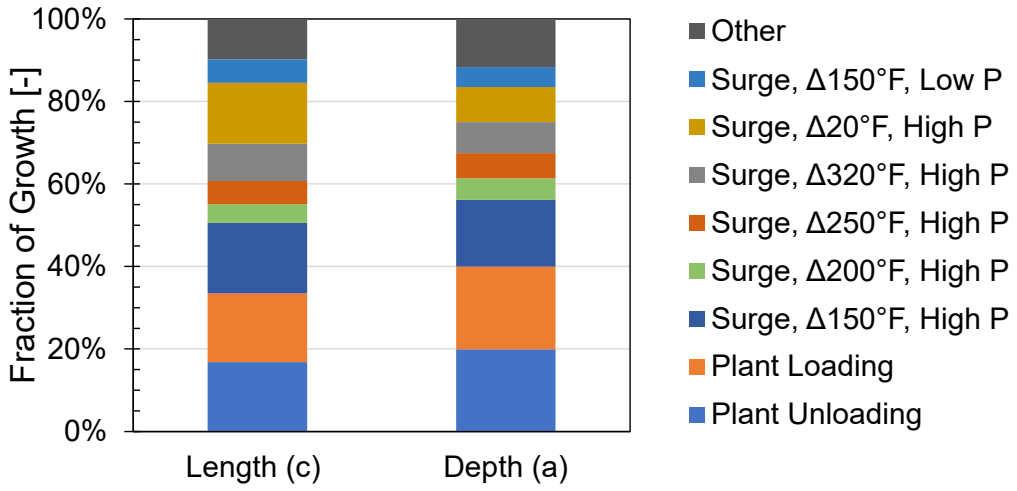

Figure 6-5
Fraction of Growth by Transient for Axial Part-Through-Wall Cracks in Case CE_AX_2

6.3 Axial Cracking Sensitivity Studies

The PIPER-CASS software includes functionality to automate execution of a set of sensitivity cases varying the values of designated inputs. The following subsections describe the set of sensitivity studies performed. For each of these sensitivity studies, an input or set of input values are changed to investigate the impact of that input on the model results. These sensitivity studies specifically focus on inputs expected to have an impact on the simulation results, or to investigate the impact of a given input or modeling decision with less precedent. Sensitivity case results are shown in Table 6-2 through Table 6-5. Results that exceed the acceptance criteria are in bolded red font. Temporal convergence sensitivity cases are discussed separately in Section 6.4.1.

For both CE cases and WEC cases, the crack becomes an idealized TW crack due to collapse of the remaining ligament, rather than becoming a TRN crack by growing to a depth of 95% of the thickness. For cases starting with 6:1 aspect ratio cracks, rupture may occur simultaneously with through-wall penetration if multiple cracks coalesced before growing through-wall, but rupture often is simulated to occur after a few years of growth of the through-wall crack. The absolute leakage probabilities in these results are low, demonstrating that defense-in-depth (leak tightness) is maintained where ruptures do not occur.

6.3.1 Crack Growth Rate and WRS Sensitivities

Sensitivity Cases A and B analyzed the impact of fatigue crack growth modeling decisions on rupture probability. Both of these input changes result in a modest increase in crack growth rates, and a marginal increase in rupture probability for the CE 2 sensitivities that remains within the acceptance criteria. As a result, the fatigue crack growth modeling decisions

involving the crack growth factor of 0.8 and the specific distribution of C_{ss} are not significant factors for the base cases considered.

Sensitivity Cases C and D explored the impact of WRS, with Sensitivity Case C resulting in increases in crack growth comparable to Sensitivity Cases A and B—although the effect for WEC cases would be smaller for deeper cracks. For WEC, Sensitivity Cases C and D resulted in no simulated ruptures. For Sensitivity Case C of the CE 2 geometry, increasing the WRS (to over 50% of the ASME Code minimum yield strength for CF8M) results in one realization (of 1.92×10^{6}) experiencing rupture.

6.3.2 Transient Sensitivities

The changes in transient importance for the transient sensitivities relative to the base case are shown for WEC cases in Figure 6-6 for growth in the depth direction and in Figure 6-7 for growth in the length direction. Equivalent figures for the CE cases are provided as Figure 6-8 for growth in the depth direction and Figure 6-9 for growth in the length direction

Sensitivity Case E on WEC cases increases the heatup and cooldown temperature change rates to the Technical Specification limit of 100°F/hr. The sensitivity results in about two-thirds more growth than the base case, but margin to rupture remained in all realizations. In this sensitivity, the contribution of the heatup transient to growth is much increased—about 40% of the overall growth.

Sensitivity Case F considers increased transient frequencies and results in a similar amount of growth as Sensitivity Case E. Because the relative increase in frequency differs by transient, the fraction of growth by transients shifts some, but the same transients remain the most important.

Sensitivity Cases H and I represent FPO: for all 80 years of operation for WEC and for 20 years starting after 60 years of base load operation (80 years total) for CE. Comparing between H and I for a given geometry shows the impact of power ramp rates. Sensitivity Cases H and I result in more growth (and more ruptures in CE cases) for thicker pipe components. In WEC Sensitivity Cases H and I, the higher frequency of loading and unloading transients due to FPO and the more rapid ramp rates during those postulated FPO transients results in the 100% to 50% power unloading transient being the largest contributor to growth of the crack over the years of service.

Cumulative rupture probabilities over 80 years for the CE cases exceed the acceptance criteria. When considering FPO, the various loading and unloading transients cumulatively dominate growth, constituting about two-thirds of all part-through-wall crack growth in Sensitivity Cases H and I. The presence of surges that rapidly change the coolant temperature in the surge line results in substantial radial gradient thermal stresses that drive surface crack growth. Comparing the CE FPO cases, the effect of ramp rate is small; the quantity of additional loading and unloading transients (and the surges therein) is the parameter that increases the growth and results in ruptures. Whereas the higher ramp rate in Sensitivity Case I results in faster

growth than Sensitivity Case H for WEC cases, the higher rise time associated with the longer transient at a lower ramp rate balances out the growth for CE cases.

For some realizations, the CE sensitivities with FPO transients have a significant amount of through-wall crack length growth before rupture. As shown in Figure 6-10, there is no contribution from the surge transients that drive part-through-wall growth because RGTS, which is self-balancing in the radial direction when the material and temperature are uniform in the axial direction, is modeled to not drive growth of idealized through-wall cracks. The transients with the largest contribution to through-wall crack growth are the leak test heatup, and cooldown transients, which involve substantial increases in primary hoop stress due to applied pressure.

Sensitivity Case M considers increased flow rates during several of the surge transients that model insurge and outsurge occurrence during heatup, cooldown, and hot standby conditions. During surge events, an increased flow rate increases the fatigue crack growth experienced due to higher RGTS. Cumulative rupture probabilities over 80 years meet the acceptance criteria for the CE 1 case and exceed the acceptance criteria for the CE 2 case.

6.3.3 Initial Crack Size Sensitivities

Sensitivity Cases G and K explore the impact of different initial crack sizes. Sensitivity Case G explores the sensitivity to crack depth. For WEC, this sensitivity increases the initial crack depth to 50% through-wall (a/t = 0.5) in order to demonstrate how the simulation predicts a substantial likelihood of rupture when larger and larger initial cracks are assumed (in this case, 50% deep with a length of at least 84 inches (2.1 m)). Because of the very long assumed initial crack length in WEC Sensitivity Case G (more than 20 times the base case length), cracks that become through-wall are already greater than the critical length, so unstable rupture coincides with through-wall penetration, leakage, and collapse of the remaining surface ligament. A similar trend (of rupture coinciding with collapse of the remaining surface ligament) would be expected if similar inputs were applied to both CE geometries; additional ruptures would occur under this Sensitivity Case for CE geometries.

Sensitivity Case K for WEC uses the same crack length of at least 84 inches (2.1 m), but with a depth of 33% of the thickness. No ruptures are simulated to occur for this case even though it assumes an extreme initial crack that is well beyond the range expected considering the required preservice examinations.

Sensitivity Case G for CE introduces a probabilistically sampled initial crack depth per the distribution shown in Figure 4-9 based on the manufacturing flaw data assessed in Lapides [27] and Appendix 2 of EPRI TR-100034 [28] for the case when pre-service radiography is credited (see Section 4.7.4.1). This case meets the acceptance criteria for all Service Levels. A similar trend is expected if the depth distribution were applied to both WEC geometries.

Sensitivity Case K for CE examines the sensitivity to initial crack length by postulating twice the number of additional cracks in the same piping region. Sensitivity Case K in both CE geometries

experiences ruptures but meets the acceptance criteria. This demonstrates how additional crack coalescence events and longer crack segments result in an increased crack growth rate in the depth direction. Increasing the number of initial cracks results in the fraction of realizations in which coalescence occurs at the start of the simulation increasing from 61% to 94%.

Sensitivity Case N analyzes the growth of an idealized through-wall crack having the same length as the initial cracks in case WEC_AX_1. Despite the higher stress intensity factor associated with through-wall cracks than part-through-wall cracks, no ruptures are calculated to occur for 80 years of simulation with this very conservative initial crack assumption.

6.3.4 Material Sensitivities

Sensitivity Case L examines the effect of using material properties for unaged CASS. Unaged CASS has the original undegraded toughness and original yield and ultimate strength values not increased by the aging process. This sensitivity case, which affects crack stability but not crack growth, resulted in acceptably low rupture probability, with no simulated ruptures occurring in the set of realizations performed.

6.3.5 Targeted Final Size Sensitivity

The purpose of the "reverse growth" Sensitivity Case O is to investigate the range of initial through-wall crack lengths that could result in unstable rupture after 80 years of operation (starting the reverse growth with a conservatively short critical through-wall crack length). The growth is simulated backwards in time as a numerical convenience. The initial through-wall crack length ($2c$) is set to the limiting critical crack size for the full range of material properties sampled across all realizations and all Service Level stability loadings, which is calculated to be 10.7 inches (271 mm) under Service Level C/D. The 0.1^{th} percentile crack size after the 80-year period of reverse crack growth (approximately the 99.9^{th} percentile of crack growth) is 0.91 inch (23 mm) smaller than the initial through-wall critical crack size.

Table 6-2
Sensitivity Case Cumulative Probabilities of Occurrence over 80 Years for Sensitivity Cases Applied to WEC_AX_1

Case Name	Service Levels with Ruptures	Cumulative Probability of Rupture			Leakage
		Service Level A	Service Level B	Service Level C/D	
A	None	< 1E-6	< 1E-6	< 1E-6	< 1E-6
B	None	< 1E-6	< 1E-6	< 1E-6	< 1E-6
C	None	< 1E-6	< 1E-6	< 1E-6	< 1E-6
D	None	< 1E-6	< 1E-6	< 1E-6	< 1E-6
E	None	< 1E-6	< 1E-6	< 1E-6	< 1E-6
F	None	< 1E-6	< 1E-6	< 1E-6	< 1E-6
G	A B C/D	**3.53E-4**	**3.57E-4**	**2.75E-3**	3.57E-4
H	None	< 1E-6	< 1E-6	< 1E-6	< 1E-6
I	None	< 1E-6	< 1E-6	< 1E-6	< 1E-6
K	None	< 1E-6	< 1E-6	< 1E-6	< 1E-6
L	None	< 1E-6	< 1E-6	< 1E-6	< 1E-6
N	None	< 1E-6	< 1E-6	< 1E-6	N/A

Table 6-3
Sensitivity Case Cumulative Probabilities of Occurrence over 80 Years for Sensitivity Cases Applied to WEC_AX_2

Case Name	Service Levels with Ruptures	Cumulative Probability of Rupture			Leakage
		Service Level A	Service Level B	Service Level C/D	
A	None	< 1E-6	< 1E-6	< 1E-6	< 1E-6
B	None	< 1E-6	< 1E-6	< 1E-6	< 1E-6
C	None	< 1E-6	< 1E-6	< 1E-6	< 1E-6
D	None	< 1E-6	< 1E-6	< 1E-6	< 1E-6
E	None	< 1E-6	< 1E-6	< 1E-6	< 1E-6
F	None	< 1E-6	< 1E-6	< 1E-6	< 1E-6
G	A B C/D	**9.43E-3**	**9.55E-3**	**6.90E-2**	9.55E-3
H	None	< 1E-6	< 1E-6	< 1E-6	< 1E-6
I	None	< 1E-6	< 1E-6	< 1E-6	< 1E-6
K	None	< 1E-6	< 1E-6	< 1E-6	< 1E-6
L	None	< 1E-6	< 1E-6	< 1E-6	< 1E-6

Table 6-4
Sensitivity Case Cumulative Probabilities of Occurrence over 80 Years for Sensitivity Cases Applied to CE_AX_1

Case Name	Service Levels with Ruptures	Cumulative Probability of Rupture			Leakage
		Service Level A	Service Level B	Service Level C/D	
A	None	< 1E-6	< 1E-6	< 1E-6	5E-7
B	None	< 1E-6	< 1E-6	< 1E-6	< 1E-6
C	None	< 1E-6	< 1E-6	< 1E-6	< 1E-6
D	None	< 1E-6	< 1E-6	< 1E-6	< 1E-6
G	None	< 1E-6	< 1E-6	< 1E-6	< 1E-6
H	A B C/D	**2.03E-5**	**3.33E-5**	6.30E-5	6.04E-05
I	A B C/D	**2.34E-5**	**3.33E-5**	7.03E-5	6.56E-05
J	None	< 1E-6	< 1E-6	< 1E-6	< 1E-6
K	A B C/D	5E-7	5E-7	1.6E-6	1.0E-06
L	None	< 1E-6	< 1E-6	< 1E-6	< 1E-6
M	None	< 1E-6	< 1E-6	< 1E-6	< 1E-6

Table 6-5
Sensitivity Case Cumulative Probabilities of Occurrence over 80 Years for Sensitivity Cases Applied to CE_AX_2

Case Name	Service Levels with Ruptures	Cumulative Probability of Rupture			Leakage
		Service Level A	Service Level B	Service Level C/D	
A	A B C/D	5E-7	5E-7	1.0E-6	2.1E-6
B	A B C/D	5E-7	5E-7	5E-7	5E-7
C	B C/D	< 1E-6	5E-7	5E-7	5E-7
D	None	< 1E-6	< 1E-6	< 1E-6	< 1E-6
H	A B C/D	**7.97E-5**	**1.11E-4**	**1.80E-4**	2.17E-04
I	A B C/D	**8.80E-5**	**1.14E-4**	**1.67E-4**	2.04E-04
J	None	< 1E-6	< 1E-6	< 1E-6	< 1E-6
K	A B C/D	5E-7	1.0E-6	2.1E-6	1.0E-06
L	None	< 1E-6	< 1E-6	< 1E-6	< 1E-6
M	A B C/D	**3.1E-6**	4.2E-6	6.3E-6	6.8E-06

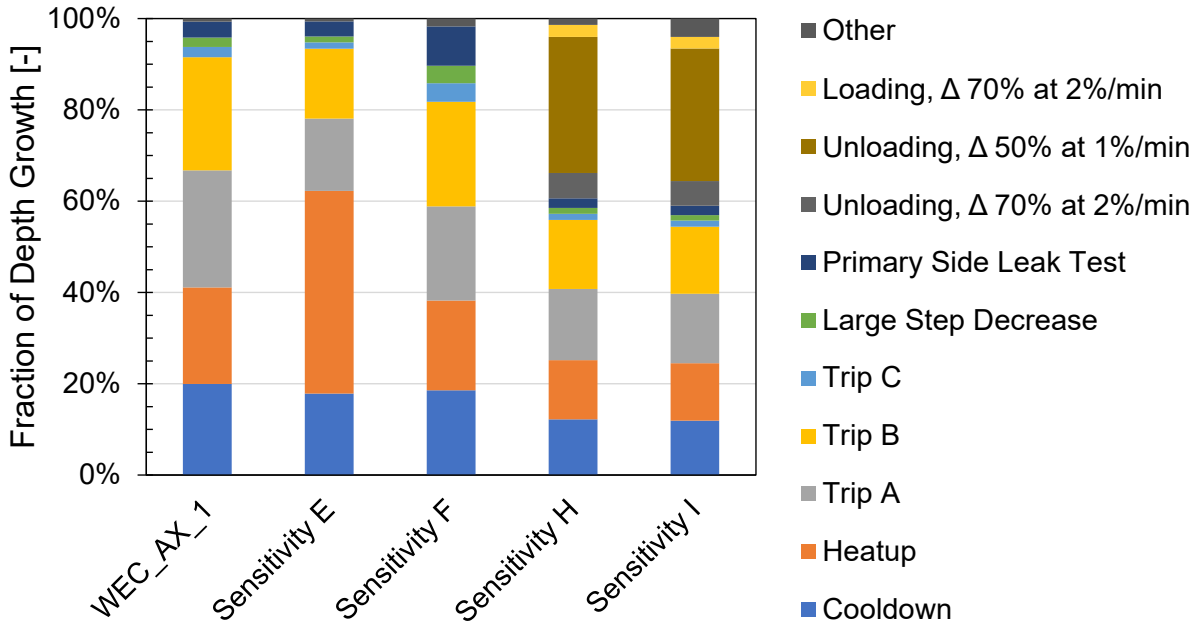

Figure 6-6
Fraction of Growth in the Depth Direction by Transient for Axial Part-Through-Wall Cracks in Case WEC_AX_1 and Sensitivity Cases E, F, H, and I

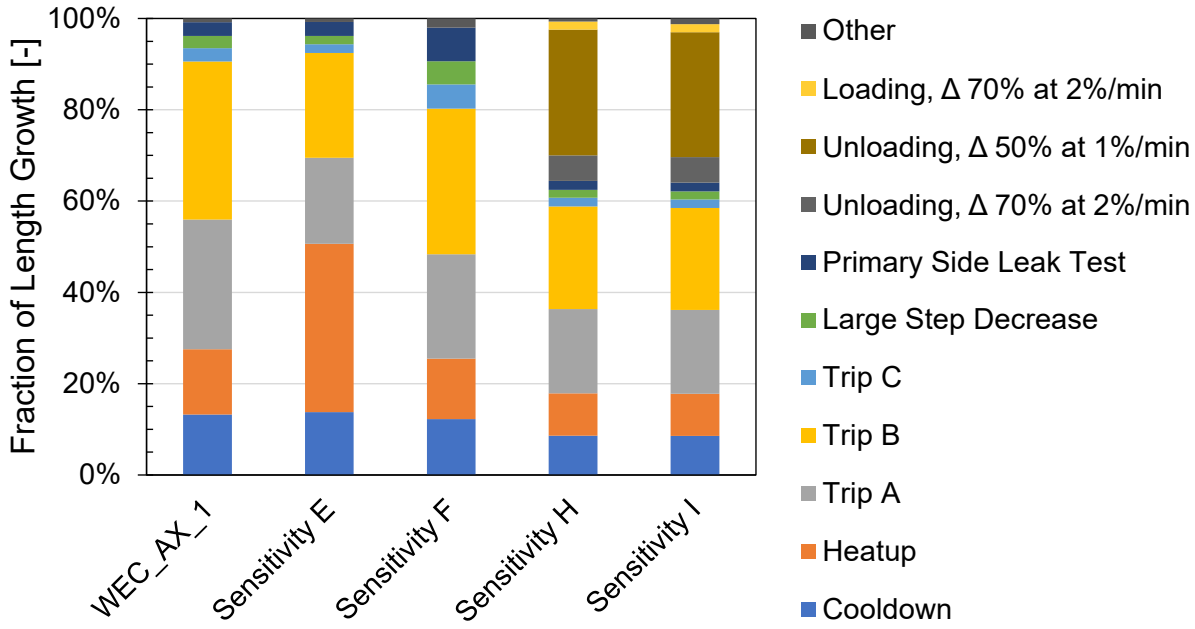

Figure 6-7
Fraction of Growth in the Length Direction by Transient for Axial Part-Through-Wall Cracks in Case WEC_AX_1 and Sensitivity Cases E, F, H, and I

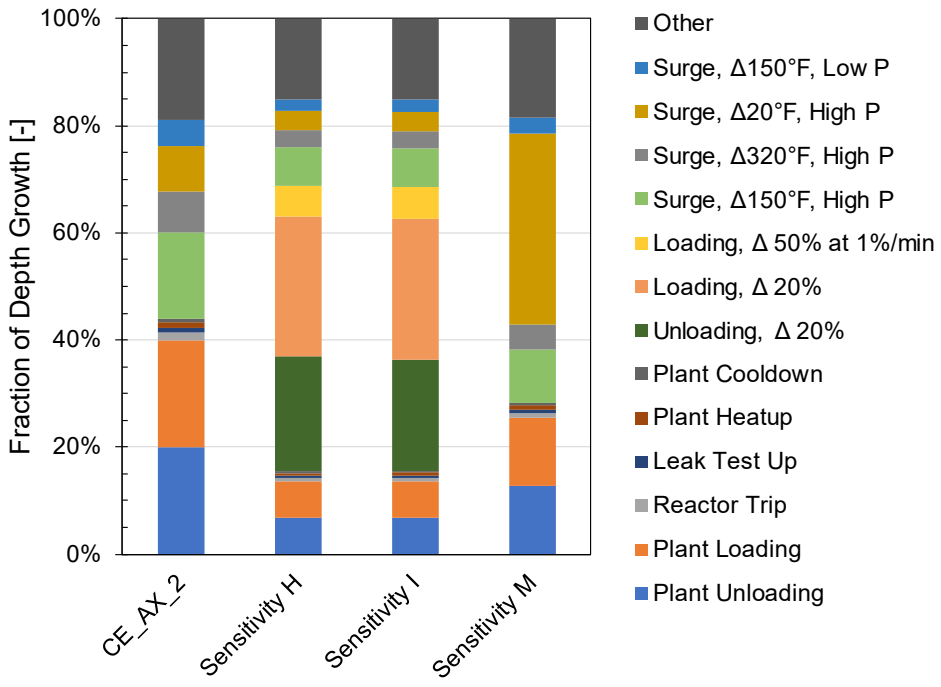

Figure 6-8
Fraction of Growth in the Depth Direction by Transient for Axial Part-Through-Wall Cracks in Case CE_AX_2 and Sensitivity Cases H, I, and M

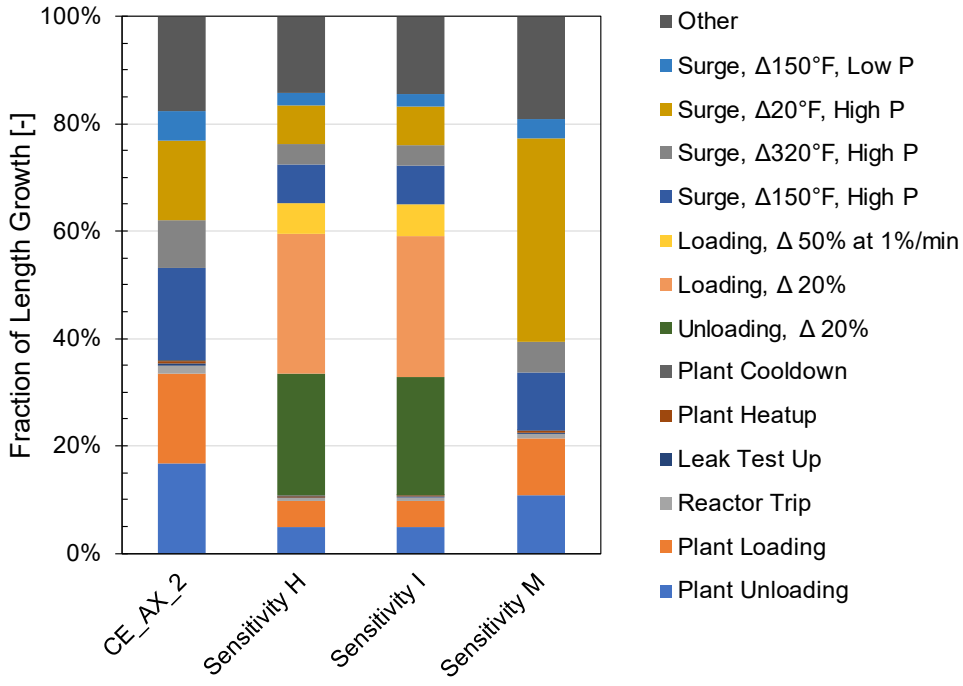

Figure 6-9
Fraction of Growth in the Length Direction by Transient for Axial Part-Through-Wall Cracks in Case CE_AX_2 and Sensitivity Cases H, I, and M

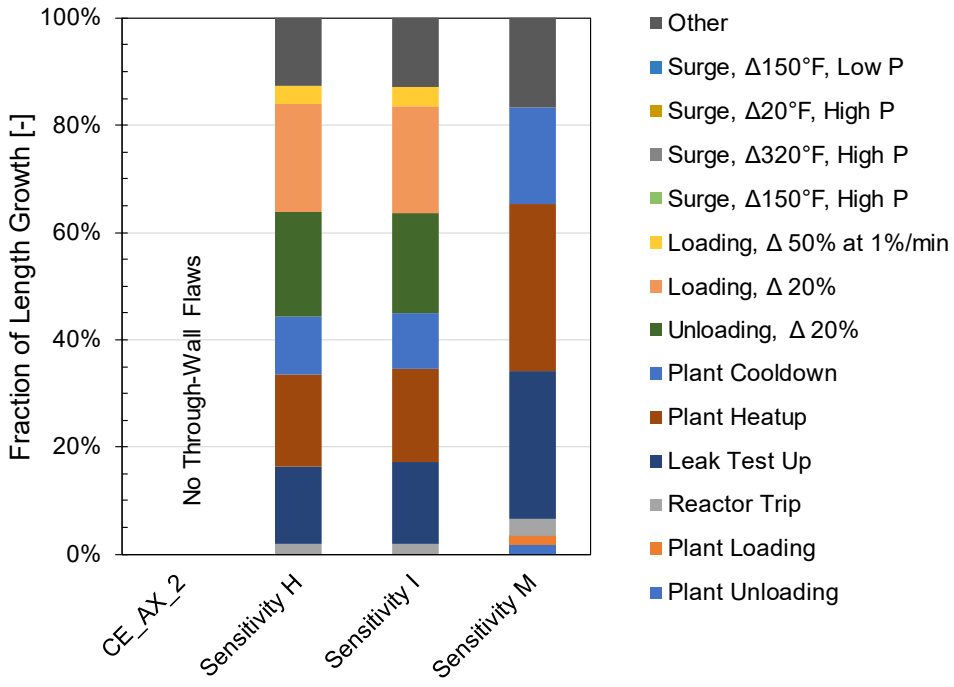

Figure 6-10
Fraction of Growth in Length by Transient for Axial Through-Wall Cracks in Case CE_AX_2 and Sensitivity Cases H, I, and M

6.4 Convergence

6.4.1 Temporal Convergence

Temporal convergence is demonstrated by running three sensitivity cases at three different timestep lengths. Axial cases are executed for an 80-year simulation time at a 5 day timestep (t1 sensitivity), 25 day timestep (t2 sensitivity), and 50 day timestep (t3 sensitivity). Detailed outputs are examined and compared between cases to ensure results are sufficiently converged. Specifically, the cumulative growth and the growth caused by each transient is compared between the three sensitivities. As shown in Table 6-6 for sensitivities on CE_AX_1, the percent difference in cumulative growth never exceeds +/- 0.5% between any two of the sensitivities, with growth due to any given transient consistent to within 1% for transients contributing 5% or more of the total growth (within 8% overall). One factor contributing to these minor differences may be that the number of transient occurrences in each timestep is required to be an integer. Further refinement of the base timestep is unnecessary, given the small difference between t1 and t2.

Further, the crack depth, crack length, aspect ratio, maximum K_I at the ID/surface, and maximum K_I at the OD/deepest point are qualitatively examined over the simulation time. No significant differences were observed during this comparison.

Table 6-6
Comparison of Cumulative Crack Growth for Temporal Convergence Sensitivity Studies

Key Transients	% Difference between t1 and t2		% Difference between t1 and t3		% Difference between t2 and t3	
	Length	Depth	Length	Depth	Length	Depth
Plant Loading	-0.18%	-0.28%	0.16%	0.16%	0.33%	0.44%
Plant Unloading	-0.14%	-0.23%	0.18%	0.18%	0.32%	0.42%
Surge, Δ150°F, High P	-0.27%	-0.37%	0.05%	0.07%	0.32%	0.44%
Surge, Δ200°F, High P	-0.06%	-0.17%	0.22%	0.22%	0.28%	0.39%
Surge, Δ250°F, High P	-0.23%	-0.35%	0.01%	0.04%	0.24%	0.39%
Surge, Δ320°F, High P	-0.41%	-0.45%	0.23%	0.22%	0.64%	0.68%
Surge, Δ150°F, Low P	-0.20%	-0.27%	-0.06%	-0.04%	0.14%	0.23%
Approx. Avg. Growth	-0.16%	-0.34%	0.14%	0.14%	0.30%	0.48%

6.4.2 Statistical Convergence

Due to the inherent discretization of Monte Carlo analyses and finite number of realizations, there is some uncertainty on the precise values of the statistics generated from the analysis results. This uncertainty is inversely related to the number of realizations included in the analysis. For continuously variable parameters and where the result reflects the outcome of a large number of realizations, this uncertainty is negligible relative to the outcome. For statistics that are based on binary outcomes (e.g., rupture or no rupture), residual uncertainty remains even if no realizations report rupture. This is reflected by the lower limit in reported values in the probability of rupture results tables.

To ensure convergence, the number of realizations for base cases is selected such that either at least 10 failures occur, or, for cases where no failures are calculated, the acceptance criteria are considered to be met when the number of realizations exceeds the 10 times the inverse of the allowable failure probability (e.g., 10^7 realizations for Service Level A, with an allowable failure probability of 10^{-6}). Showing that the base case results meet the acceptance criteria with at least one order of magnitude of margin (i.e., < 10^{-7} ruptures observed versus the limiting acceptance criterion of 10^{-6}) meets category SC-1 for RG 1.245 [10]. The base case runs for a total of 10^7 realizations are generated by running five separate analyses at 2×10^6 realizations, which natively permits a bootstrapping analysis. For base cases with ruptures or leaks at probabilities of ≤ 10^{-6}, the difference between each of the five cases is at most one occurrence of the event, indicating good convergence.

This approach can be validated by calculating the probability of a simulation experiencing no ruptures due to statistical non-convergence for the simulation time and number of realizations modeled. Given *N* independent trials, the probability of observing zero occurrences of an event having a probability, *p*, is given by the binomial distribution and can be simplified to Equation 1.

$$P(0; N, p) = (1 - p)^N$$ Equation 1

where, in the context of statistical convergence versus the acceptance criteria:

p is the acceptance criterion corresponding to the maximum allowable probability of rupture

N is the number of Monte Carlo realizations run

$P(0; N, p)$ is the probability of observing no failure events in the conducted number of realizations if the true probability of failure were to meet or exceed the acceptance criterion

For the base cases, the probability that no failures would occur over 9.6×10^6 realizations if the actual risk meets or exceeds the Service Level A acceptance criterion (the lowest allowable failure probability, of 10^{-6}) is 0.01%. For the sensitivity cases having 1.92×10^6 realizations, the equivalent probability is 15%. This gives high confidence that the fully converged failure probability is less than the acceptance criterion for the base cases and reasonable confidence for the sensitivity cases.

7 CIRCUMFERENTIAL CRACKING RESULTS AND DISCUSSION

7.1 Circumferential Cracking Base Case Results

The two base cases, for each of the main loop geometries, are described in Section 4.6 with case numbering nomenclature defined in Table 4-9. The acceptance criteria are based on the allowable rupture probability, as discussed in Section 5. Rupture probability results from PIPER-CASS are the cumulative conditional probability of rupture during a 2 year period of continued operation following flaw acceptance given the occurrence of the transient generating the limiting loading for that Service Level.

Results for the base cases are shown for each Service Level in Table 7-1. Only for the WEC 1 geometry under Service Level D (faulted) loading is the rupture probability large enough to be quantified for the number of realizations considered. As seen in Figure 7-1, the amount of crack growth is predicted to be small for the period of continued operation versus the crack size (multiple inches long).

Table 7-1
Base Case Cumulative Probabilities of Occurrence over 2 Years of Continued Operation

Case Name	Service Levels with Ruptures	Cumulative Probability of Rupture			
		Service Level A	Service Level B	Service Level C	Service Level D
WEC_CIRC_1	D	< 1E-7	< 1E-7	< 1E-7	8.3E-7
WEC_CIRC_2	None	< 1E-7	< 1E-7	< 1E-7	< 1E-7

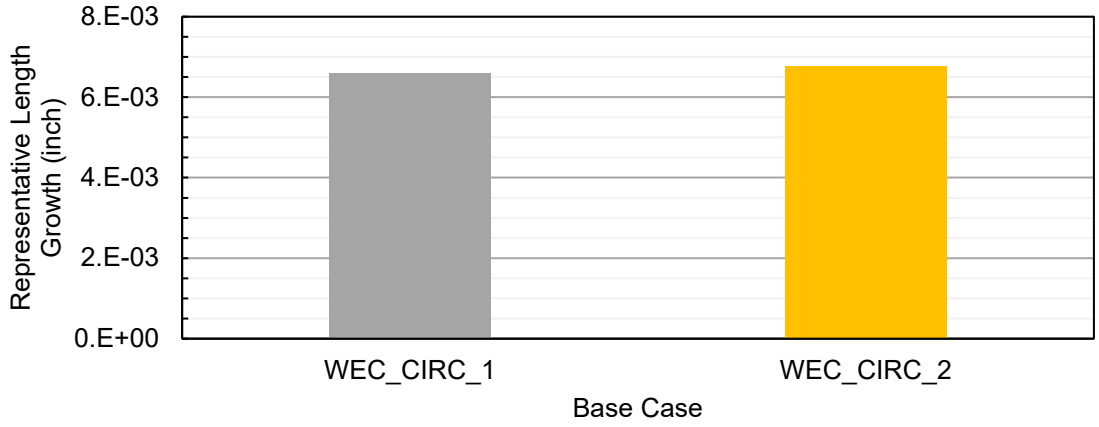

Figure 7-1
Crack Length Growth Representative of Each Base Case

7.2 Input and Transient Importance

In each of the base case realizations with ruptures, rupture occurs at the first timestep (before any crack growth occurs). The sampled inputs in these realizations represent the intersection of low material toughness (leading to a smaller critical crack size) and substantial undersizing of the flaw at detection (i.e., an initial crack length larger than the nominal size, which is set to the allowable size for the applied loads). Figure 7-2 shows the relationship between the value of several sampled parameters and the critical through-wall crack length for a sampling of realizations. The results of this assessment indicate similar factors are at play as for axially oriented cracking, as described in Section 6.2.1. The reduction in the realizations with a critical through-wall half-length at 0.8 radian (45.8°) is due to the plastic J-integral not being an entirely smooth equation[18]. Because the cracks being considered have a median half-angle (Θ) around 16° (roughly 0.3 or π/11 radian), this discontinuity does not affect the results presented herein.

As seen in Figure 7-3, the majority of crack growth that does occur is due to the heatup, cooldown, and OBE transients. These are all transients that include a sizable change in pressure or mechanical stresses, which promote through-wall growth. Crack growth is of reduced importance for the circumferential cracking cases in WEC main loop piping relative to axial cracking because relatively little crack propagation occurs.

[18] The xLPR-TWC_Fail method [54] results in a discontinuity in $dJ/d\Theta$ at $\Theta = \pi/4$ and $\pi/3$ due to the shift from equation 2.41 to 2.42 of NUREG/CR-4853.

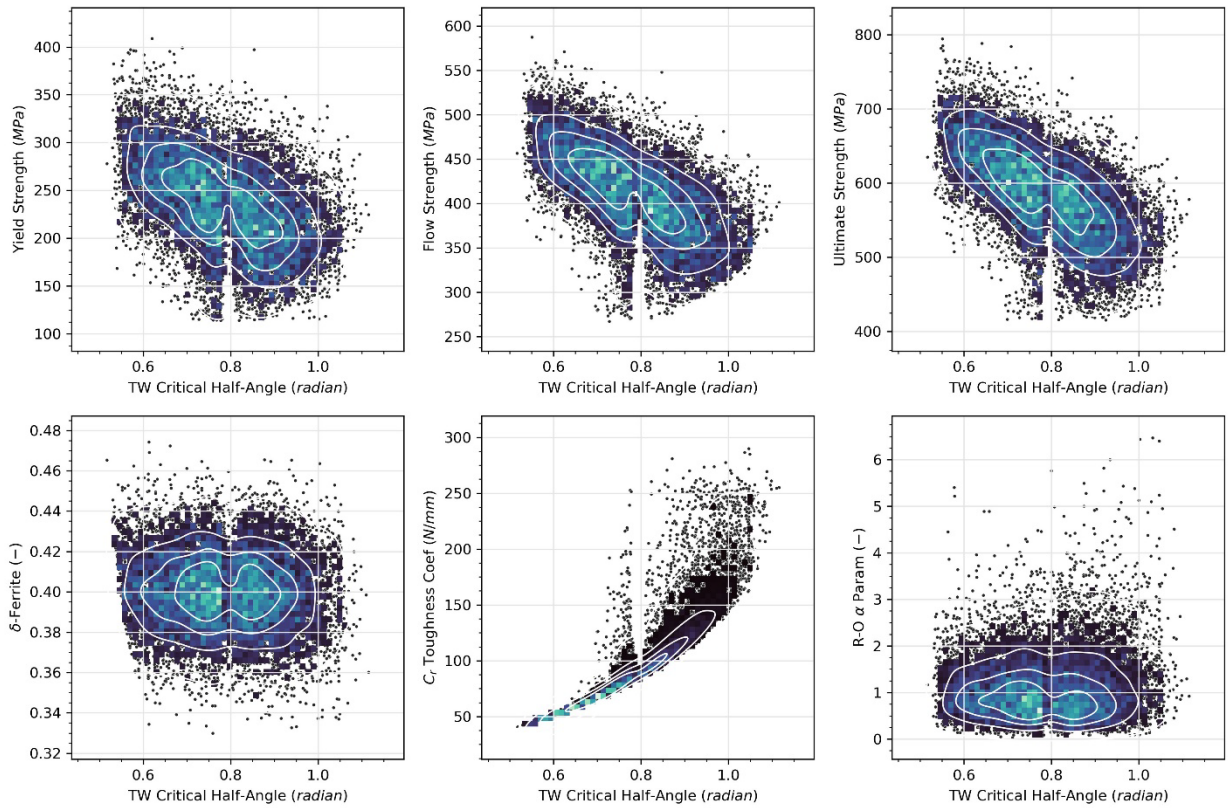

Figure 7-2
Impact of Sampled Values on Critical Crack Half-Angle at Service Level A for Case WEC_CIRC_1

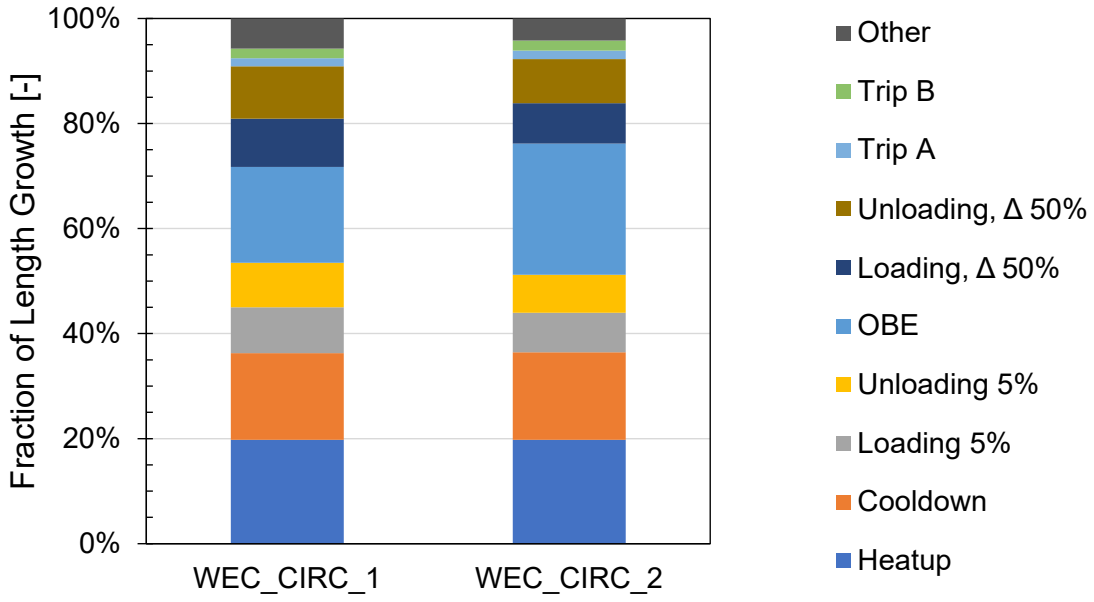

Figure 7-3
Fraction of Growth in Length by Transient for Circumferential Base Cases

7.3 Circumferential Cracking Sensitivity Studies

Sensitivity case results are shown in Table 7-2 and Table 7-3 for cases based on WEC 1 and WEC 2 geometries, respectively. The following subsections describe the results.

7.3.1 Crack Growth Rate, WRS, and Transient Sensitivities

Whereas substantial crack growth occurs in some cases evaluating axially oriented cracking, the much shorter duration evaluation for circumferentially oriented cracking deemphasizes the importance of sensitivity cases that predominantly impact the amount of crack growth. These sensitivities on fatigue crack growth rate (FCGR) parameters (A and B) and transients (E, F, and H) have a negligible to modest impact on the probability of rupture. Figure 7-4 depicts the fraction of crack growth that is caused by each transient for some of these key cases. As expected, Sensitivity Case E increases the growth due to heatup and cooldown, and Sensitivity Case F increases growth due to 5% power change loading and unloading transients due to the factor of 10 increase in their frequency.

Since the axial stress from WRS is self-balancing through the wall, it does not contribute significantly to through-wall crack growth. Consequently, Sensitivity Case C with a weld repair WRS profile is evaluated using a part-through-wall crack, and its effect is observed by comparing against Sensitivity Case G. For Sensitivity Case C, depth growth is faster due to less compressive WRS over the first half of the thickness (see Figure 4-5), but length growth is slower because of the greater magnitude of compressive WRS at the ID surface. There are no realizations with ruptures in either Sensitivity Case C or G.

7.3.2 Initial Crack Size Sensitivities

Sensitivity Case G assesses the growth of a 50% part-through-wall crack to ensure that the growth and stability of through-wall cracks bounds shallower ones. Despite being influenced by WRS and RGTS, Sensitivity Case G has slower length growth than the through-wall cracks in the base case; it does not include any realizations with ruptures.

The probability of rupture for Sensitivity Case P is within an order of magnitude of the acceptance criterion for Service Level D loading. Over 90% of the ruptures in this case occur prior to any crack growth, highlighting that the limiting factor is, as with the base case, the intersection of low material toughness and substantial flaw undersizing (i.e., a longer sampled initial crack length). The realizations that rupture after one or more time steps of crack growth are already very close to the critical crack size at instantiation. The results of Sensitivity Case P highlight the importance of flaw length sizing uncertainty on the PFM results. For larger uncertainties (i.e., RMSE on 2Θ over 1.0 inch), the probability of rupture would increase above the acceptance criteria for a nominal (i.e., measured) crack length of $2\Theta = 32°$. To meet the acceptance criteria with larger sizing uncertainties, the nominal crack length could be shortened.

7.3.3 Material and Loading Sensitivities

Sensitivity Case L examines the effect of using material properties for unaged CASS (higher toughness but lower strength in the PFM), and it results in no simulated ruptures occurring in the set of realizations performed. The other material Sensitivity Cases (Q and R) affect multiple aspects of the PFM due to the increased allowable loads for these cases and, in the case of Sensitivity Case Q for CF8, the increased FCGR coefficient. The allowable loads for Sensitivity Case R are greater than those for Sensitivity Case Q. Both of these cases yield no realizations with ruptures, and the two cases have similar increases in the amount of crack growth.

The probability of rupture for Sensitivity Case S, which increases membrane stress, is within an order of magnitude of the acceptance criterion for Service Level D loading. As with Sensitivity Case P, over 90% of the ruptures occur prior to any crack growth. Whereas Sensitivity Case P resulted in an increase in the rupture probability due to an increase in the initial crack size, Sensitivity Case S yields a similar effect by reducing the through-wall crack critical length. Given that both the base case and Sensitivity Case P apply their respective loadings that yield stresses equal to the maximum allowable, the increase in probability of rupture for this sensitivity case reflects the reduced margin in the Nonmandatory Appendix C combined loading approach for increased but allowable membrane stresses.

Table 7-2
Sensitivity Case Results for WEC_CIRC_1

Case Name	Service Levels with Ruptures	Cumulative Probability of Rupture			
		Service Level A	Service Level B	Service Level C	Service Level D
A	D	< 1E-6	< 1E-6	< 1E-6	5E-7
B	D	< 1E-6	< 1E-6	< 1E-6	5E-7
C	None	< 1E-6	< 1E-6	< 1E-6	< 1E-6
E	D	< 1E-6	< 1E-6	< 1E-6	1.0E-6
F	D	< 1E-6	< 1E-6	< 1E-6	2.1E-6
G	None	< 1E-6	< 1E-6	< 1E-6	< 1E-6
H	D	< 1E-6	< 1E-6	< 1E-6	5E-7
L	None	< 1E-6	< 1E-6	< 1E-6	< 1E-6
P	C D	< 1E-6	< 1E-6	4.7E-6	3.80E-5
Q	None	< 1E-6	< 1E-6	< 1E-6	< 1E-6
R	None	< 1E-6	< 1E-6	< 1E-6	< 1E-6
S	D	< 1E-6	< 1E-6	< 1E-6	3.44E-5

Table 7-3
Sensitivity Case Results for WEC_CIRC_2

Case Name	Service Levels with Ruptures	Cumulative Probability of Rupture			
		Service Level A	Service Level B	Service Level C	Service Level D
A	None	< 1E-6	< 1E-6	< 1E-6	< 1E-6
B	None	< 1E-6	< 1E-6	< 1E-6	< 1E-6
C	None	< 1E-6	< 1E-6	< 1E-6	< 1E-6
E	None	< 1E-6	< 1E-6	< 1E-6	< 1E-6
F	None	< 1E-6	< 1E-6	< 1E-6	< 1E-6
G	None	< 1E-6	< 1E-6	< 1E-6	< 1E-6
H	None	< 1E-6	< 1E-6	< 1E-6	< 1E-6
L	None	< 1E-6	< 1E-6	< 1E-6	< 1E-6
P	D	< 1E-6	< 1E-6	< 1E-6	2.1E-6
Q	None	< 1E-6	< 1E-6	< 1E-6	< 1E-6
R	None	< 1E-6	< 1E-6	< 1E-6	< 1E-6
S	D	< 1E-6	< 1E-6	< 1E-6	3.6E-6

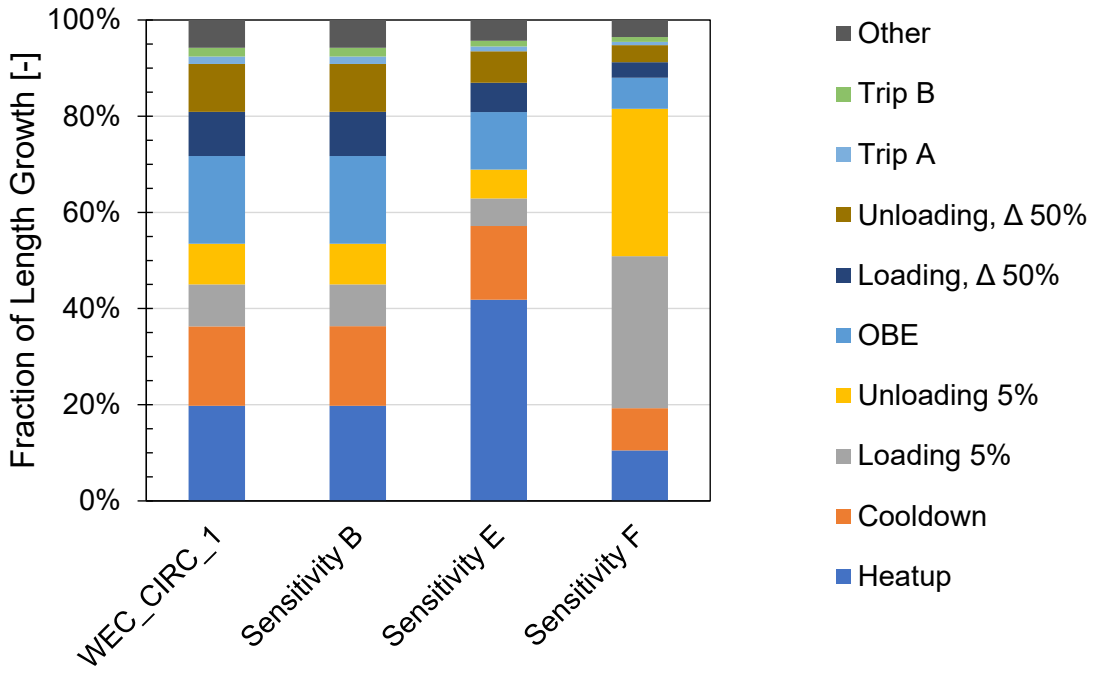

Figure 7-4
Fraction of Growth in Length by Transient for WEC_CIRC_1 and Sensitivity Cases

7.4 Convergence

A temporal convergence study was also performed for the circumferential cracking cases using the same timesteps as for the axial cracking cases. A comparison of the detailed outputs indicates that results are sufficiently converged. Specifically, Table 7-4 shows the percent difference in cumulative growth is within +/- 0.6% among the three sensitivities, with growth due to any given transient consistent to within 3% for transients contributing more than 5% of the total growth (within 8% overall). Further refinement of the base timestep is unnecessary, given the small difference between t1 and t2.

As with the axial cases, the circumferential base case runs for a total of 10^7 realizations are generated by running five separate analyses at 2×10^6 realizations. For base cases with ruptures or leaks at probabilities of $\leq 10^{-6}$, the difference between each of the five cases is at most one occurrence of the event, indicating good convergence.

Table 7-4
Comparison of Cumulative Crack Growth for Temporal Convergence Sensitivity Studies

Key Transients	Difference in Length Growth		
	t1 vs. t2	t2 vs. t3	t1 vs. t3
Heatup	0.15%	0.33%	0.49%
Cooldown	1.28%	-0.92%	0.35%
Loading 5%	1.41%	-0.17%	1.24%
Unloading 5%	1.50%	-0.46%	1.04%
Loading 50%-100%	-0.26%	0.50%	0.24%
Unloading 100%-50%	-0.13%	-0.01%	-0.14%
OBE	-1.72%	2.70%	0.93%
Approx. Average Growth	0.06%	0.50%	0.57%

7.5 Assessment of Margin on Stress

In addition to a PFM assessment of the acceptability of the alternative flaw evaluation approach proposed in Section 3, a deterministic evaluation of the margin was performed by plotting the maximum allowable bending stress and the critical bending stress for different crack sizes. Figure 7-5, generated from the base case material definition at the median strength and toughness, shows how there is greater margin on through-wall crack stability (indicated by the distance between the blue solid and dashed lines) for shorter cracks. Where the part-through-wall crack critical stress is lower than the through-wall critical stress, instability of a part-through-wall crack would yield ligament collapse; above the through-wall critical stress, rupture would result. For comparison, Figure 7-6 plots the critical stresses using the median strength but 1st percentile of toughness parameters. Margin is also reduced for lower structural factors.

These plots illustrate why the proposed approach has a maximum limit of applicability, and the monotonic nature of the changing margin for through-wall crack length confirms that the largest allowable flaw length for which this methodology is validated by the PFM bounds shorter flaws.

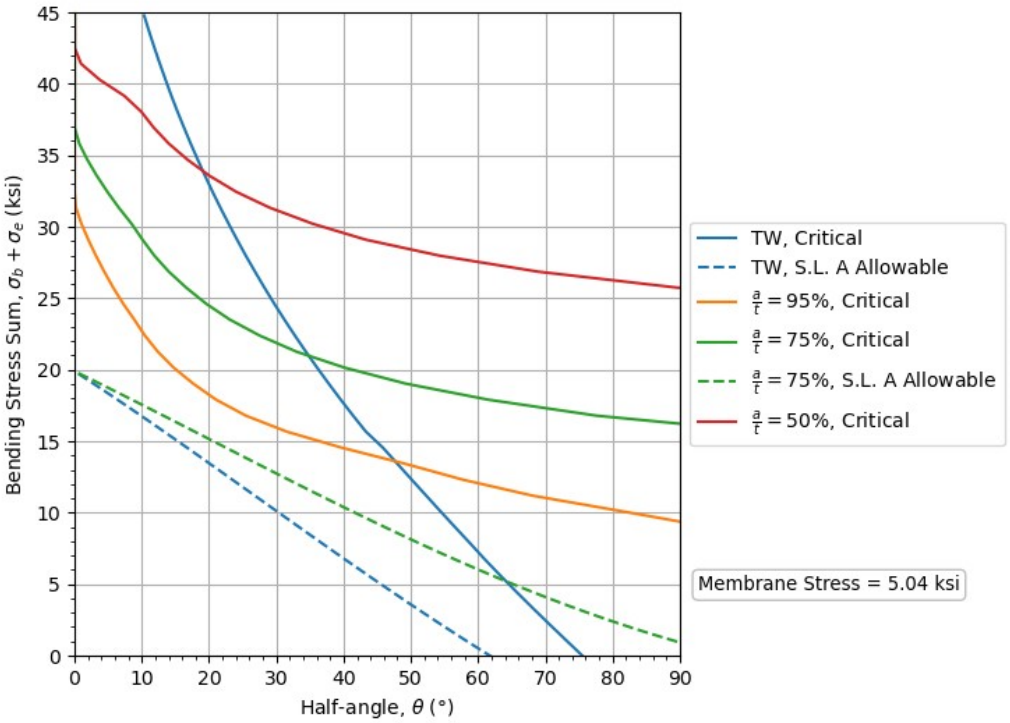

Figure 7-5
Comparison of Allowable and Critical Bending Stress by Crack Size (Median Toughness)

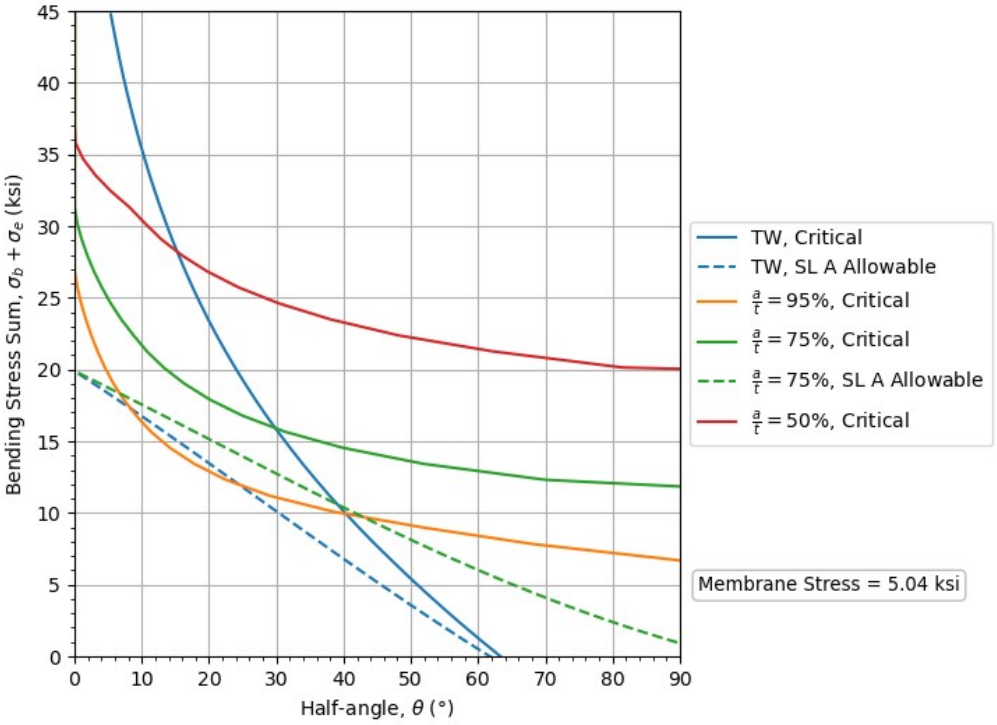

Figure 7-6
Comparison of Allowable and Critical Bending Stress by Crack Size (1st Percentile Toughness Parameters)

7.6 Consideration of Surge Line Piping Components

The proposed flaw evaluation methodology is not applicable on a generic basis to surge line piping components. Transient information applicable to CE surge line locations includes a substantial frequency of stratification and surge events that are expected to be conservative versus the actual transient count in a given fuel cycle, particularly for plants that maintain pressurizer outflow during heatup, cooldown, and hot standby. Stratification events generate global bending stresses that promote growth of cracks in the PFM evaluation. Together with the distributions that include conservatively low toughness material, prediction of ruptures can exceed the acceptance criteria. A plant-specific analysis for which less severe as-aged material toughness or less severe transient definitions are appropriate could be used to justify the proposed flaw evaluation methodology and determine an appropriate limit of applicability.

8 UNCERTAINTIES

As described in Section 2 and Appendix B, the models in PIPER-CASS are largely adapted from xLPR modules. Detailed discussion of sources and treatment of uncertainty for these xLPR modules is provided in the xLPR Uncertainty Report [35]. This xLPR report provides significant discussion of input variable uncertainty, model uncertainty, model parameter uncertainty, and completeness uncertainty. Consequently, this section focuses on key input or modeling uncertainties and assumptions that apply to PIPER-CASS but not to xLPR (i.e., uncertainties not covered in the xLPR Uncertainty Report).

In addition to the discussion in xLPR Uncertainty Report [35] of xLPR modules relevant to PIPER-CASS, the key uncertainties are as follows:

- *Single-loop Monte Carlo:* Unlike xLPR, the framework of PIPER-CASS does not contain a dual-loop structure to separately handle aleatory and epistemic uncertainties. Although separation of sampled uncertainties into epistemic and aleatory uncertainties is a method for obtaining an improved understanding in uncertainties of an analysis output, the simpler single-loop structure is sufficient given the extremely low failure probabilities obtained. Under these circumstances, there would be little advantage gained from separating epistemic and aleatory uncertainties. Furthermore, sensitivity studies are then leveraged to determine the importance of uncertainty on different input parameters.
- *Fracture toughness:* Uncertainty in aged fracture toughness and aged flow strength of CASS material is a key source of overall modeled uncertainty because these parameters essentially control the critical crack size. This source of uncertainty was addressed as detailed in Section 4.2 by calibrating the input parameters to achieve the overall variability and correlation apparent in available data. Additionally, the inputs captured the potential for as-aged material strength to be below the Section II-D minimum and for the material toughness to be below the “lower bound” value from NUREG/CR-4513, Rev. 2 [3].
- *Material strength, as aged:* Limited data are available for the as-aged yield and ultimate tensile strengths of CF8M materials. This source of uncertainty was assessed as discussed in Section 4.2.2 by considering the available data and with comparison against an aging factor applied to strength data for unaged material. Furthermore, as shown in the input importance study documented in Sections 6.2.1 and 7.2, the critical crack length is more directly correlated to the toughness than the material strength. This means that the limited data for aged strength values are not key to the stability modeling.
- *Component geometry and material:* The PFM modeling assumes that the flaw or flaws are propagating as cracks and located in a section of straight pipe. As discussed in Section 4.1, this assumption is appropriate considering that the examination coverage required by Subarticle IWB-2500 (Examination Categories B-F and B-J) includes the weld and a short section of base metal on either side of the weld. Per the requirements of IWB-3641, the procedures in Nonmandatory Appendices C and H of ASME Code, Section XI, which are

based on equations applicable to a section of straight pipe, are applicable to a flaw in the initial portion of an elbow closest to the adjoining weld.

As also discussed in Section 4.1, the effect of differences in pipe diameter and wall thickness for the subject piping lines (WEC main loop CASS piping and CE surge line CASS piping) are explicitly assessed in the set of PFM base cases (Table 4-9). The WEC cases reflect the range of main loop piping diameters, with wall thickness specified to increase with pipe diameter. The CE cases reflect the reduced wall thickness at the similar metal welds, as well as the variation in the value of this reduced wall thickness among the CE plants with CASS surge lines.

xLPR explicitly models the different material regions making up a dissimilar metal weld, whereas PIPER-CASS applies a simplified model of a single material representing a section of straight piping, inclusive of any welds. Furthermore, for dissimilar metal welds, the standard approach for evaluating stability considers the material strength properties from the base metal and the toughness properties from the weld metal. However, for the aged CASS components evaluated in this effort, the toughness of the CASS base metal is degraded and becomes limiting. Thus, both material strength and toughness properties for the aged CASS base metal material are therefore applied in PIPER-CASS, with no need to consider multiple material zones.

- *Flaw shape:* Because the shape of flaws growing by fatigue tends to be more regular than the branching intergranular growth of cracks by primary water stress corrosion cracking (PWSCC), the uncertainty associated with assuming idealized planar crack shapes is reduced for PIPER-CASS relative to xLPR.
- *Transient scheduling:* In PIPER-CASS, the occurrence of transients is sampled (discussed in Section B.3.2) to reflect epistemic uncertainty in the time and frequency at which transients occur at different plants. Including this uncertainty in transient scheduling is of greater importance for PIPER-CASS because fatigue crack growth is dominant for CASS material. In contrast, xLPR, which was developed with a focus on PWSCC but also models fatigue cracking, applies a deterministic transient schedule based on a user-input frequency and number of cycles per event.
- *Transient pressure and temperature time histories*: This report applies the transient histories in MRP-393 [22] for WEC cases, which reflect example best-estimates of typical plant transients. Additionally, the frequency of transient occurrence is set to appropriately reflect realistic plant operating practices, rather than the higher design basis frequency. Sensitivity studies (Sections 6.3.2 and 7.3.1) are executed to address the potential effect of more severe transients or more frequent transients.

  For axial cracking, these sensitivity studies included the effect of additional loading and unloading transients due to flexible power operation for 20 years (CE cases) or 80 years (WEC cases) out of an 80 year plant life for each component geometry considered. As a further sensitivity on the best-estimate transient frequencies for WEC cases, a sensitivity study increased the frequency of each transient by a factor of 1.3 to 12. The Heatup and Cooldown transients drive crack growth for WEC cases, so a more aggressive variant of

these transients was also considered with temperature histories changing at a rate of 100°F/hr (55.6°C/hr), the maximum allowed rate for typical PWR technical specifications. For circumferential cracking, similar sensitivity studies for transients during one fuel cycle of continued operation (2 years) are included, although the amount of crack growth in base cases and sensitivities is small. In this manner, the analyses address the variability across the industry of RCS transients resulting in fatigue loading.

If a transient time history is assumed to be truncated prior to reaching equilibrium, a non-conservatism may be applied in the fatigue crack growth inputs, as the rise time may be truncated. In this effort, the potential for truncated transient time histories was assessed and addressed by (if needed) adding an additional point to the end of the transient time history to allow the pipe temperature to equilibrate. Allowing for equilibration of the pipe temperature following a transient produces more realistic crack growth results.

9 CONCLUSIONS

This report describes the new PFM analysis code for analysis of CASS piping components, PIPER-CASS. In this report, PIPER-CASS is applied to evaluate the need for NDE capable of detecting axial flaws in CASS surge line or CASS main loop piping and the need for NDE capable of depth-sizing circumferential flaws in CASS main loop piping. The results support development and revision of examination requirements to accommodate the current NDE limitations for CASS piping components in PWRs. Specifically, this report documents the results of the project scope for CASS components with axially and circumferentially oriented cracks present in the main loop piping of WEC PWRs and surge line piping of CE PWRs. The key conclusions related to axial and circumferential cracking are presented in the following sections.

For both axial and circumferential cracking, a nominal δ-*Fe* content of 40% in CF8M material was assumed in the analyses performed to bound the full range of CASS piping material. The analyses modeled the influence of degraded toughness for fully thermally aged CF8M material with a nominal δ-*Fe* content of 40%, with consideration of EPFM fracture of both part-through-wall and through-wall axial cracks.

9.1 Axial Cracking

Primary Result for Axial Cracking

The available PFM modeling results show that periodic examination to detect axially oriented flaws is unnecessary to ensure pipe structural and leak tight integrity of WEC main loop CASS piping under base load operation or FPO and of CE surge line CASS piping for base load operation.

In addition to the primary result stated in the box above, further conclusions of the axial cracking scope are as follows:

- PFM modeling under normal base loading conditions yields a rupture probability that meets the acceptance criteria in Table 5-1 to cover 80 years of operation for WEC main loop piping and CE surge line piping.[19] Furthermore, the relevant base and sensitivity cases for WEC main loop piping and CE surge line piping under normal base loading conditions showed extremely low cumulative probabilities of leakage (i.e., below 10^{-4} over 80 years).
- Surge lines in CE plants operating under FPO have an increased concern for fatigue crack growth due to the potential for a large number of insurge/outsurge transients to be triggered by FPO power shifts.

[19] As discussed in Section 5, the acceptance criteria ensure a rupture risk comparable or below that implied for ASME Code Section XI for acceptance of flaws when material behavior is fully ductile and fracture toughness is not limiting.

For CE surge line piping, the PFM analyses including FPO explicitly consider the thermal gradient stresses associated with insurge and outsurge events conservatively assumed to occur with each change in power level in addition to such events during heatup, cooldown, and hot standby. Given the fatigue crack growth predicted under this conservative assumption, the results show that 20 years of FPO (following 60 years of base loaded operation) does not meet the acceptance criteria. The number of flow reversals in the surge line during FPO has a greater effect on fatigue crack growth than the power ramp rate, and the flow rate during surge events is also a significant factor. Given the potential role of insurge/outsurge transients triggered by FPO power shifts, this report does not conclude that periodic examinations are unnecessary to detect axially oriented flaws in CE surge line CASS piping under FPO.

- For WEC main loop piping, the PFM cases specific to FPO show acceptable results for 80 years of FPO. The analyses show a benefit for significantly reduced fatigue crack growth when the power ramp rate is limited to less than 0.5% per minute for routine loading and unloading operations, based on the results for WEC main loop piping cases. Furthermore, the relevant base and sensitivity cases for WEC main loop piping under FPO conditions showed extremely low cumulative probabilities of leakage (i.e., below 10^{-4} over 80 years).
- The initial crack conditions applied in the analyses robustly address the possibility of degradation due to fatigue crack growth. Fatigue crack growth for 80 years is modeled to bound the concerns for both fatigue crack initiation and manufacturing flaws. Based on data for CASS material crediting preservice radiographic testing, an initial crack depth of 25% through-wall is applied as the baseline initial crack depth. Furthermore, the potential for coalescence of multiple pre-existing initial cracks on the same axial growth plane was explicitly considered in the analyses.
- Performance monitoring for hypothesized cracking degradation of CASS piping components in the subject piping systems is ensured by the requirements for detection of circumferentially oriented flaws and axially oriented flaws extending into dissimilar metal weld locations. Because the potential causes of axial fatigue cracking (local thermal radial gradient stresses and pressure fluctuations) yield biaxial stresses, instances of axially oriented cracking are likely to be associated with some amount of circumferential cracking. Additionally, examinations of the non-CASS material at dissimilar metal welds would provide an opportunity to detect axial cracking propagating from the CASS material. Furthermore, there have been very few such instances of cracking in stainless steel at inspectable locations analogous to the in-scope locations with CASS. Continued inspection of these non-CASS areas provides further performance monitoring.
- The above conclusions are supported by a robust set of sensitivity studies that address the modeling and input uncertainties.

9.2 Circumferential Cracking

Primary Result for Circumferential Cracking

The available PFM modeling results show that an alternative flaw evaluation methodology that does not rely on depth sizing information ensures pipe structural integrity for one fuel cycle (2 years) of continued operation when applied to circumferential cracking in WEC main loop CASS piping components.

Flaws with an end-of-evaluation-period full-length (2Θ) of 32° or less meet the limit of applicability regardless of depth.

In addition to the primary result stated in the box above, further conclusions of the circumferential cracking scope are as follows:

- The alternative flaw evaluation methodology, summarized in the following subbullets, applies to plants performing both base load operation and FPO.
  - Following detection of a circumferential flaw, determine the flaw length in accordance with a qualified length sizing process.
  - Assuming the flaw is an idealized through-wall crack (a/t = 100% and equal angular extents at the ID and OD), determine the end of evaluation period size by performing a deterministic crack growth calculation.
  - Compare the crack length at the end of the evaluation period against the limit of applicability (2Θ of 32°), and compare the design loads against the allowable bending and membrane stresses calculated per C-6320 using a/t = 1.0. If crack length and the design loads are both lower, then the flaw is acceptable for one fuel cycle of continued operation.
- Applying the acceptance criteria in Table 5-1, PFM modeling under FPO conditions (bounding of base load conditions) showed acceptable results for cumulative probability of rupture for two years of continued operation following detection of a flaw with an end-of-evaluation period full-length (2Θ) of 32°.

  A component- or plant-specific analysis that could justify less conservative transient or material toughness inputs may demonstrate the acceptability of the alternative flaw evaluation methodology for CASS surge line piping components or for flaws with a full-length (2Θ) longer than 32° in CASS main loop piping components.
- The assumption of an idealized through-wall crack for both the PFM and modified flaw evaluation methodology removes the need to have a qualified depth sizing process. Assuming the presence of an idealized through-wall crack since time zero (the start of the evaluation period) is a conservative approach from a stress intensity factor and crack stability standpoint. A sensitivity case demonstrates it is also conservative for fatigue crack growth versus a part-through-wall crack.

- A qualified length-sizing process with an uncertainty of RMSE = 0.75 inch on the full crack length (2Θ) meets the acceptance criteria. A slightly larger length sizing uncertainty can also be accommodated, but a shortened limit of applicability may be necessary to support values of RMSE beyond 1.0 inch.
- The above conclusions are supported by a robust set of sensitivity studies that address the modeling and input uncertainties.

The alternative flaw evaluation methodology is compatible with repeated use on a given flaw, with the PFM technical basis being valid for one fuel cycle (2 years) from the latest examination of the flaw. The methodology is intended to supplant the IWB-3640 flaw evaluation methodology (including the limitation of the acceptable depth to $a/t \leq 75\%$). However, other requirements may still limit the acceptability of returning the flawed component to service, such as Technical Specification requirements disallowing operation with pressure boundary leakage. The alternative flaw evaluation methodology is not generically applicable to surge line piping components.

9.3 Applicability to Other Piping Components

The applicability of the WEC main loop piping results to CASS locations in the main loop piping of B&W, CE, and AP-1000 plants (i.e., at the RCP nozzles) was evaluated to determine whether the WEC results can be leveraged as a basis for exclusion of examination for axial flaws in CASS material without dedicated analyses of each of the relevant RCP locations. Note that this does not include the weld between the RCP nozzle and SG nozzle in the AP-1000 design. To determine the applicability of the results, key geometries and loads for each of the relevant locations were identified and compared to the WEC geometries and loads. Key parameters affecting the PFM evaluations include pressure stresses, piping loads affecting subcritical growth (for circumferential cracking), pipe wall thickness, and transient profiles. These are discussed below and summarized in Table 9-1.

Hoop pressure stresses drive axial crack stability and thus are a key point of comparison between the WEC CASS main loop piping and the B&W, CE, and AP-1000 RCP main loop CASS locations. The hoop pressure stresses calculated for the WEC locations are bounding of the CE and AP-1000 locations and are representative of the B&W locations, where the B&W hoop pressure stress is about 6% greater than that of the bounding WEC location.

Similarly, the axial pressures stress for the WEC locations bound the CE and AP-1000 locations and is within 6% of the B&W location. Differences in static piping loads between components and locations are of reduced importance for the circumferential cracking results because the analysis methodology sets the loads to yield the maximum allowable stress, rather than being based on loads typical for one class of component.

Wall thickness affects both the distance over which cracks must grow to become through-wall as well as the magnitude of the gradient stresses. Larger wall thicknesses extend the distance over which cracks must grow but also result in larger RGTS that contribute to fatigue crack

growth. Therefore, the effect of wall thickness on crack growth and probability of rupture is not monotonic. The WEC analyses consider wall thicknesses of 2.32 inches and 3.09 inches, which approximately bound the thicknesses of each of the B&W (2.5 inches), CE (3.1 inches), and AP-1000 (2.56 inches) locations and demonstrate that structural and leak tight integrity is maintained for a range of pipe thicknesses.

The results of the PFM analyses demonstrate that axial and circumferential crack growth in WEC CASS main loop piping is driven by transients with large rise times and large pressure changes, namely heatup and cooldown transients. The heatup and cooldown transient profiles among the designs do not differ substantially and support the conclusion that the WEC heatup and cooldown transients for main loop piping [22] are representative of the B&W, CE, and AP-1000 locations.

Applicability of WEC Main Loop Piping Results to Other Plant Designs

Comparison of the geometry and load differences, including hoop stresses, wall thickness, and dominant transient profiles, shows that the conclusions of the PFM analyses for WEC CASS main loop piping extend to CASS locations at RCP nozzles in B&W, CE, and AP-1000 plants.

Table 9-1
Geometry and Load Differences for CASS Locations in WEC, B&W, CE, and AP-1000 Plants

Case/ Component	ID (inch)	OD (inch)	t (inch)	R_i/t	Norm. Op. P (psig)	Avg. Hoop Pressure Stress (ksi)	Avg. Axial Pressure Stress (ksi)	Ref.
Case WEC 1	22.9	27.5	2.32	4.9	2,250	11.1	5.1	This report
Case WEC 2	31.4	37.6	3.09	5.1	2,250	11.4	5.2	This report
B&W RCP Suction	28	33	2.5	5.6	2,155	12.1	5.5	[36], [37]
B&W RCP Discharge	28	33	2.5	5.6	2,155	12.1	5.5	[36], [37]
CE RCP Suction	29.9	36.1	3.1	4.8	2,250	10.9	4.9	[38]
CE RCP Discharge	29.9	36.1	3.1	4.8	2,250	10.9	4.9	[38]
AP-1000 RCP Discharge	22	27.1	2.56	4.3	2,235	9.6	4.3	[39]

9.4 Suggested Focus Areas for Future Developments

Key challenges in the development of qualification requirements for UT inspection of CASS piping components (i.e., a Section XI, Mandatory Appendix VIII, Supplement 9) have included the challenges in demonstrating the detectability of axial cracking in CASS and the depth sizing of circumferential cracking in CASS. This report provides a basis for acceptance of circumferential flaws in main loop piping components without depth sizing information and for the structural integrity of CASS piping in the presence of undetected axial cracking. ASME Code Committee actions have been initiated within Task Group Inspectability with the goal of developing ASME Code Cases to implement the alternative inspection requirements for axial cracking and the alternative circumferential flaw evaluation methodology.

Given the results and conclusions of this report, it is suggested to focus on demonstrating the following UT inspection capabilities:

- UT length sizing capabilities for circumferential cracking capable of meeting a sizing uncertainty (RMSE) of 1.0 inch or less. For circumferential cracking in the main loop piping, increases in the RMSE beyond 1.0 inch would decrease the maximum measured flaw length for which the proposed flaw evaluation methodology is applicable.
- UT depth sizing capabilities for circumferential cracking in the relatively thinner CASS piping components applicable to surge line geometry. The proposed circumferential flaw evaluation methodology is not generically applicable to these locations.

10 REFERENCES

1. ASME Boiler & Pressure Vessel Code, Section XI, Division 1, *Rules for Inservice Inspection of Nuclear Power Plant Components: Rules for Inspection and Testing of Components of Light-Water-Cooled Plants*, 2019 Edition.
2. *Nondestructive Evaluation: Cast Austenitic Stainless Steel Round-Robin Study—Summary of Results, Revision 1*. EPRI, Palo Alto, CA: 2018. 3002010314.
3. U.S. NRC, NUREG/CR-4513, *Estimation of Fracture Toughness of Cast Stainless Steels during Thermal Aging in LWR Systems*, Revision 2, Published May 2016. [NRC ADAMS Accession No.: ML16145A082].
4. Letter from C.I. Grimes (U.S. NRC) to D.J. Walters (NEI), "License Renewal Issue No. 98-0030, 'Thermal Aging Embrittlement of Cast Austenitic Stainless Steel Components'," dated May 19, 2000. [NRC ADAMS Accession No.: ML003717179]
5. Chen, Y., Alexandreanu, B., and Natesan, K., "Technical Letter Report on the Cracking of Irradiated Cast Stainless Steels with Low Ferrite Content," Argonne National Laboratory Report ANL-14/16, 2014.
6. *Nondestructive Evaluation: Flaw Tolerance Evaluation of Thermally Aged Cast Austenitic Stainless Steel Piping,* EPRI, Palo Alto, CA: 2009. 1019128.
7. *Probabilistic Fracture Mechanics Evaluation of PWR Cast Austenitic Stainless Steel Piping Components.* EPRI, Palo Alto, CA: 2021. 3002020449.
8. *Probabilistic Fracture Mechanics Evaluation of PWR Cast Austenitic Stainless Steel Piping Components – Axial Cracking Methods and Results.* EPRI, Palo Alto, CA: 2022. 3002025221.
9. K. Fuhr, M. Wolfson, G. White, M. Burkardt, and D.J. Shim, "Probabilistic Fracture Mechanics Evaluation of PWR Cast Austenitic Stainless Steel Piping Components – Axial Cracking Methods and Results," *Proceedings of the ASME 2023 Pressure Vessels & Piping Conference,* July 16-21, 2023, Atlanta, Georgia, USA. PVP2023-107363.
10. U.S. NRC Regulatory Guide 1.245, Revision 0, "Preparing Probabilistic Fracture Mechanics Submittals," January 2022. [NRC ADAMS Accession No.: ML21334A158].
11. U.S. NRC, NUREG-2247, "Extremely Low Probability of Rupture Version 2 Probabilistic Fracture Mechanics Code," August 2021. [NRC ADAMS Accession No.: ML21225A736]
12. U.S. NRC, NUREG/CR-7278, Technical Basis for the use of Probabilistic Fracture Mechanics in Regulatory Applications, Revision 0, Published January 2022. [NRC ADAMS Accession No.: ML22014A406].
13. *Materials Reliability Program: Technical Basis for ASME Section XI Code Case N-838 – Flaw Tolerance Evaluation of Cast Austenitic Stainless Steel (CASS) Piping Components (MRP-362 Rev. 1)*, EPRI, Palo Alto, CA: 2016. 3002007383.

14. ASME Code Case N-838, “Flaw Tolerance Evaluation of Cast Austenitic Stainless Steel Piping,” Section XI, Division 1, American Society of Mechanical Engineers, New York, Approval Date: August 3, 2015.
15. Letter from Palo Verde to U.S. NRC, “License Renewal Pressurizer Surge Line Inspection,” dated July 26, 2023. [NRC ADAMS Accession No.: ML23207A248]
16. ABB Combustion Engineering, *Pressurizer Surge Line Flow Stratification Evaluation*, CEN 387-NP, Revision 1-NP, December 1991.
17. R. C. Cipolla and W. H. Bamford, “Technical Basis for Code Case N-809 on Reference Fatigue Crack Growth Curves for Austenitic Stainless Steels in Pressurized Water Reactor Environments,” *Proceedings of the ASME 2015 Pressure Vessels and Piping Conference*, July 19-23, 2015, Boston, MA. PVP2015-45884.
18. U.S. NRC, NUREG/CR-6142, *Tensile-Property Characterization of Thermally Aged Cast Stainless Steels*, Published February 1994. [NRC ADAMS Accession No.: ML052580136].
19. ASME Boiler & Pressure Vessel Code, Section II Part D, *Materials Properties*, 2019 Edition.
20. *Evaluation of Flaws in Austenitic Steel Piping*. EPRI, Palo Alto, CA: 1986. NP-4690-SR.
21. xLPR Version 2.0 Technical Basis Document, “Welding Residual Stress Modeling Development,” xLPR-MSGR-WRS, Version 1.0, October 2016. [NRC ADAMS Accession No.: ML16341B049].
22. *Materials Reliability Program: Characterization of U.S. Pressurized Water Reactor (PWR) Fleet Operational Transients (MRP-393)*. EPRI, Palo Alto, CA: 2014. 3002003085.
23. Structural Integrity Associates, Inc., “Flaw Tolerance Evaluation of St. Lucie Surge Line Welds Using ASME Code Section XI, Appendix L,” Report No. 1301103.401, Revision 0, dated May 08, 2015. [NRC ADAMS Accession No. ML15314A161]
24. *Materials Reliability Program: Generic Flaw Tolerance Evaluation to Address Environmentally Assisted Fatigue for PWR Surge Lines (MRP-464).* EPRI, Palo Alto, CA: 2022. 3002020922.
25. *Flexible Operations: Effects of Flexible Operations on Primary-to-Secondary Leakage*. EPRI, Palo Alto, CA: 2017. 3002010416.
26. *Materials Reliability Program: Influence of Flexible Power Operations on Thermal Fatigue (MRP-459): Evaluation of Pressurizer Piping and MRP Thermal Fatigue Guidance*. EPRI, Palo Alto, CA: 2021. 3002020502.
27. M. E. Lapides, “Radiographic In-Service Inspection of Cast Austenitic Nuclear Plant Components,” *Materials Evaluation*, 44, January 1986.
28. Appendix 2, “Quality of Castings; ‘Residual Flaws,’” *Cast Austenitic Stainless Steel Sourcebook*. EPRI, Palo Alto, CA: 1991. TR-100034.
29. T. Griesbach, D. Dedhia, D. O. Harris, N. Cofie, A. Alleshwaram, and K. Amberge, “Further Validation of the Technical Basis of Code Case N-838 for Flaw Tolerance Evaluation of CASS

Piping," *Proceedings of the ASME 2015 Pressure Vessels and Piping Conference*, July 19-23, 2015, Boston, MA. PVP2015-45191.

30. xLPR Version 2.0 Technical Basis Document, "PWSCC & Fatigue Crack Growth and Coalescence Module Development," xLPR-MSGR-CGR, Version 1.0, June 2016. [NRC ADAMS Accession No.: ML16341B051]
31. ASME Code Case N-809, "Reference Fatigue Crack Growth Rate Curves for Austenitic Stainless Steels in Pressurized Water Reactor Environments," Section XI, Division 1, American Society of Mechanical Engineers, New York, Approval Date: June 23, 2015.
32. *Materials Reliability Program: Supplement 9 Draft—Qualification Requirements for Cast Stainless Steel Piping Welds (MRP-424).* EPRI, Palo Alto, CA: 2017. 3002010517.
33. "xLPR Software Requirements Description for xLPR Framework," xLPR-SRD-FW, Version 5.0, May 2020.
34. Letter from B. E. Thomas (NRR) to J. W. Lubinski (NRR), "Acceptance Criteria for Use with xLPR Version 2 Code," dated November 7, 2016. [NRC ADAMS Accession No.: ML16271A436].
35. xLPR Version 2.0 Technical Basis Document, "Sources and Treatment of Uncertainty," xLPR-TR-Uncert, Version 1.0, November 2018. [NRC ADAMS Accession No.: ML19337C165].
36. xLPR-GR-IG, *Inputs Group Report*, Version 1.0. December 19, 2017. [NRC ADAMS Accession No. ML19337B876].
37. Arkansas Nuclear One – Unit 1, *SAR Amendment 29*, May 05, 2020 [NRC ADAMS Accession No. ML20133J853].
38. B. Ganta and W. Bamford, *Flaw Evaluation of CE Design RCP Suction and Discharge, and Safety Injection Nozzle Dissimilar-Metal Welds*, WCAP-16925-NP, Revision 1, July 2009 [NRC ADAMS Accession No. ML092740086].
39. Southern Nuclear, "Chapter 5 – Reactor Coolant Systems and Connected Systems," *VEGP 3&4 - UFSAR*, Revision 10, June 15, 2021. [NRC ADAMS Accession No. ML21179A123].
40. NumPy v1.21 Reference, "Legacy Random Generation," accessed December 2023. https://numpy.org/doc/1.21/reference/random/legacy.html
41. xLPR Version 2.0 Technical Basis Document, "Cyclic Stress Intensity Factors Due to Operating Transients – Module Development (TIFFANY)," xLPR-MSGR-TIFF, Version 1.0, January 2016. [NRC ADAMS Accession No.: ML16341B048].
42. xLPR Version 2.0 Program: Module, Framework, and Model Activities, "xLPR Version 2.0 Stress Requirements," xLPR-TR-Stress, Version 1.1, March 2016.
43. xLPR Version 2.0 Program: "xLPR User Manual for xLPR V2.0 Framework and Modules," xLPR-UM, Version 1.2, September 2016.
44. xLPR Version 2.0 Technical Basis Document, "Surface and Through-Wall Crack Stress Intensity Factor Module Development," xLPR-MSGR-KSol, Version 1.0, June 2016. [NRC ADAMS Accession No.: ML16341B046].

45. xLPR Version 2.0 Technical Basis Document, “Surface-to-Through-Wall Crack Transition Module Development,” xLPR-MSGR-CTM, Version 1.0, April 2016. [NRC ADAMS Accession No.: ML16341B044].

46. S. X. Xu, D. R. Lee, D. A. Scarth, and R. C. Cipolla, “Closed-Form Relations for Stress Intensity Factor Influence Coefficients for Axial ID Surface Flaws in Cylinders for Appendix A of ASME Section XI,” *Proceedings of the ASME 2014 Pressure Vessels & Piping Conference*, July 20-24, 2014, Anaheim, CA. PVP2014-28222.

47. S. X. Xu, D. A. Scarth, and R. C. Cipolla, “Technical Basis for Proposed Weight Function Method for Calculation of Stress Intensity Factor for Surface Flaws in ASME Section XI Appendix A,” *Proceedings of the ASME 2011 Pressure Vessels & Piping Division Conference*, July 17-21, 2011, Baltimore, MD. PVP2011-57911.

48. S. X. Xu, D. A. Scarth and R. C. Cipolla, “Calculation of Stress Intensity Factor for Surface Flaws Using Weight Functions with Piece-Wise Cubic Stress Interpolation,” *Proceedings of the ASME 2012 Pressure Vessels & Piping Conference*, July 15-19, 2012, Toronto, Canada. PVP2012-78236.

49. D. Rudland, D.-J. Shim, and S. Xu, “Simulating Natural Axial Crack Growth in Dissimilar Metal Welds due to Primary Water Stress Corrosion Cracking,” *Proceedings of the ASME 2013 Pressure Vessels and Piping Conference*, July 14-18, 2013, Paris, France. PVP2013-97188.

50. D.-J. Shim, S. Xu, and D. Lee, “Closed-Form Stress Intensity Factor Solutions for Circumferential Through-Wall Cracks in Cylinder,” *Proceedings of the ASME 2014 Pressure Vessels & Piping Conference*, July 20-24, 2014, Anaheim, CA. PVP2014-28049.

51. United States Patent, “Device for and method of one-way cryptographic hashing,” US6829355.

52. ASME Code Case N-809-1, “Reference Fatigue Crack Growth Rate Curves for Austenitic Stainless Steels in Pressurized Water Reactor Environments,” Section XI, Division 1, American Society of Mechanical Engineers, New York, Approval Date: October 9, 2020.

53. ASME Code Case N-809-2, “Reference Fatigue Crack Growth Rate Curves for Austenitic Stainless Steels in Pressurized Water Reactor Environments,” Section XI, Division 1, American Society of Mechanical Engineers, New York, Approval Date: March 2, 2023.

54. xLPR Version 2.0 Technical Basis Document, “Crack Stability,” xLPR-MSGR-Stability, Version 1.0, June 2016. [NRC ADAMS Accession No.: ML16341B050].

55. *Ductile Fracture Handbook – Application to: Power Plants, Offshore Structures, Petrochemical Plants, Transportation Systems, Volume 3*, EPRI, Palo Alto, CA: 1991. NP-6301-D, V3.

56. A. Simon, “Errata List for Ductile Fracture Handbook (NP-6301),” Dominion Engineering, Inc. Memo M-5841-00-02, Rev. 1, October 2021.

57. xLPR Version 2.0 Technical Basis Document, “In-Service Inspection,” xLPR-MSGR-ISI, Version 1.0, June 2016. [NRC ADAMS Accession No.: ML16341B045].

A MATERIAL DATA

The material data in Appendix E of MRP-362 Rev. 1 [13] for fully aged CF8M at approximately 600°F is applied to develop input distributions for the PIPER-CASS runs performed in this report. Table A-1 contains the material strength and toughness information applied herein. For heats "75" and "AA" that had multiple toughness specimens for a single material heat with a single value of strengths, the toughness (as expressed by $J_{0.08}$) was averaged between the two specimens.

For convenience, a column is also provided in Table A-1 for the value of $J_{0.08}$ normalized to 25% δ-*Fe* using the relations for centrifugally cast material in NUREG/CR-4513 Rev. 2 [3]. Similar values would be obtained using the relations for statically cast material. To estimate $C_{v,sat}$ using the δ-*Fe*, the fitted equation in Figure 39 of that report is applied.

Table A-1
Material Data (from Appendix E of MRP-362 Rev. 1 [13])

Heat	Yield Strength [MPa (ksi)]	Ultimate Strength [MPa (ksi)]	δ-*Fe* [%]	$J_{0.08inch}$ [kJ/m² (lb/in)]	$J_{0.08inch}$ Normalized to 25% δ-*Fe* [kJ/m² (lb/in)]
75 [t/c]	254.4 (36.9)	575.7 (83.5)	24.8	365.9 (2,090)	362.1 (2,068)
205	175.1 (25.4)	502.6 (72.9)	21.0	470.0 (2,684)	375.8 (2,146)
74	217.9 (31.6)	488.8 (70.9)	15.5	444.4 (2,538)	240.8 (1,375)
AA [1/2]	199.9 (29.0)	489.5 (71.0)	10.3	673.3 (3,845)	218.5 (1,248)
pipe	171.0 (24.8)	503.3 (73.0)	15.3	505.3 (2,886)	269.3 (1,538)
C	210.3 (30.5)	630.2 (91.4)	23.1	246.2 (1,406)	222.5 (1,271)
D	230.3 (33.4)	627.4 (91.0)	17.4	269.3 (1,538)	169.2 (966)
E	250.3 (36.3)	730.8 (106.0)	23.0	107.2 (612.0)	96.3 (550)
3296	383.3 (55.6)	643.3 (93.3)	33.8	63.6 (363)	93.6 (534)
4331	333.0 (48.3)	672.2 (97.5)	23.9	125.7 (718)	118.7 (678)
2/3 elb	259.9 (37.7)	661.9 (96.0)	30.0	76.2 (435)	96.2 (550)
A	275.8 (40.0)	679.1 (98.5)	32.0	100.0 (571)	137.2 (784)
elb	222.7 (32.3)	584.0 (84.7)	27.0	62.5 (357)	69.0 (394)

B DESCRIPTION OF PIPER-CASS PFM CODE

The PIPER-CASS (Piping Integrity Probabilistic Evaluation for Reactors – Cast Austenitic Stainless Steel) PFM code focuses on modeling of fatigue crack growth and stability of CASS piping components, including thermally aged material with low toughness. This PFM code applies many of the same models as the xLPR program, but it applies them within a framework that promotes scalability and productivity for power users.

Table B-1
Module Comparison Versus xLPR

Module Name	Description	Relation to xLPR
Simulation Framework	Performs the Monte Carlo analysis (including random sampling and time loop); handles input/output, including numeric results, visualizations, and plain-text logging to file	Entirely new; Implemented in Python instead of GoldSim to avoid limitations of graphical programming (e.g., provides improved performance and version control)
Post-Processing	Automatically saves text files containing results and generates relevant figures	Entirely new
Materials	Models the probabilistic and correlated nature of material properties including strength and toughness	Significantly different; PIPER-CASS includes relationships reflecting nature of variability in CASS material properties, including correlation among YS, UTS, and toughness
Loading	Determines the stresses due to steady-state loading	Same models, with extended functionality to distinguish between Service Levels
Stress	Calculates stresses and loading applicable to growth and stability	Same models
Transients	Models the occurrence and temperature/pressure driven stresses from plant transients (precalculated)	Same models, with extended functionality; In PIPER-CASS, module is automatically run by program, and additional inputs provide greater flexibility when defining operating transients (e.g., arbitrary number of transients with different flow rates and thermal solver time steps)
Stress Intensity Factor	Performs the calculation of stress intensity factors by universal weight function method (precalculated for transient loadings)	Same models
Crack Growth	Calculates growth of cracks due to fatigue	Same model, for CASS fatigue
Crack Transition	Models crack evolution from part-through-wall to through-wall	Same models

Module Name	Description	Relation to xLPR
Crack Coalescence	Models interaction of multiple coplanar cracks (IWA-3330 proximity rules applied)	Same models
Axial Stability	Performs net section collapse (NSC) and elastic plastic fracture mechanics (EPFM) stability checks on axially oriented cracks (like xLPR, stability is checked independently for each crack)	Same NSC models and TW EPFM model, with extended functionality; PIPER-CASS has improved numeric solver for through-wall crack stability, and it adds a part-through-wall crack EPFM stability model
Circumferential Stability	Performs NSC and EPFM stability checks on circumferentially oriented cracks; multiple crack stability of all co-planar cracks by NSC	Same NSC models and TW EPFM model, with extended functionality; PIPER-CASS has improved numeric solver for through-wall crack stability, and it adds a part-through-wall crack EPFM stability model

B.1 Model Instantiation

The pre-processing phase of the framework includes all subroutines and functions necessary to transform user inputs into the full data structures required for processing the time loop. In general, PIPER-CASS is designed to perform as many realization-invariant and time-invariant calculations during pre-processing as possible to reduce the computational impact of repeated computations within the time loop. Loads, stresses, stress intensity factors for transients, and critical crack sizes for through-wall cracks are all precalculated. The critical size for part-through-wall cracks is not precalculated (see Section B.8 for more details).

Inputs to PIPER-CASS can be specified as deterministic inputs or as inputs to be sampled probabilistically. Where feasible, probabilistic values are sampled prior to the execution of the time loop. This facilitates input validation of sampled parameters and improves simulation runtime by leveraging vectorized array operations and allowing for more pre-calculation of time-invariant values (e.g., critical through-wall cracks sizes). Crack size and location parameters are sampled on a per-crack basis; other inputs are sampled on a per-realization basis.

PIPER-CASS utilizes a seeded Mersenne Twister pseudo-random number generator (MT19937) [40]. To permit precisely repeated runs, the seed may be set by user input, and the utilized seed is always printed to an output file (whether user-specified or generated). For multiprocessing, each spawned worker thread re-seeds the pseudo-random number generator using a unique seed to provide independent samples between workers.

B.2 Materials Model

The material strength, elasticity (*E*), J-integral material resistance (J-R) curve parameters, Ramberg-Osgood (RO) exponent, fatigue crack growth (FCG) equation parameters, and thermal material properties are specified by user input. Temperature dependent properties for water (as in xLPR-TIFF [41]) and the thermal conductivity of CASS (from ASME Code Section II-D M, 2015 Ed.) are included within the code for interpolation.

The material toughness (J-R curve parameters; $J_R = C_r \Delta a^m$) may be specified directly or may be derived from the correlation equations in NUREG/CR-4513 (Rev. 1 or Rev. 2). To ensure that probabilistically sampled correlated parameters are correctly distributed, material properties used in the EPFM stability calculation for the analyses documented in this report are derived from more fundamental material inputs using the correlations in NUREG/CR-4513 Rev. 2 [3]. PIPER-CASS includes the correlation equations for static cast or centrifugally cast CF8M or CF8/CF8A. The room temperature Charpy Impact Energy at saturated thermal aging (C_{vsat}) is calculated from the input δ-*Fe* content and the material composition parameter (ϕ). The variability in material composition and toughness behavior is accounted for by scaling the calculated C_{vsat} by a separate factor that is probabilistically sampled. Then, fracture resistance at thermally aged conditions, as given by the C_r and m parameters in the J_R material resistance curve, is calculated from correlations with C_{vsat}. With reference to the equations of NUREG/CR-4513, Rev. 2, the value of C_{vsat} is calculated using Equation 24 and the C_r and m parameters are calculated from C_{vsat} using Equations 28, 29, and 44 for statically cast CF8M or using Equations 37, 38, and 44 for centrifugally cast CF8M [3].

The user specifies the at-temperature yield strength (σ_y) and ultimate strength (σ_u). These may be specified as either the values reflecting saturated thermal aging (fully aged) or as an unaged strength with a corresponding aging factor. Per the common approach as reflected in ASME Code, Section XI, the aged flow strength (σ_f) is a derived parameter taken as the average of the aged yield and ultimate strengths. User specified correlation coefficients among σ_y, σ_u, and toughness (C_{vsat} variability) may also be specified. These coefficients modify the variance of the normal or lognormal distribution used for sampling. The aging factors for σ_y and σ_u may also be correlated with one another.

The implementation of the Ramberg-Osgood (RO) equation in PIPER-CASS utilizes σ_y as the reference stress[20]: $\epsilon/\epsilon_o = \sigma/\sigma_y + \alpha\,(\sigma/\sigma_y)^n$. Depending on user input, the RO α parameter is either calculated as $0.002E/\sigma_y$ [33, p. 36] or using the correlation with σ_f of CF8M in Equation A-11 of MRP-362 Rev. 1 [13].

Refer to Section 4.2 for specific details on the material property distributions applied. This module is considered Category M-4 in the context of RG 1.245.

[20] Conversion from other reference stresses is performed using Eq. 7 of NUREG/CR-6142 [18].

B.3 Loading and Stress Models

For all runs, PIPER-CASS accepts weld residual stress (WRS), normal operating conditions, and transient conditions. For normal operating conditions and transient conditions, both the pressure and temperature conditions are specified. In runs where circumferentially oriented cracks are modeled, membrane and bending stresses from deadweight, thermal expansion, and transient conditions (e.g., seismic events) are also included. These models are considered Category M-3 in the context of RG 1.245.

B.3.1 Constant Loading

The normal operating conditions specified for PIPER-CASS runs include both pressure and temperature. For circumferential cracking runs of PIPER-CASS, membrane and bending due to deadweight and normal thermal expansion are also included. The normal operating condition is stored for at-runtime calculation of stress intensity factor and is also used for pre-calculation of transient loading. As in xLPR, the normal thermal expansion (NTE) stresses included in circumferential crack runs are scaled with the fluid temperature during transients, and NTE loads are included when calculating crack stability.

WRS (hoop WRS for axial cracking and axial WRS for circumferential cracking) is superimposed on the operating conditions when calculating the stress intensity factor during normal operation. WRS tends to have a small effect on fatigue crack growth because time-invariant stresses only affect the load ratio. Since they are relieved by material yielding, WRS effects are not included in crack stability evaluations.

In summary, the module is functionally equivalent to xLPR-Stress [42] with the following minor differences: xLPR considers whether the applied loads would cause rupture without any cracks, which only results in a warning message in PIPER-CASS. PIPER-CASS also evaluates stability separately for each Service Level, while xLPR considers stability for all load conditions together (although safe shutdown earthquake conditions are considered separately).

B.3.2 Transient Loading

Transients are modeled as a combination of changes in internal pressure, mechanical loading, and/or fluid temperature. Transients in PIPER-CASS may be set to affect only crack growth, only crack stability, or both. Each transient is assigned to one of Service Level A, B, C, and D.

Radial gradient thermal stresses (RGTS) are calculated from the changes in fluid temperature using the same models as the TIFFANY module of xLPR [41]. The first time point in each transient sets the initial uniform temperature of the piping segment. Subsequent variation in temperature generates thermal gradient stresses that drive FCG. Like TIFFANY, 101 radial nodes are utilized when calculating the radial gradient of the temperature. The variation in internal pressure also generates stresses in the pipe wall. After the transient hoop stress is calculated,

the minimum and maximum stress intensity factors during each transient are calculated and stored in interpolation objects, as described in Section B.4. RGTS are relieved by small-scale yielding and self-balancing through the wall, so, consistent with xLPR, RGTS do not impact stability of any cracks or growth of through-wall cracks.

As in TIFFANY [41], the normal thermal expansion stresses vary linearly with zero stress at room temperature and the user-input values at normal operating temperature. Additional variations in global membrane or bending stresses (such as thermal stratification or seismic events) during a transient are modeled in PIPER-CASS by directly inputting these stresses as part of a transient and superimposing them on the extremes of the pressure and temperature stresses. This modeling behavior is the same as implemented by TIFFANY [41] for a "Type II" stress; the K_I from the user-input stress is added to the maximum K_I and subtracted from minimum K_I. Consistent with TIFFANY, PIPER-CASS only applies variations in global membrane and bending stresses due to transients to circumferential cracking; because they are axial stresses, they do not affect fatigue crack growth of axial cracks.

A listing of differences between TIFFANY and PIPER-CASS include:

- PIPER-CASS simplifies the equations by only modeling a single material (rather than two layers of different metals).
- PIPER-CASS permits an arbitrary number of transients (rather than being limited to 20).
- PIPER-CASS permits the user to specify a different flow rate and stress solver timestep for each transient. The xLPR-TIFF preprocessor uses a single global flow rate and programmatically selected timestep that may not be refined enough to capture rapid fluctuations.
- PIPER-CASS includes the stress and stress intensity factor for time = 0 when determining the minimum / maximum K_I. xLPR-TIFF does not include the first timepoint (time = 0 state) when calculating minimum / maximum K_I.
- PIPER-CASS uses superposition to reduce computation time for circumferential cracks. The K_I-solution is obtained for membrane-only and maximum global bending-only, then the bending K_I is scaled by the angular position to find K_I for each angular point. Additionally, angular points over a range 0 to π are stored, leveraging symmetry. xLPR directly evaluates each point in the full 0 to 2π range.
- PIPER-CASS provides diagnostic plots of the transient stress history, and it warns the user if the end of the thermal transient definition may be inadvertently truncating the rise time used for FCG.

The modifications from TIFFANY, particularly the ability refine flow rate and timestep in the RGTS solver, provide better modeling of the rapid changes in fluid temperature caused by insurges and outsurges in pressurizer surge lines.[21]

Transients may be specified to occur on a deterministic frequency (equivalent to a value of 0 for the xLPR front-back loading ratio [43]), or the rate of occurrence may vary randomly each timestep of the time loop used to simulate crack growth. For infrequent transients (nominal frequency of < 75% timesteps), a random number is sampled for each timestep to determine whether the transient occurs at that timestep. Otherwise, an integer number of occurrences is sampled between 0 and twice the nominal frequency. Each transient may be assigned a different onset and termination time outside of which there are no occurrences.

PIPER-CASS produces several plots for each transient which help ensure the input is correctly specified, in particular that the flow rate, thermal calculation timestep, and final time point are specified appropriately. These plots provide key intermediate results from the thermal and stress solutions for each transient. Examples of these plots (Figure B-1, Figure B-2, Figure B-3, Figure B-4, and Figure B-5) are shown for a heatup transient. A key improvement versus xLPR is that the user is notified if the cumulative rise time is being truncated by the end of the transient time history definition. If the residual temperature differential profile (Figure B-5) is hotter at the ID and the rise time (Figure B-3) is increasing at the end of the transient, the stress at the ID of the pipe may continue to become more tensile as the temperature equilibrates, so the rise time may continue to increase if another time point were added to extend the duration of the final pressure and temperature state. The user is notified in such cases because this affects the FCG rate.

[21] References to the timestep in this report refer to the time loop timestep for simulating crack growth (typically 1 month), unless specified to be the timestep for the thermal stress solver. The transient thermal and stress solver operates as a pre-processor with an independently set timestep (typically on the order of seconds) for each transient.

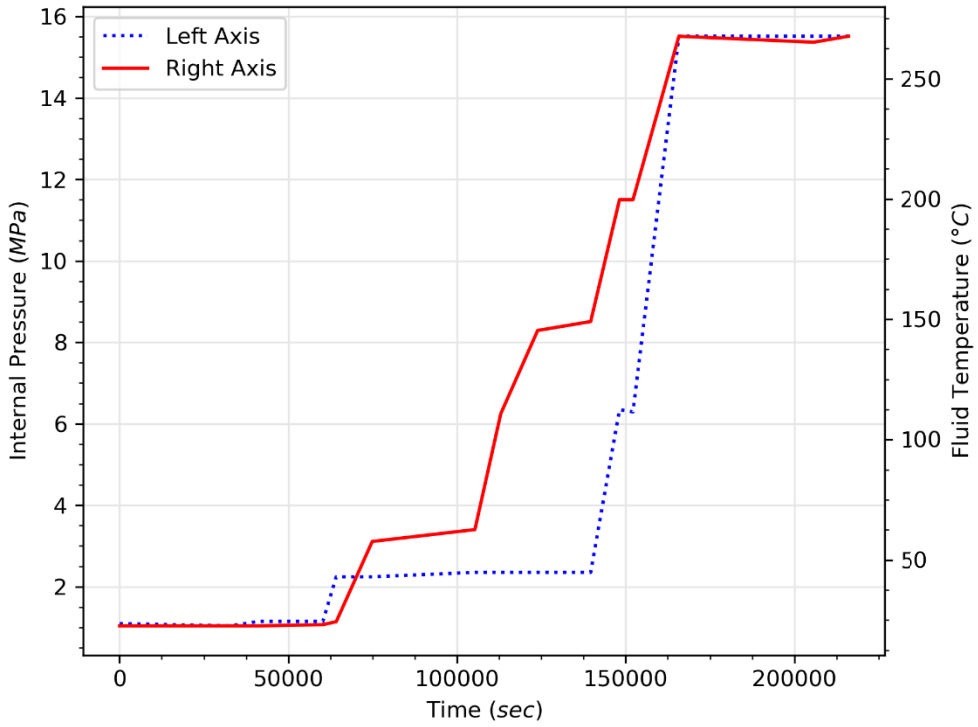

Figure B-1
Fluid Temperature and Pressure History of the Heatup Transient

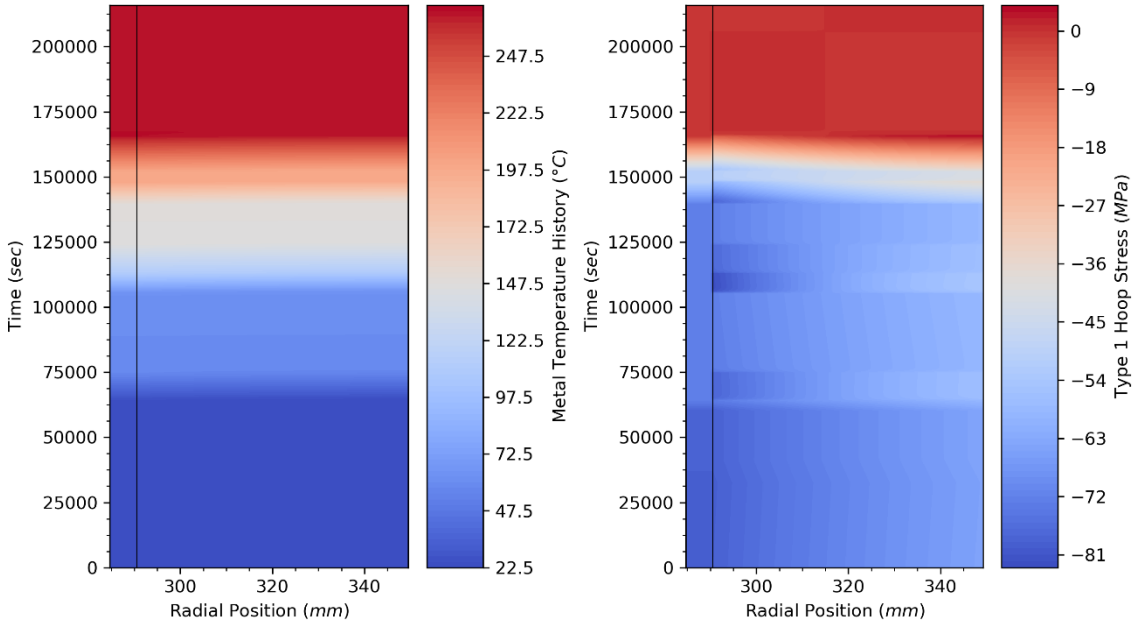

Figure B-2
Time History of Radial Temperature and Stress Through the Pipe Wall for the Heatup Transient (Inside the ID (< 290 mm) Shows Coolant Temperature and Hoop Pressure Stress)

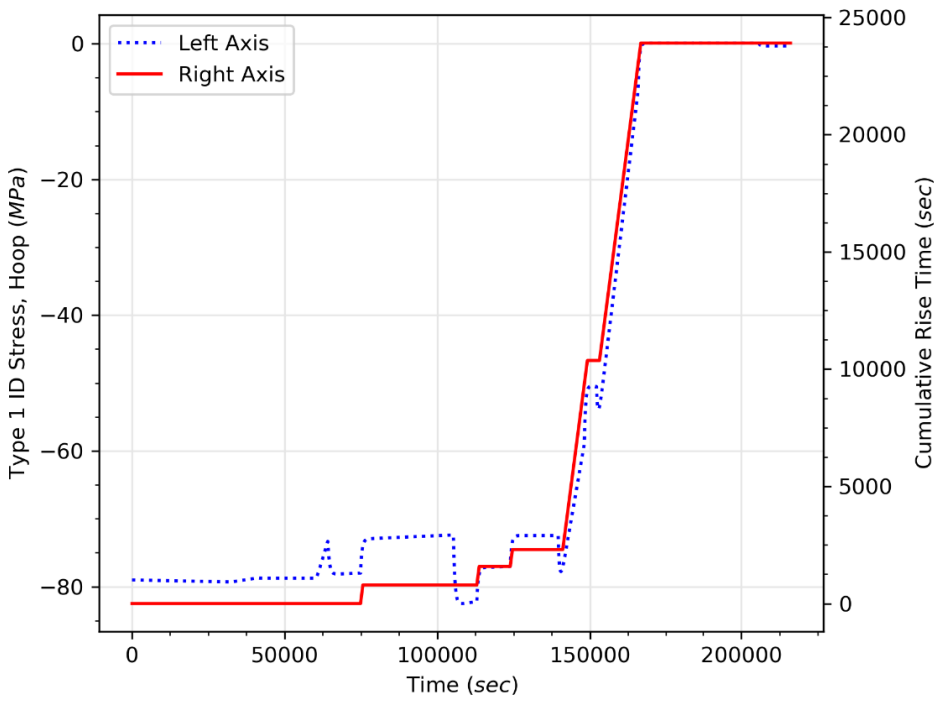

Figure B-3
Time History of ID Stress and Cumulative Rise Time for the Heatup Transient

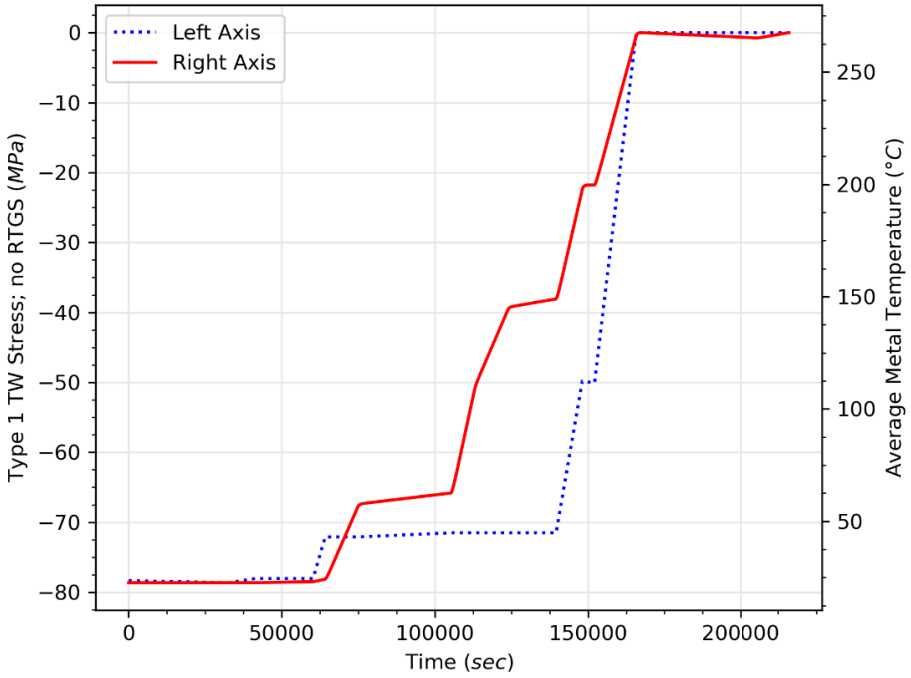

Figure B-4
Time History of Stress Applied for Through-Wall Crack Growth from Heatup Transient

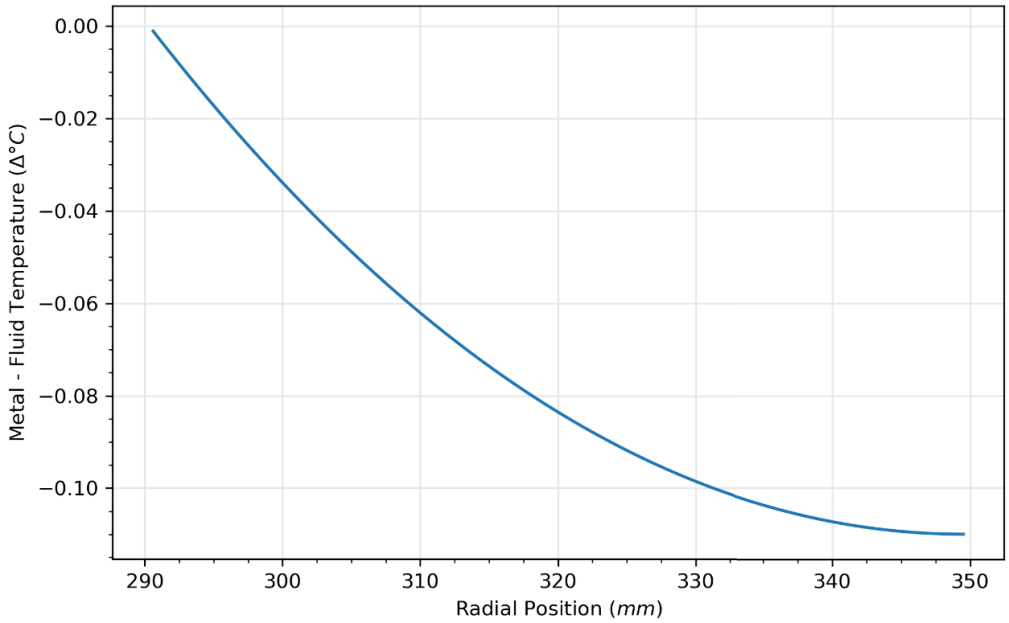

Figure B-5
Radial Gradient of Temperature Difference Between Pipe Metal and Fluid at End of Heatup Transient

B.4 Stress Intensity Factor Calculation

The stress intensity factor (K_I) is calculated from the through-wall stress distribution using the same equations as xLPR-KPW [44], xLPR-CTM [45], and xLPR-KTW [44]. These are weight function method solutions ([46], [47], [48], [49], [50]) that can handle an arbitrary stress profile defined on uniform discrete points varying in the radial dimension through the pipe wall.[22] For part-through-wall cracks, the crack is modeled as semi-elliptical in shape (i.e., semi-elliptical surface crack, SESC). Through-wall cracks may be idealized (rectangular) or transitioning (trapezoidal). The transitioning through-wall crack (TRN) is calculated by finding the stress intensity factor for an equivalent size idealized through-wall crack (TW) equal to the length of the TRN at the ID, then applying adjustment factors from xLPR-CTM to scale the K_I at the ID and OD. These models are considered Category M-3 in the context of RG 1.245.

The normal operating K_I (due to pressure stress, crack face, and WRS) is superimposed with the transient minimum and maximum transient K_I (due to the change in pressure stress and thermal gradient stresses) for calculating fatigue crack growth using the same equations as xLPR-TIFF [41]. For each timestep, the K_I for all cracks is calculated once for normal operating loads and once for each transient which contributes to growth in that timestep, as in xLPR-TIFF.

[22] *K* from global bending stress (for circumferential cracks only) is calculated using the method of influence coefficients [46]. The total *K* for growth is then applied as the sum of membrane and bending components.

The K_I for normal operating stresses is calculated directly each timestep. In contrast, the K_I for transients is pre-calculated as multidimensional interpolation objects for SESC and TW crack shapes that yield K_I for any valid crack size. For TRN cracks, the TW transient K_I is obtained by interpolation then the correction factor for the TRN shape is calculated directly for that timestep.

The transient K_I calculation involves a computationally intensive thermal stress solver performed for each transient time history (Section B.3.2). Prior to the time loop, multi-dimensional transient stress intensity factor arrays (crack depth versus crack aspect ratio for SESC and normalized crack length for TW cracks) are calculated at a grid of user-specified points. These points are specified with a density at least as great as the hard-coded grid in xLPR-TIFF. The following K_I values are pre-calculated:

- Minimum and maximum K_I at the surface point and deepest point for part-through-wall cracks, as a function of crack aspect ratio, relative crack depth, and (for circumferential cracks only) crack center circumferential position.
- Minimum and maximum K_I for through-wall cracks, as a function of crack length and (for circumferential cracks only) crack center circumferential position. The crack length is specified as normalized crack length (circumferential extent for circumferential cracks; crack length divided by characteristic length for axial cracks).
- Minimum and maximum inner diameter (ID) stresses.
- Rise times (stress at the ID becoming more tensile at a rate ≥ 6.9 mPa/hr (1 ksi/hr)).

Each of these pre-calculated arrays are stored in Python objects that provide a linear interpolation method that prevents extrapolation. Interpolation in the time loop is much more computationally efficient than directly calculating these values for individual crack shapes at each timestep. These interpolation objects are saved to disk as non-human readable serialized interpolation objects that can be reloaded during subsequent runs of PIPER-CASS with the same inputs. All inputs used to generate these arrays are hashed as a unique name for the file using the SHA256 algorithm [51]. By hashing any arbitrary set of inputs, PIPER-CASS can quickly determine if the required tables have already been calculated. Further, the inputs are also saved in the object and are matched to the current input to ensure the correct tables are loaded from disk.

B.5 Crack Growth Calculation

Fatigue crack growth at each of the modeled crack tips (surface and deepest points for surface cracks, ID and OD surface tips for through-wall cracks) is performed independently based on the minimum and maximum K_I for each transient that occurs in the timestep during which growth is evaluated. Any transients defined as Service Levels C or D do not contribute to crack growth.

PIPER-CASS implements the fatigue growth models for austenitic stainless steels from xLPR-CGR [30]. The xLPR program provides recommended fatigue crack growth rate equation parameters:

coefficient, ΔK_I threshold scaling factor, exponent, alloy factor, rise time, load ratio effects, and temperature effects for austenitic stainless steel [30]. To account for growth in different alloys, the load ratio effect and FCG rate coefficient differ by category of stainless steel alloy. This model is considered Category M-3 in the context of RG 1.245. As with xLPR, RGTS is modeled to not cause growth in through-wall cracks. An option is included to apply FCG model parameters per ASME Code Case N-809 [31], which differs from xLPR in the choice of alloy factor (i.e., FCG rate coefficient) for CF8M and CF3M and of ΔK_I threshold for growth ($\Delta K_{I,th}$) for each of the alloys.

Differences among the alloy factors (FCG rate coefficients) recommended by xLPR-CGR [30], N-809 [31], and N-809-1 [52] are shown in Table B-2. PIPER-CASS applies the stainless steel alloy factor for CF8M as recommended by xLPR. In Code Case N-809, the Type 304 curve was applied to define the behavior for Type 304 and Type 316 as a conservative simplification [17]. Similarly, the Type 304L curve was applied to define the behavior for Type 304L and Type 316L. In each case, the same coefficients were assumed to extend to the cast equivalents. Revision N-809-1 [52], which modified the stress ratio, R, effect specified in N-809, applies the same alloy coefficients as N-809. Figure B-6 shows the ratio of growth rates predicted by N-809 and N-809-1 to the median growth rate modeled in PIPER-CASS for a selection of $K_{I,min}$ and ΔK_I values. For reference, the 90th percentile of the distribution of FCG rate variability applied by PIPER-CASS is 1.7 times higher than the median. N-809-2 [53] does not change the equations or parameter values from N-809-1; it adds an alternate methodology for the calculation of an "effective rise time" parameter that yields a different FCGR for transient cycles with non-monotonic rising K_I.

Table B-2
Stainless Steel Alloy Factor Comparison Between N-809 [31] and xLPR [30]

CASS Alloy	Wrought Alloy Equivalent	Value of C_{SS} $\left[\frac{\mathrm{mm}}{\mathrm{cyc}}\ \left(\mathrm{MPa}\sqrt{\mathrm{m}}\right)^{-n_{SS}}\right]$	
		CC N-809, -1, and -2	xLPR Median
CF8	304	9.10×10^{-6}	9.10×10^{-6}
CF3	304L	1.39×10^{-5}	1.39×10^{-5}
CF8M	316	9.10×10^{-6}	7.28×10^{-6}
CF3M	316L	1.39×10^{-5}	9.10×10^{-6}

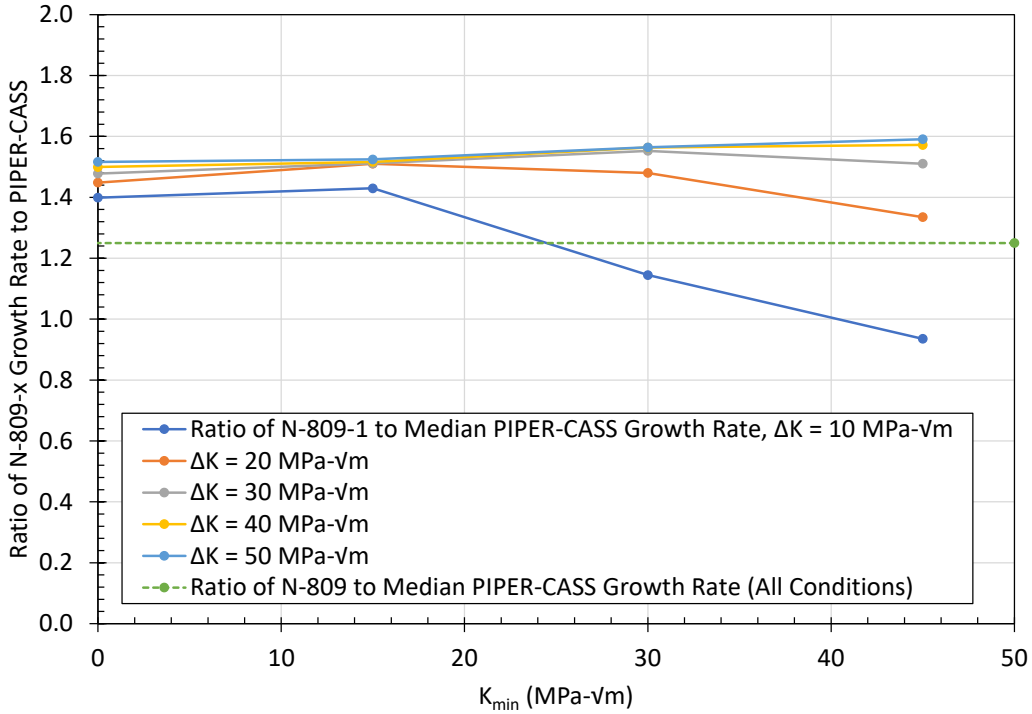

Figure B-6
Comparison of Fatigue Crack Growth Models

B.6 Crack Transition Modeling

In PIPER-CASS, cracks transition between different crack types in the same manner as xLPR [45]. This model is considered Category M-3 in the context of RG 1.245. Surface cracks transition from semi-elliptical shapes to transitioning (trapezoidal) through-wall cracks if the crack depth exceeds 95% of the component thickness. Transitioning through-wall cracks transition to idealized through-wall cracks if the ratio of the ID length to the OD length is less than 1.05. Axial and circumferential surface cracks may also transition to idealized through-wall cracks (skipping TRN) by failing a stability check under Service Level A, B, or C loading. Under Service Level D loading, unstable surface cracks are checked for stability under that loading as a through-wall crack, but the surface crack does not transition, consistent with the treatment of safe shutdown earthquake loading in xLPR.

B.7 Crack Coalescence Modeling

Coplanar pairs of cracks can coalesce into a larger crack, to account for increased crack growth rates due to crack interaction when cracks are within close proximity of each other. PIPER-CASS implements rule-based coalescence models as in xLPR-Coalescence [30], with key modifications from xLPR-Coalescence as described below. These rule-based coalescence models vary for different pairwise combinations of crack types and follow the same methodology as xLPR. This model is considered Category M-3 in the context of RG 1.245.

The key differences between PIPER-CASS and xLPR-Coalescence are:

- PIPER-CASS does not have an idealized through-wall crack (TW) / transitioning through-wall crack (TRN) distance rule modifier option, only physical overlap causes coalescence.
- In PIPER-CASS, coalescence for each crack is only evaluated against the nearest unabsorbed crack on the right (for axial orientations) or clockwise direction (for circumferential orientations, includes 0/2π wrap-around), but this evaluation is repeated until no further coalescences are predicted for the set of cracks in each realization.
- PIPER-CASS models pair-wise coalescence of axial cracks in addition to pair-wise coalescence of circumferential cracks.

B.8 Crack Stability Calculation

The stability models implemented in PIPER-CASS are largely build on xLPR-AxCS, xLPR-SC_fail, and xLPR-TWC_fail [54], with added functionality to evaluate EPFM stability of part-through-wall cracks, modifications to improve EPFM stability model solution convergence, and added functionality to separately evaluate stability for each Service Level. The models adapted from xLPR are considered Category M-3 in the context of RG 1.245.

As with xLPR, the stability of through-wall cracks is determined by comparison against the critical crack length. However, for part-through-wall cracks, stability of the crack size at each timestep is directly evaluated. The net-section collapse (NSC) criterion is evaluated by comparing the applied stress against the critical stress, and the EPFM stability of a crack of a given size can be determined by solving for the crack extension at which $J=J_R$ then stable cracks are those where the derivative of J_R is greater than J.

Interaction of multiple cracks in the context of stability is only considered by the circumferential NSC solution, which is the same as xLPR. For other categories, interaction of multiple cracks is not considered by the stability module (i.e., it is assumed that any cracks that do not interact enough to cause coalescence do not interact for stability); see instead coalescence in Section B.7.

The classification of stresses that do and do not impact crack stability is the same as in xLPR. For axial cracks, only stresses due to pressure generate a hoop stress contributing to instability. For circumferential cracks, stresses contributing to instability include axial membrane stresses due to the end cap pressure, stresses (both membrane and global bending) imposed by static loads, and any “Type II” stresses imposed by transients. Thermal gradient stresses are relieved by yielding and self-balancing over the wall thickness (in axially uniform areas of hoop stress and in any cross-section in axial stress), so they are considered to not impact crack stability.

In addition to the models applied in xLPR, PIPER-CASS includes EPFM stability models for constant-depth part-through-wall cracks. These models (and the part-through-wall NSC solutions) are applied for SESC cracks by evaluating the stability of an equivalent size constant-

depth crack with the same ID length and depth as the SESC (i.e., it circumscribes SESC geometry). Both the axial part-through-wall crack EPFM model and the circumferential part-through-wall crack EPFM model are considered Category M-4 in the context of RG 1.245.

As is the approach taken by xLPR, stability for transitioning through-wall cracks is evaluated considering an equivalent idealized through-wall crack with length equal to the average of the inner and outer lengths of the transitioning through-wall cracks.

Example results of the circumferential through-wall crack stability model are shown in Figure B-7 for Service Level A loading. Each of 10 realizations of the simulation is plotted with the corresponding minimum critical crack size marked. For this example, NSC produces the limiting crack size for seven realizations while EPFM produces the limiting crack size for three realizations.

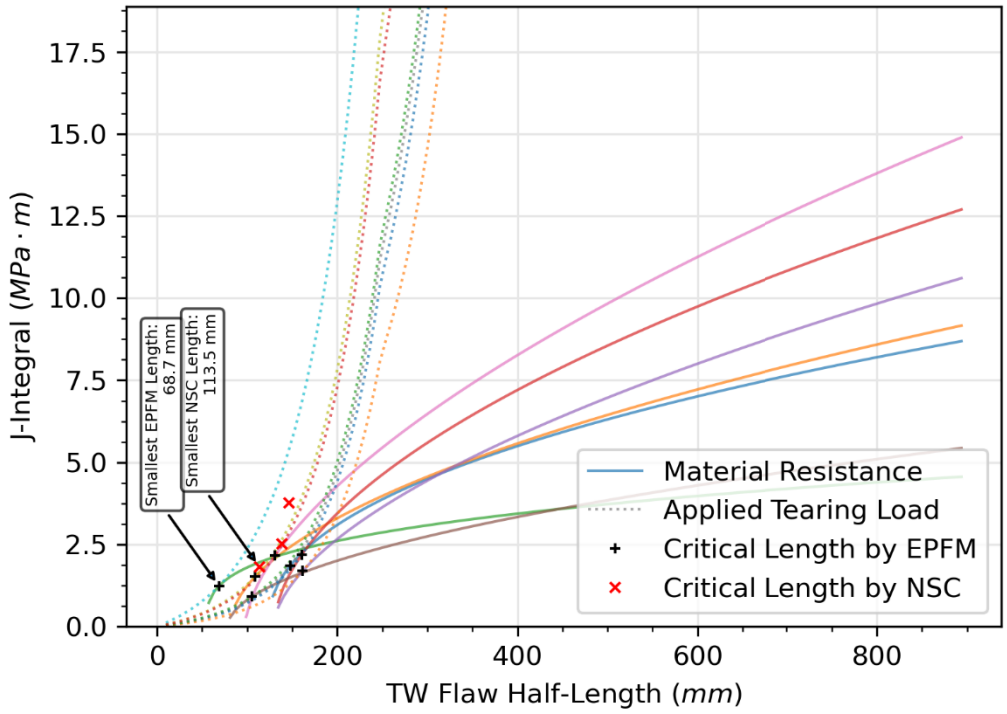

Figure B-7
Example of J-Integral and Critical Through-Wall Crack Sizes at the Mean Radius (R_m) for Circumferential Cracks at Service Level A for 10 Realizations (EPFM Limiting for 3 Realizations, NSC Limiting for 7 Realizations)

B.8.1 Axial Cracking

B.8.1.1 Net-Section Collapse (NSC)

For axial surface cracks, the constant depth surface crack plastic collapse solution from xLPR-AxCS is applied. If the pressure exceeds the critical pressure, ligament blow-out occurs, and the surface crack is modeled to become an idealized through-wall crack.

For axial through-wall cracks, the limit load solution from xLPR-AxCS is applied. If the crack is unstable, a rupture occurs.

B.8.1.2 Elastic-Plastic Fracture Mechanics (EPFM)

For axial surface cracks, EPFM stability is evaluated using either the infinite length axial crack or the finite semi-elliptical surface crack J-integral solutions from the EPRI Ductile Fracture Handbook [55] (with correction of identified errata [56]).[23] The critical crack depth yielding instability does not completely align between these models at the limit of applicability for the finite length model. The following approach is taken to yield a monotonic and continuous critical depth as a function of length, as seen in Figure B-8. For cracks longer than the limit of applicability of the finite length model ($c/a > 20$), the J-integral is calculated using that for an infinite length axial crack. For shorter cracks, ligament collapse is predicted when the crack depth would lead to instability using the solution for both an infinite length axial crack and the finite length semi-elliptical axial crack solutions. The current crack stability is directly determined by comparison of the derivative of J-integrals with respect to crack depth extension when the applied loading and material resistance J-integrals are set to be equal. As with NSC, ligament instability results in crack transition to an idealized through-wall crack.

For axial through-wall cracks, the EPFM solution from xLPR-AxCS is applied. A different numeric solver approach than xLPR-AxCS is applied to solve the implicit equations, as described in Section B.8.3. If the crack is unstable, a rupture occurs.

[23] The influence coefficient H1 is only available for $R_i/t=10$, and these values are assumed to be reasonable for application to the pipe geometries being evaluated using PIPER-CASS.

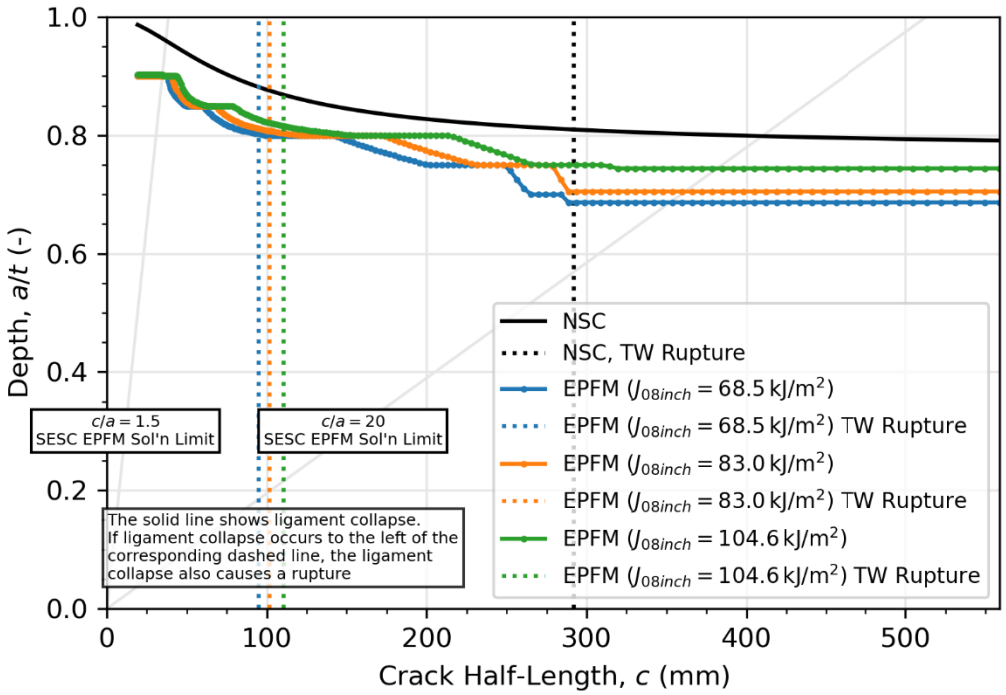

Figure B-8
Example Collapse Depths of Axial Surface Cracks for PIPER-CASS Approach Considering Both Finite and Infinite Solutions

B.8.2 Circumferential Cracking

B.8.2.1 Net-Section Collapse (NSC)

For circumferential surface cracks, the NSC solution from xLPR-SC_Fail [54] is applied. For the multiple circumferential crack NSC models, transitioning through-wall and idealized through-wall cracks are represented as equivalent surface cracks having a constant depth of 99% through-wall. If more than one crack is present and the bending moment exceeds the critical bending moment, this is treated as a rupture. If the realization has only one crack and that crack is a part-through-wall crack, then instability results in ligament collapse and crack transition to an idealized through-wall crack.

For circumferential through-wall cracks, the net section collapse solution from xLPR-TWC_Fail [54] is applied.

B.8.2.2 Elastic-Plastic Fracture Mechanics (EPFM)

For circumferential surface cracks, PIPER-CASS evaluates EPFM stability using the J-integral solutions developed in MRP-362 R1, Appendix B [13] for a constant-depth circumferential crack under combined tension and bending loading. This solution leverages the tabulated values for h_1 from the EPRI Ductile Fracture Handbook [55]. As with NSC, ligament instability results in crack transition to an idealized through-wall crack.

For circumferential through-wall cracks, the LBB.ENG2 model from xLPR-TWC_Fail [54] is applied.

B.8.3 Through-Wall Crack Critical Size Solver

The critical crack lengths for a through-wall crack under the load condition of each transient selected to affect crack stability (and normal operation) are pre-calculated once prior to entering the time loop. In the time loop, the current length of any through-wall cracks is compared to these stored critical lengths.

The critical through-wall crack size is a function of material parameters and applied loads, so each realization has its own critical through-wall crack size when material parameters are probabilistically sampled. Calculation of the critical through-wall size involves solving for the minimum size at which rupture is predicted by the stability criteria of either the NSC or EPFM models.

PIPER-CASS applies an interpolation-search method with multiple initial guesses to ensure the global solution (i.e., smallest critical crack size) is found. This method replaces the Newton-Raphson and backup downhill-simplex method solvers in the xLPR stability modules (xLPR-AxCS and xLPR-TWC_fail). In certain instances, particularly with low-toughness material like thermally aged CASS, the non-smooth nature of the applied J-integral curve causes the Newton-Raphson solver to yield a local solution to the EPFM model equations that over-estimates the critical crack size. If the Newton-Raphson solver fails to converge, the downhill-simplex solver may silently yield an unconverged solution.

B.9 Inspection

The inspection module of PIPER-CASS uses the same models as in xLPR-ISI [57] to model piping NDE examinations, but inspections are not included in the cases considered by this report.

B.10 User Interface: Input and Output

User input for PIPER-CASS is stored in text files that use the YAML markup language to designate the input data structure. Deterministic and distributed input parameters can be specified. A large number of statistical distributions are available, and they may be truncated, scaled, or shifted by the user. The input file and other options (e.g., input and output directory) are specified by the user via command line interface at runtime. PIPER-CASS generates outputs that include plain text results, figures and image results, and log files. The richness of output can be changed by user settings from providing intermediate results at each timestep to only providing summary results at the end of the modeled period. For repeatability of runs, the input file and the random number generator seed(s) are always echoed. For deterministic (i.e.,

single realization) runs, PIPER-CASS includes a utility that can create a video visualizing the time history of crack geometry for a single realization.

In the event of an error, PIPER-CASS writes the error message to the log, writes key data from the program state to file, and exits. Extensive at-runtime validation of the user inputs and intermediate calculation results are included with custom descriptive error messages.

Additional ancillary files are also provided that assist with debugging, graphics generation, cloud computing deployment, and other tasks. These files do not affect the results of the simulation and are not detailed in this report.

B.11 Verification and Validation

The PFM results presented in this report were produced using PIPER-CASS v1.1, which was developed and tested in accordance with the requirements of a custom software project plan (CSPP) developed by Dominion Engineering, Inc. (DEI) for this purpose. The plan imposes appropriate quality assurance requirements for development and testing of custom PFM engineering analysis software. These quality assurance requirements in substantial part were modeled after the quality assurance requirements established under the xLPR PFM project. The xLPR quality assurance requirements were designed to fulfill a specific set of software work practice requirements within NQA-1-2008 (including Addenda 2009).

The governing CSPP and DEI procedures incorporated by reference outline personnel qualification requirements, assign responsibilities, define the custom software documentation that forms the baseline of the lifecycle documentation, and give guidance on configuration control as well as code style. PIPER-CASS software baseline documentation includes the following documents:

- Custom Software Project Plan (CSPP)
- Software Requirements Specification (SRS)
- Requirements Traceability Matrix (RTM)
- Software Design Description (SDD)
- Software Implementation Files (SIF)
- User Instructions (UI)
- Software Test Plan (STP)
- Software Test Report (STR)

The quality-affecting work activities for developing and managing commercially developed software are established in the governing CSPP. This document specifies any coding standards to be used, identifies key personnel and their associated roles and responsibilities, and defines

controls that govern SIF development. Key aspects of the various software baseline documentation are as follows:

- The required functionality of the software is captured in the SRS. The requirements specification consists of a number of uniquely identified requirement items, each of which should be complete, verifiable, consistent, and traceable. At their core, the requirements given in the SRS describe what the software must do, but not necessarily how it is implemented. Key types of requirements include input constraints, specification of particular numerical or analytical solutions to be used, information that is recorded as an output, design assumptions, and security features. The sum of the software requirements describes the totality of the required functionality for the software, and verification that the software requirements are met indicates that the software is implemented as designed.
- An RTM is developed to document the traceability of software requirements and test cases. This matrix provides a mapping between the SRS and STP. The RTM demonstrates requirement coverage such that each requirement in the SRS is verified by one or more test cases given in the STP.
- The software design is documented in the SDD. This document provides a detailed description of the software components and interfaces, as well as the models and assumptions that inform those design choices. While the SRS defines what the software must do, the SDD describes how those requirements are implemented. As appropriate, the SDD captures information about the control and process flow of the computations and describes each software module and its constraints.
- Software implementation files contain the code that comprises PIPER-CASS and its supporting utilities. These files contain code in text-based or binary-based formats, and are separated into distinct modules by function, as described in the SDD. The software implementation files are version-controlled, and the modification history of each file is retained. The SIF were prepared by qualified software developers and developed in accordance with the governing coding standards for the Custom Software as specified by the CSPP.
- The user instructions provide information about how to install and run the software. These instructions are included with the SIF, and include information associated with the preparation of inputs, steps necessary to use the software, expected results of successful operation, and verification instructions for operating the automated test suite.
- The requirements and instructions for the work activities associated with testing the custom software are specified and documented within the STP. The STP provides the procedure to verify that the software meets all of the requirements as defined in the SRS. Each requirement is verified to be met through one or more uniquely identified test cases. Test cases are either conducted manually by a software tester or executed by automated testing software.

  Leveraging automated tests provides a number of benefits, including the ability to perform both functional testing (by testing that the software output produces the expected result given a certain set of inputs) and unit testing (by testing that individual functions or

modules perform as expected, in isolation from the other software modules) and the option to validate software performance during development following an incremental codebase change. Throughout software development, the automated test suite was periodically executed to quickly identify any unintended behavior or introduced bugs. Where the expected results match those for xLPR modules, xLPR module-level test cases were incorporated as automated functional tests within the STP to provide additional confidence in the software performance. The xLPR modules which have some applicable tests to the PIPER-CASS software are the coalescence (xLPR-Coalescence), growth (xLPR-CGR), inspection (xLPR-ISI), stress intensity factor (xLPR-KPW and xLPR-KTW), TIFFANY (xLPR-TIFF), transition (xLPR-CTM), and stability (xLPR-AxCS, xLPR-SC_fail, and xLPR-TWC_fail) modules.

- The results of the testing for each software baseline are documented in the associated STR. If each test case is successful, then the software is deemed acceptable. If one or more test failures reveals deviations from the requirements specifications, then the deviations must be resolved, either by resolving the errors and demonstrating that the previously failing tests now pass, or by dispositioning the errors as acceptable.

C BENCHMARKING VERSUS XLPR

Given the commonalities between PIPER-CASS and xLPR, benchmarking cases are developed to identify differences in the calculated results given an equivalent set of inputs. Cases are considered for circumferential and axial crack orientations. Benchmarking focused on deterministic (single realization with constant input values) cases rather than probabilistic runs. Since PIPER-CASS and xLPR use the same or compatible equations for stress intensity factor, fatigue crack growth, coalescence, and stability, the deterministic results should match in cases focusing on these modules. As noted in Section B.11, xLPR test cases for these modules are also leveraged in the V&V for PIPER-CASS. Reasons were identified for all significant differences in results, and it was ensured that for the benchmarking, PIPER-CASS—albeit a modified version that incorporates the xLPR approach for any differences—provides agreement with xLPR results.

C.1 Incorporation of xLPR Differences

Remaining differences were identified and dispositioned as either an intentional difference in approach taken by PIPER-CASS or as an issue in the xLPR codebase. Issues in the xLPR codebase have been reported to the developers of xLPR. Extensive use of “debug mode” within the integrated development environments (IDE) was used in the disposition of differences, as this allowed variable values to be tracked and compared at runtime.

For this benchmark, a modified version of PIPER-CASS was created which adopted differences from xLPR modules with the goal of obtaining agreement in benchmarking results. Because PIPER-CASS is subject to git version control, the modified code for this benchmark is maintained separately from the primary version of PIPER-CASS used for this report. As PIPER-CASS is written in plaintext code (rather than a programmable graphical user interface (GUI) like the xLPR framework), simple text comparison also can be used to review the differences implemented into this branch of PIPER-CASS. The changes made to reflect intentional differences versus the documented xLPR approach are listed in Table C-1. Additional changes to PIPER-CASS needed to align with the state of the xLPR codebase are listed in Table C-2; these items have been submitted to the xLPR maintenance program to be addressed in future releases of xLPR. Other differences in approach with xLPR represent additional functionality in one code or the other that can be matched by changing the inputs of one code or the other.

Table C-1
Modifications to Match xLPR due to Intentional Differences Versus Documented xLPR Approach

PIPER-CASS	Modification to Match xLPR
Includes EPFM stability modules for part-through-wall cracks	These modules are disabled
Ramberg-Osgood exponent (n) is directly input by the user	Use equation from xLPR Requirement RFW-L1-52 [33, pg. 36] to calculate n based on σ_y and σ_u
Raise an error and exit the program if a through-wall crack grows beyond the range of pre-calculated ΔK_I	Allow growth of through-wall cracks beyond a limited range of pre-calculated ΔK_I due to transients, clipping the ΔK_I at the limit
Continue crack growth until rupture occurs under all of A, B, C, and D	Halt growth when rupture occurs due to any of Service Level A, B, or C transients

Table C-2
Additional Modifications to Match Behavior of xLPR Codebase

PIPER-CASS	Modification to Match xLPR v2.0d Behavior
Applies the normal operating pressure as part of axial stability calculations	For only axial stability calculations, reduce the normal operating pressure by a factor of R_i / R_m.
In the axial TW crack EPFM stability module, truncate the values of the nondimensionalized length ("rho") and RO n to the limits of the look-up tables when obtaining values for the look-up tables.	Additionally, truncate the values of rho and RO n through all parts of the J-integral calculation, including analytical equations.
Calculate K_I for transitioning through-wall cracks using the half-length at R_i.	Calculate K_I for transitioning through-wall cracks using the average half-length at R_m.
Pre-calculate the ΔK_I for through-wall cracks for each transient, applying the maximum and minimum values for the current transient.	For each transient, apply the maximum and minimum values of K_I across all transients that have already been evaluated up to and including the current transient when finding ΔK_I.[24]
Additionally, the version of the xLPR framework used for comparisons was modified so that the K_I influence factors for transitioning through-wall cracks are correctly applied for all transients.	

[24] This behavior is addressed in xLPR v2.2. Unmodified PIPER-CASS was confirmed to agree with the output of TIFFANY from xLPR v2.2 for the benchmark case transients.

C.2 Inputs for Benchmarking Cases

Equivalent inputs are passed to xLPR and PIPER-CASS so that any differences in results could be identified, traced, and dispositioned. A higher material toughness is applied in the benchmarking case to avoid differences due to difficulty in achieving convergence with the xLPR EPFM stability solver at low toughness values. To match xLPR, the toughness is directly specified as an input instead of being calculated from the material composition factor and δ-*Fe* level using the correlations described in Section B.2. Benchmarking cases applied the same transient definitions, including a Cooldown transient modified to increase growth rates.

C.3 Results of Benchmarking

As seen in Figure C-1 (axial) and Figure C-3 (circumferential), near-perfect agreement was obtained for deterministic fatigue crack growth rates between PIPER-CASS and xLPR after incorporating the modifications described in Section C.1. This is reinforced by the agreement in stress intensity factor values for the normal operating condition shown in Figure C-2 and Figure C-4. These plots demonstrate the agreement in stress intensity factors and crack growth modules for semi-elliptical, transitioning through-wall, and idealized through-wall crack shapes.

The left side of Figure C-1 demonstrates that the part-through-wall ligament stability models are in agreement, as the crack transitions to an idealized through-wall crack with a depth around 91% through-wall. Because xLPR was unable to grow the axial crack to the full critical length (see right side of Figure C-1), the value of the critical length found by xLPR was extracted from the final GoldSim file. xLPR calculated a critical through-wall length of 898.5 mm and PIPER-CASS reported 898.0 mm, a difference within the convergence tolerance of the stability solver.

For the circumferential case, the 80-year simulation contains the full progression from semi-elliptical surface crack to rupture as an idealized through-wall crack. The transition points are evident in the stress intensity factor plot, Figure C-4. The agreement in the stability modules is evident in the right side of Figure C-3: the crack ruptures and stops growing at the same size for xLPR as PIPER-CASS.

This benchmarking serves as an additional verification atop the testing suite described in Section B.11, and it reinforces the confidence in the PIPER-CASS codebase.

Comparison between PIPER-CASS and xLPR

Near-perfect agreement was obtained for deterministic fatigue crack growth behaviors between PIPER-CASS and xLPR, providing additional confidence in the PIPER-CASS code base.

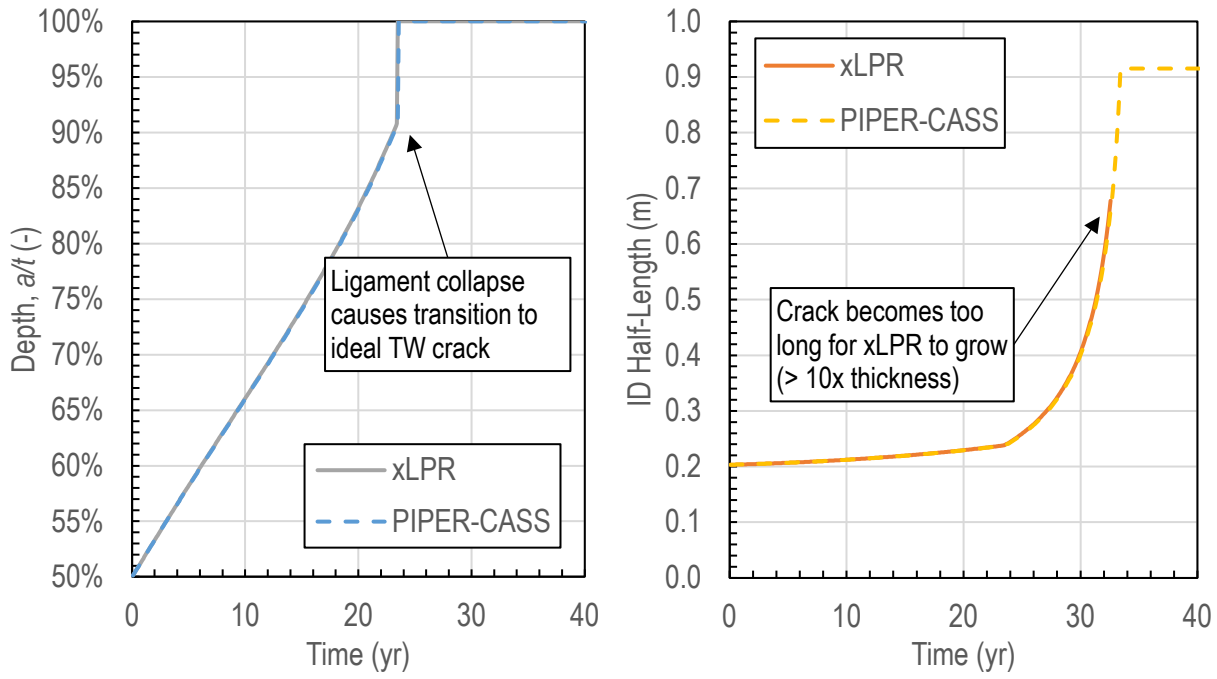

Figure C-1
Comparison of Crack Size for Axial Crack Orientation Deterministic Benchmarking Case

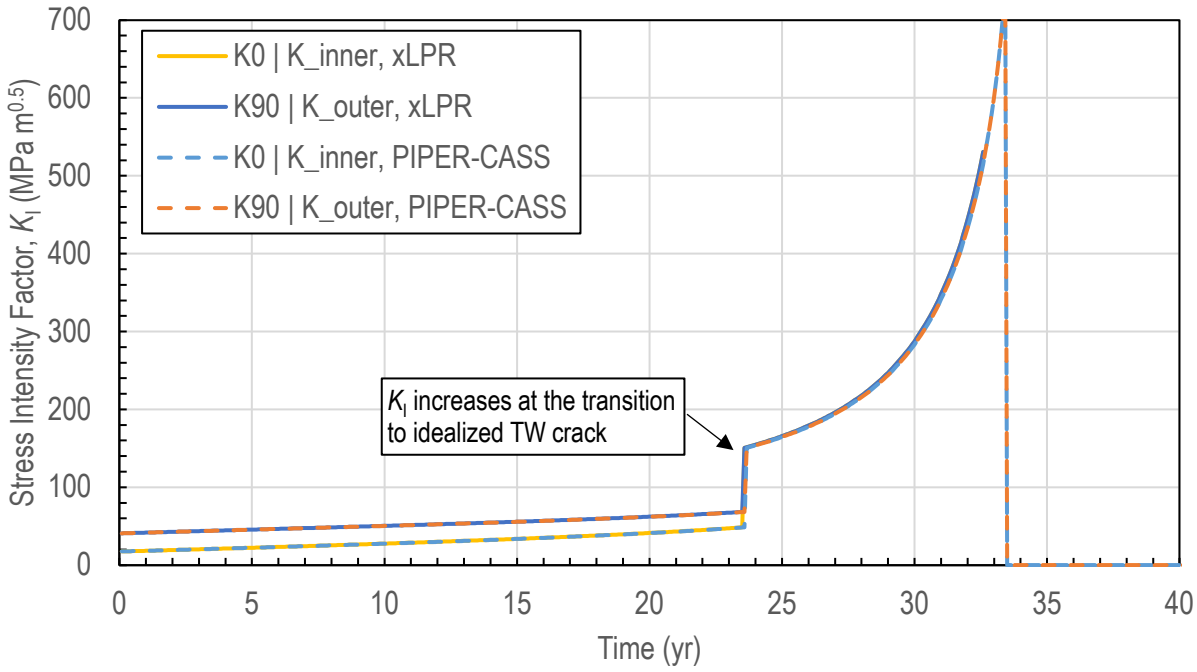

Figure C-2
Comparison of K_I for Axial Crack Orientation Deterministic Benchmarking Case

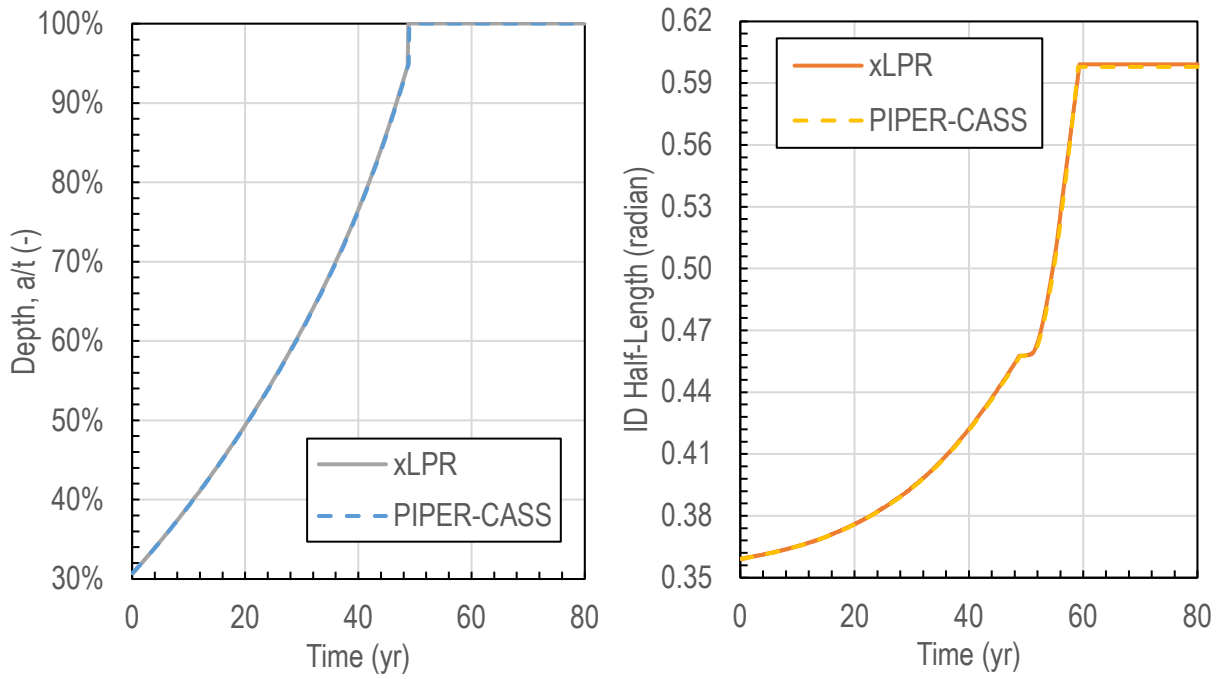

Figure C-3
Comparison of Crack Size for Circumferential Crack Orientation Deterministic Benchmarking Case

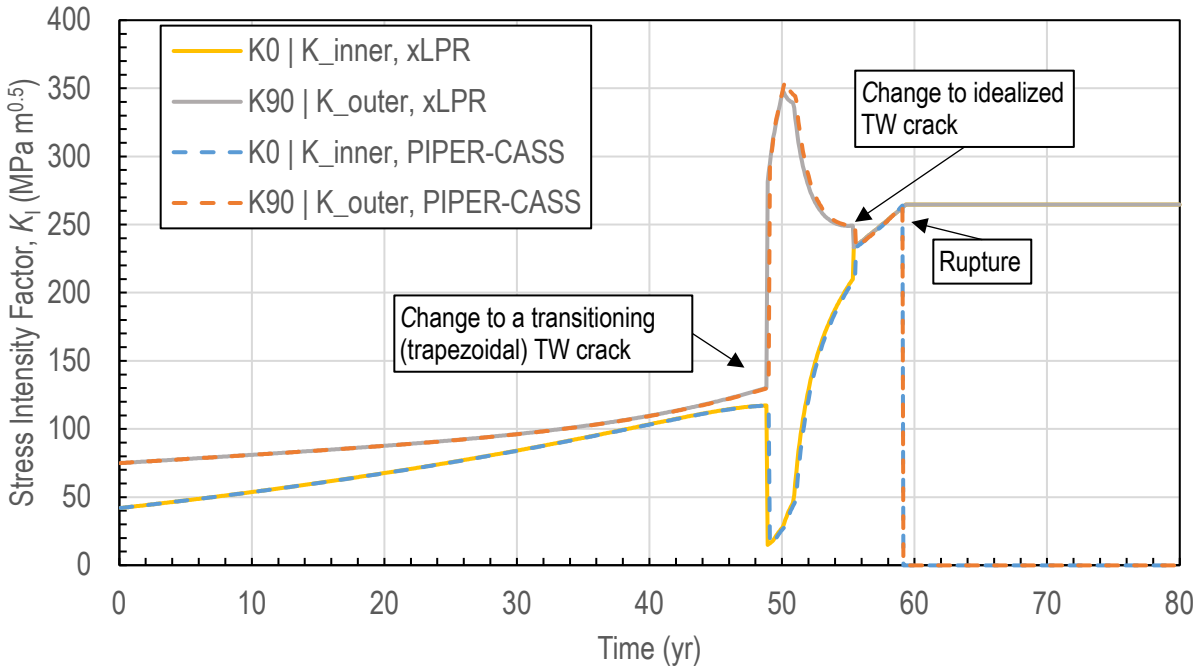

Figure C-4
Comparison of K_I for Circumferential Crack Orientation Deterministic Benchmarking Case

C.4 Continued Differences in EPFM Stability versus xLPR

Given the focus in this work on aged CASS, it is important that the EPFM stability modules converge to the appropriate critical length even at low material toughness. When solving equations to find the EPFM critical crack length, the solver method used in PIPER-CASS finds the smallest crack size that satisfies the equations for critical crack length. For some combinations of inputs, the xLPR stability modules report a larger critical crack length, as their Newton-Raphson solver converges to a different local minimum of the error function. Additionally, an EPFM stability model for axial part-through-wall cracks is added to PIPER-CASS and not present in xLPR.

For axial cracks, the truncation of ρ and RO n in the xLPR EPFM through-wall axial crack stability solver leads the Newton-Raphson method to occasionally fail to converge or converge at an erroneous critical length. Consequently, the axial benchmarking case is run with the EPFM stability check disabled in PIPER-CASS, and inputs are chosen to result in the net-section collapse solution being limiting in xLPR.

For circumferential cracks, a different set of material strengths and toughness are used to ensure the Newton-Raphson solver in the xLPR EPFM stability module converges to a solution. The xLPR-TWC_Fail method [54] includes a discontinuity in the derivative of the applied plastic J-integral ($dJ/d\Theta$) at $\Theta = \pi/4$ and $\pi/3$. This discontinuity can cause the Newton-Raphson solver to fall into a stable oscillation and reach the iteration limit for certain combinations of inputs. This xLPR module has a fallback solver using the downhill simplex (DHS) method that, when used, returns an unconverged value as the critical length, as seen in Figure C-5. When xLPR returns this unconverged solution, a warning message is returned to the user, but the xLPR run is not terminated. Consequently, the toughness inputs in the circumferential benchmarking cases are different from the axial cases to ensure that both xLPR and PIPER-CASS would obtain converged NSC and EPFM stability results.

xLPR tests embedded in the PIPER-CASS automated testing suite verify that EPFM through-wall crack stability modules for axial and circumferential cracks yields the same values as the xLPR module if the xLPR module converges appropriately to the smallest crack size satisfying the conditions $J=J_R$ and $dJ/dc=dJ_R/dc$ using the Newton-Raphson solver.

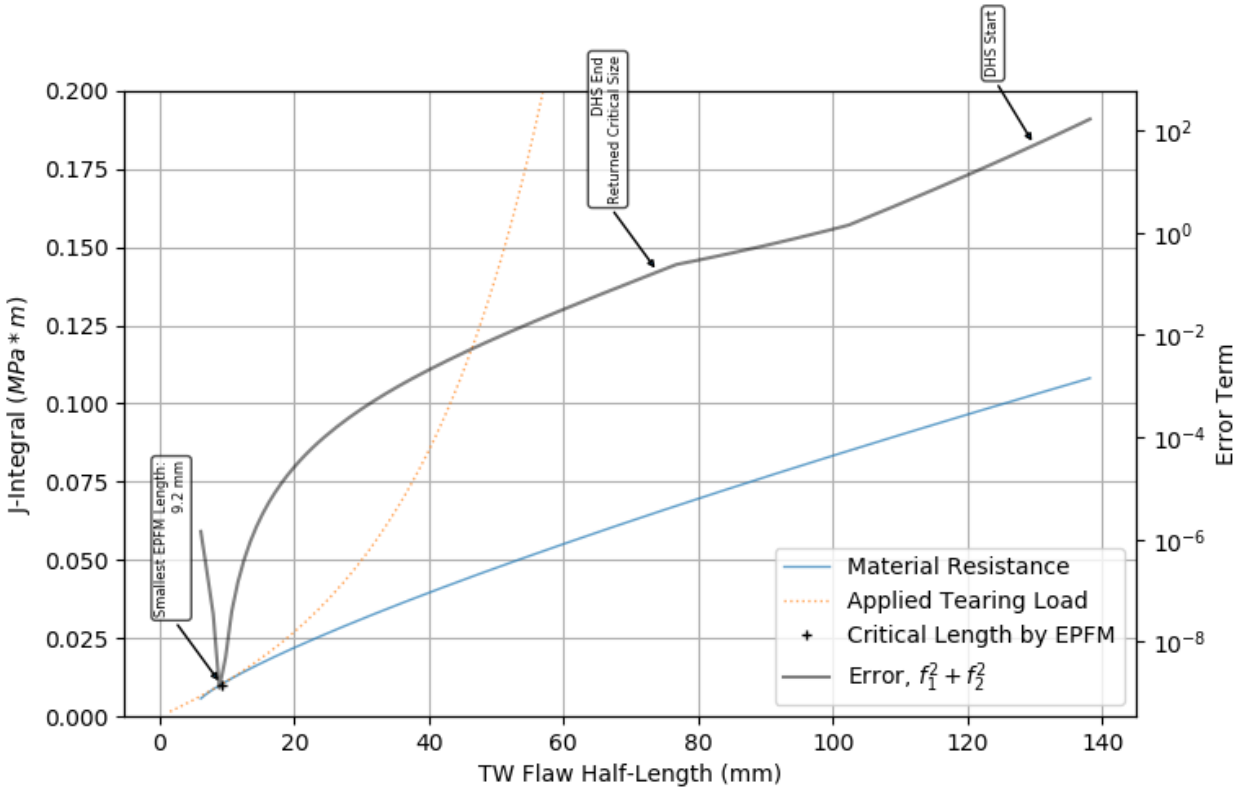

Figure C-5
Example of xLPR TWC_Fail Module DHS Solver Performance (for xLPR-STP-TWC_fail v2.1 Test Case #42)

D TRANSLATED TABLE OF CONTENTS

DISCLAIMER OF WARRANTIES AND LIMITATION OF LIABILITIES

材料可靠性计划：PWR 铸造奥氏体不锈钢管道组件的概率断裂力学评估 (MRP-479)

3002023893

最终报告，2024 年 6 月

EPRI 项目经理
D. Shim

EPRI 核质量保证计划的所有或部分要求适用于本产品。	YES NO

EPRI
3420 Hillview Avenue, Palo Alto, California 94304-1338 USA
800.313.3774 · 650.855.2121 · askepri@epri.com · www.epri.com

免责声明和责任限制

本文档由下文所列的组织编写，作为美国电力研究协会 (EPRI) 赞助或共同赞助的工作说明文档。EPRI、EPRI 的任何成员、任何赞助人、以下组织或代表其中任何组织行事的任何人：

(A) 不对以下事项做任何明示或暗示的保证或陈述：(I) 本文档中披露的任何信息、设备、方法、工艺或类似品项的使用，包括适销性和特定用途的适用性，或 (II) 此类使用不侵犯或干扰私有权利，包括任何一方的知识产权，或 (III) 本文档适用于任何特定用户的状况；或

(B) 对因您选择或使用本文档或本文档中披露的任何信息、设备、方法、工艺或类似品项而导致的任何损害或其他责任（包括任何间接损害，即使 EPRI 或任何 EPRI 代表已被告知此类损害的可能性），不承担任何责任。

本文提及任何特定的商业产品、工艺或服务，包括其商品名称、商标、制造商或其他相关信息，并不一定构成或暗示 EPRI 对其的认可、推荐或青睐。

根据与美国电力研究协会 (EPRI) 的合同，以下组织参与了本报告的编制：

Dominion Engineering, Inc.

本产品的技术内容**并非**依据满足 10 CFR 50 附录 B 要求的 EPRI 质量计划手册编制。本产品**不**受 10 CFR 第 21 部分的要求约束。

注

有关 EPRI 的更多信息，请致电 800.313.3774 联系 EPRI 客服协作中心，或者发送电子邮件至 askepri@epri.com。

Together…Shaping the Future of Energy®

致谢

根据与美国电力研究协会 (EPRI) 的合同，下列组织亦参与了本报告的编制：

Dominion Engineering, Inc.
12100 Sunrise Valley Drive, Suite 220
Reston, VA 20191

主要研究者
K. Fuhr
M. Wolfson
G. White
M. Burkardt

本报告所述研究由 EPRI 发起。

摘要

铸造奥氏体不锈钢 (CASS) 材料的材料微观结构对超声检查技术的可靠性提出了挑战。与此同时，相关方尚未依据美国机械工程师协会 (ASME) 锅炉及压力容器规范第 XI 卷，强制性附录 VIII 的规定，制定用于检查 CASS 管道的超声检测 (UT) 程序、人员和设备的资格要求。根据目前的研究，检查 CASS 管道组件时面临的最困难挑战是，轴向裂纹的检测和周向裂纹的深度测量。

除了超声检测 (UT) 的局限性外，CASS 材料还受到热老化的影响，这会导致断裂韧性随着时间推移而下降。韧性下降的程度取决于特定组件的 δ 铁素体 (δ-*Fe*) 含量。考虑到在较低的断裂韧性下，临界裂纹尺寸减小，我们需要关注的 CASS 材料失效模式是裂纹（例如从预先存在的制造缺陷）扩展到可能导致组件无法发挥全部效能的尺寸。暴露于压水反应堆 (PWR) 冷却剂的 CASS 材料的主要裂纹扩展机制是疲劳开裂。工厂经验和测试表明，PWR 环境中的奥氏体不锈钢材料一般具有抗应力腐蚀开裂的能力，而 CASS 材料所含的 δ 铁素体有望对应力腐蚀开裂敏感性产生有益影响。

本报告描述了概率断裂力学 (PFM) 评估方法以及其在应对 CASS 管道超声检测资格挑战方面的结果。PFM 分析可评估 CASS 管道中存在的轴向缺陷及其作为裂纹扩展的结构影响，未考虑在役检查。额外的 PFM 分析可评估替代性缺陷评估方法提供的结构裕量，该方法在检测到周向裂纹时不需要深度尺寸信息。PFM 评估使用专门为此项目开发的软件代码 PIPER-CASS（反应堆管道完整性概率评估 — 铸造奥氏体不锈钢）进行。PIPER-CASS 专注于 CASS 管道组件（包括低韧性的热老化材料）的疲劳裂纹扩展和稳定性建模。

这项工作的目的是帮助制定 ASME 锅炉及压力容器规范强制性附录 VIII 关于 CASS 的补充条款 9，以及第 XI 卷当前关于 CASS 管道组件的检查和缺陷验收要求的替代方案。

关键词

ASME 锅炉及压力容器规范 (BPVC)
铸造奥氏体不锈钢 (CASS)
疲劳裂纹扩展
概率断裂力学 (PFM)
无损检查 (NDE)

执行摘要

交付编号：3002023893

产品类型：技术报告

产品标题：材料可靠性计划：PWR 铸造奥氏体不锈钢管道组件的概率断裂力学评估 (MRP-479)

主要受众：铸造奥氏体不锈钢 (CASS) 管道组件相关规范和标准的制定者

次要受众：压水反应堆 (PWR) 被许可人和监管机构的技术人员

关键研究问题

有哪些分析解决方案可以补充当前的 CASS 管道组件无损检查 (NDE) 功能，尤其是用于检测轴向开裂和测量周向开裂的深度尺寸？

研究概览

本报告描述了概率断裂力学 (PFM) 评估方法和结果，旨在协助确立适用于 CASS 组件的替代性检查要求。这项工作的目的是帮助制定 ASME 锅炉及压力容器规范第 XI 卷，强制性附录 VIII 针对 CASS 的补充条款 9，并完善第 XI 卷 IWB-2500 子条款（检查类别 B-F 和 B-J）针对 CASS 管道的检查要求。对于轴向开裂，我们研究了假如不定期进行无损检查 (NDE)，核安全（破裂概率）和纵深防御（密封性）会受到怎样的影响。对于周向开裂，我们提出了一个替代性的缺陷评估程序，用于验收检测到的开裂，而不依赖合格的深度尺寸测量能力。

关键成果

- 为此，一套基于 Python 的 PFM 代码 PIPER-CASS（反应堆管道完整性概率评估 — 铸造奥氏体不锈钢）应运而生。此 PFM 代码应用了许多与 xLPR 程序相同的模型，但侧重于对疲劳裂纹扩展和弹塑性断裂力学 (EPFM) 裂纹稳定性进行建模。
- PFM 建模结果表明，在主回路 CASS 管道（包括基本负载压水反应堆 (PWR) 以及在灵活功率运行 (FPO) 模式下运行的压水反应堆 (PWR)）和波动管线 CASS 管道（包括基本负载，但不包括 FPO）中，不必定期检测轴向开裂，以确保管道结构和密封完整性。由于 FPO 功率转换可能会触发大量波动瞬态，因此在 FPO 下运行的 CE 工厂波动管线对疲劳裂纹扩展的担忧日益增加。

- PFM 建模结果表明，对于检测到的角度全长达 32° 的裂纹，所提出的替代性缺陷评估方法可确保 CASS 主回路管道组件在检测到周向裂纹后持续运行一个燃料周期并保持结构完整性。

为何如此重要

CASS 材料的异质微观结构会阻碍超声检查 (UT) 某些方面的合格性。已有技术基础证明无需检测 CASS 管道中的轴向开裂，这就消除了 UT 程序的挑战，可靠地满足了性能演示合格标准。由于不具备对 CASS 管道中周向裂纹或裂缝样缺陷深度尺寸的合格测量能力，无法应用标准缺陷评估程序，因此需要替代程序来确保继续运行并尽量减少不必要的紧急维修状况。

如何应用结果

这项工作有望为 ASME 规范委员会的行动提供技术基础，解决 CASS 组件的检查难题。这包括开发新的 ASME 规范案例，并制定适用于合格 CASS 检查的第 XI 卷强制性附录 VIII 补充条款 9 的内容，以及第 XI 卷 IWB-2500 子条款（检查类别 B-F 和 B-J）特定于 CASS 管道检查要求的潜在替代性方案。

学习和参与机会

- EPRI 于 2023 年 1 月发布了极低断裂概率 (xLPR) 概率断裂力学代码 2.2 版 (EPRI 3002023872)。有些 xLPR 代码模块经过修改后应用于 PIPER-CASS。
- MRP-362 第 1 修订版 (EPRI 3002007383) 介绍了 CASS 管道缺陷容限评估的技术依据，以支持 ASME 规范案例 N-838。我们使用了全老化 CASS 管道的 PFM 模型来确定缺陷尺寸验收限值，以满足一套针对各种负载工况的失效概率验收标准。
- EPRI 3002010314 记录了一项循环研究，用以确定无损检查 (NDE) 技术在一组包含真实表面和几何条件的有缺陷 CASS 样本上的性能。
- MRP-424 (EPRI 3002010517) 包含一份 CASS 管道焊缝检查要求草案，提供了一个框架，可据此起草最终版本的第 XI 卷强制性附录 VIII 补充条款 9。

EPRI 联系信息： Do Jun Shim，技术总监，dshim@epri.com

计划： 核电，P41；PWR 材料可靠性计划 (MRP)，P41.01.04

实施类别： 参考文献 — 技术基础

目录

图片列表

表格列表

材料可靠性計畫：PWR 澆鑄奧氏體不鏽鋼管線元件概率斷裂力學評估 (MRP-479)

3002023893

總結報告，2024 年 6 月

EPRI 專案經理
D. Shim

EPRI 核電品質保證計畫之全部或部分規定適用於本產品。	YES NO

EPRI
3420 Hillview Avenue, Palo Alto, California 94304-1338 USA
800.313.3774・650.855.2121・askepri@epri.com・www.epri.com

擔保免責聲明與責任限制

本文件的編纂是由以下指名的組織承辦，美國電力研究所 (ELECTRIC POWER RESEARCH INSTITUTE, INC.，以下簡稱 EPRI) 贊助或共同贊助的工作所進行。EPRI、EPRI 任何成員、任何共同贊助者、下列組織或是代表上述任一方行使工作者均未：

(A) 針對以下事項明示或暗示任何保證或背書：(I) 本文件所揭露之任何資訊、設備、方法、流程或類似項目的使用 (II) 這類資訊的使用並未侵犯或干涉私有權利，包含任一方的智慧財產權，或 (III) 本文件適用於任何特定使用者的情況；

(B) 承擔任何因您選擇使用本文件或本文件揭露之任何資訊、設備、方法、流程或類似項目所衍生的損害或其他責任 (包含任何間接損害，即便 EPRI 或任何 EPRI 代表已得知造成這類損害的可能性)。

本文件憑特定商品名稱、商標、製造商或其他方式參照任何特定商業產品、流程或服務，不構成或暗示其獲得 EPRI 的支持、推薦或贊同。

根據 EPRI 合約，此報告的編纂工作是由以下組織所進行：

Dominion Engineering, Inc.

本產品的技術內容並**非**根據 EPRI 品質計畫手冊準備，因此也並未符合 10 CFR 50 附錄 B 的要求。本產品**不**符合 10 CFR 第 21 部分的要求。

注意

如需有關 EPRI 的進一步資訊，請撥打電話 800.313.3774 或寄送電子郵件至 askepri@epri.com 與 EPRI 客戶協助中心聯絡。

Together...Shaping the Future of Energy®

銘謝

本報告係由以下組織根據與 EPRI 所簽合約編纂而成：

Dominion Engineering, Inc.
12100 Sunrise Valley Drive, Suite 220
Reston, VA 20191

主要研究員
K. Fuhr
M. Wolfson
G. White
M. Burkardt

本報告所述研究由 EPRI 贊助。

摘要

澆鑄奧氏體不鏽鋼 (CASS) 材料微結構對超音波檢驗方法可靠性造成問題。因此，並未針對 CASS 管線檢驗用超音波 (UT) 程序、人員與設備，制定符合美國機械工程師 (ASME) 協會鍋爐與壓力容器規範第 XI 段強制附錄 VIII 的資格要求。根據目前研究，檢驗 CASS 管線元件時最大的挑戰是偵測軸向裂縫與環狀裂縫的深度尺寸。

除了 UT 檢驗限制外，CASS 材料也受到加熱老化影響，導致斷裂韌度會隨時間退化。韌度退化程度取決於特定元件的鐵素體 (δ-*Fe*) 成分。由於斷裂韌度降低後，關鍵裂縫尺寸也會減小，對 CASS 材料故障模式的關心包含裂縫成長 (例如：來自先前已有的製造裂隙) 以及可能影響元件完整性的裂縫尺寸。CASS 材料暴露於加壓水反應爐 (PWR) 冷卻劑後，可能造成裂縫成長的主要機制為疲勞裂縫。發電廠的經驗與檢測顯示，PWR 環境中的奧氏體不鏽鋼材料通常能夠抵抗應力侵蝕裂縫，但 CASS 材料的鐵素體成分，可能有益於對應力侵蝕裂縫的靈敏度。

本報告描述了概率斷裂力學 (PFM) 法，並說明其用於解決 CASS 管線 UT 檢驗的資格和獲得的結果。PFM 分析評估在未使用運行中檢驗方法的情況下，CASS 管線出現和增生軸向裂隙造成的結構影響。額外的 PFM 分析則評估了替代裂隙評估方法提供的結構邊際，這種方法在偵測到環狀裂縫時，不需要取得深度尺寸資訊。我們使用特別為此專案開發的 PIPER-CASS (反應爐管線完整度概率評估：澆鑄奧氏體不鏽鋼) 軟體程式碼，進行 PFM 評估。PIPER-CASS 著重在為疲勞裂縫成長與 CASS 管線元件的穩定度建立模型，包含低韌度的加熱老化材料。

本研究旨在幫助制定強制附錄 VIII 關於 CASS 的增補條款 9，以及針對第 XI 段目前關於 CASS 管線元件檢驗與裂隙驗收要求的替代方案。

關鍵字

ASME 鍋爐與壓力容器規範 (BPVC)
澆鑄奧氏體不鏽鋼 (CASS)
疲勞裂縫成長
概率斷裂力學 (PFM)
非破壞性檢驗 (NDE)

執行摘要

交付編號：3002023893

產品類型：技術報告

產品標題：材料可靠性計畫：PWR 澆鑄奧氏體不鏽鋼管線元件概率斷裂力學評估 (MRP-479)

主要受眾：與澆鑄奧氏體不鏽鋼 (CASS) 管線元件相關規範與標準的製訂人員

次要受眾：加壓水反應爐 (PWR) 授權與監管單位的技術人員

重點研究問題

現存哪些分析解決方案可補充目前的 CASS 管線元件非破壞性檢驗 (NDE) 功能，尤其是可進行軸向裂縫以及環狀裂縫深度尺寸的偵測？

研究概述

本報告說明支援 CASS 元件替代檢驗要求的概率斷裂力學 (PFM) 法與結果。本研究旨在幫助制定 ASME 鍋爐與壓力容器規範第 XI 段，強制附錄 VIII 中關於 CASS 的增補條款 9 並完善第 XI 段 IWB-2500 子條款 (檢驗類別 B-F 與 B-J) 關於 CASS 管線的檢驗要求。假設週期性 NDE 沒有任何益處，對於軸向裂縫，已針對核能安全 (斷裂概率) 與多層防禦 (滲漏密度) 進行檢查。在不仰賴合格深度尺寸判斷功能下，針對環狀裂縫採用替代裂隙評估程序，以進行驗收和裂縫偵測。

主要發現

- 在此研究中，我們開發了採用 Python 的 PFM 程式碼，稱為 PIPER-CASS (反應爐管線完整性概率評估：澆鑄奧氏體不鏽鋼)。此 PFM 程式碼套用許多與 xLPR 計畫相同的模型，但著重在為疲勞裂縫成長與彈性塑膠斷裂力學 (EPFM) 裂縫穩定性建立模型。
- PFM 模型結果顯示定期檢驗 CASS 主迴路管線 (包含基本負載 PWR 以及在彈性能源運轉 (FPO) 下運作的 PWR) 和 CASS 管線調節管線 (包含基準負載但不含 FPO) 的軸向裂縫，對於確保管線結構與滲漏密度完整性並無必要。在 FPO 下運作的 CE 發電廠調節管

線，增加了對疲勞裂縫成長的關心，因為可能因 FPO 能源轉換，而產生大量的調節暫態。

- PFM 模型結果顯示，對於偵測到的角度總長度達 32° 的裂縫，所提議採用的替代裂隙評估法可確保 CASS 主迴路管線元件在偵測到環狀裂縫後持續運作一個燃料循環並保持結構完整性。

這為何很重要

CASS 材料的異質微結構會對超音波檢驗 (UT) 的特定方面的合格性造成阻礙。技術基準展示偵測 CASS 管線的軸向裂縫對於因應 UT 程序面對的阻礙，以穩定展現達到合格標準並無必要。針對 CASS 管線中的環狀裂縫與類裂縫的裂隙缺乏深度尺寸判斷功能，導致無法應用標準裂隙評估程序，因此需要替代程序才能允許持續運作，並限制不必要的緊急修復。

如何應用結果

此研究預期可為 ASME 規範委員會提供技術基準，以採取行動進行 CASS 元件的檢驗。其中包含新的 ASME 規範案例，與制定強制附錄 VIII 第 XI 段增補條款 9 中關於合格 CASS 檢驗的內容，以及第 XI 段 IWB-2500 子條款 (檢驗類別 B-F 與 B-J) 關於 CASS 管線的檢驗要求的潛在替代方案。

學習和參與機會

- EPRI 於 2023 年 1 月發布極低斷裂機率 (xLPR) 概率斷裂力學程式碼第 2.2 版 (EPRI 3002023872)。有數種 xLPR 程式碼模組經過修改，以應用於 PIPER-CASS。
- MRP-362 修訂版 1 (EPRI 3002007383) 提出 CASS 管線裂隙容差評估的技術說明，以支持 ASME 規範案例 N-838。運用完全老化的 CASS 管線 PFM 模型，以制定裂隙尺寸驗收限制，滿足各負載服務等級的一系列故障概率驗收標準。
- EPRI 3002010314 記錄循環研究，以確定在一系列有裂隙的 CASS 試樣上採用 NDE 技術的效果，這些試樣包含實際表面與幾何條件。
- MRP-424 (EPRI 3002010517) 包含 CASS 管線熔接檢驗要求草案，為最終版的強制附錄 VIII 第 XI 段增補條款 9 提供架構。

EPRI 聯絡人：Do Jun Shim，技術執行人員，dshim@epri.com

計畫：核能，P41；PWR 材料可靠性計畫 (MRP)，P41.01.04

實施類別：參考：技術基準

目錄

附圖目錄

附表目錄

Programme de fiabilité des matériaux : Évaluation probabiliste de la mécanique de la rupture des composants de tuyauterie en acier inoxydable austénitique moulé des REP (MRP-479)

3002023893

Rapport final, juin 2024

Responsable de projet EPRI
D. Shim

Tout ou une partie des spécifications du programme de qualité nucléaire d'EPRI s'applique à ce produit.	YES NO

EPRI
3420 Hillview Avenue, Palo Alto, Californie 94304-1338 États-Unis
800.313.3774 ▪ 650.855.2121 ▪ askepri@epri.com ▪ www.epri.com

EXONÉRATION DE GARANTIES ET LIMITATION DE RESPONSABILITÉS

LE PRÉSENT DOCUMENT A ÉTÉ PRÉPARÉ PAR LES ENTREPRISES CITÉES CI-DESSOUS DANS LE CADRE DE TRAVAUX SPONSORISÉS OU CO-SPONSORISÉS PAR L'ELECTRIC POWER RESEARCH INSTITUTE, INC. (EPRI). NI EPRI, NI UN MEMBRE D'EPRI, NI UN COSPONSOR, NI LA OU LES ENTREPRISE(S) CI-DESSOUS, NI AUCUNE PERSONNE AGISSANT EN LEUR NOM :

(A) N'OFFRE DES GARANTIES OU REPRÉSENTATIONS EXPRESSES OU IMPLICITES QUELLES QU'ELLES SOIENT, (I) QUANT À L'UTILISATION D'INFORMATIONS, D'APPAREILS, DE MÉTHODES, DE PROCÉDÉS OU D'ÉLÉMENTS SIMILAIRES FIGURANT DANS CE DOCUMENT, Y COMPRIS LA VALEUR MARCHANDE ET L'ADAPTATION À UN USAGE PARTICULIER, OU (II) QU'UNE TELLE UTILISATION N'ENFREINT PAS OU N'INTERFÈRE PAS AVEC DES DROITS PARTICULIERS, OU (III) QUE CE DOCUMENT CORRESPOND À TOUTES LES CIRCONSTANCES PARTICULIÈRES DE L'UTILISATEUR ; OU

(B) N'ASSUME AUCUNE RESPONSABILITÉ POUR TOUS DOMMAGES OU AUTRES (Y COMPRIS LES DOMMAGES CONSÉCUTIFS, MÊME SI EPRI OU UN REPRÉSENTANT D'EPRI A ÉTÉ AVERTI DE LA POSSIBILITÉ DE TELS DOMMAGES) RÉSULTANT DE VOTRE SÉLECTION OU UTILISATION DE CE DOCUMENT OU INFORMATIONS, APPAREILS, MÉTHODES, PROCÉDÉS OU ÉLÉMENTS SIMILAIRES FIGURANT DANS CE DOCUMENT.

DANS CE DOCUMENT, LES REFERENCES A DES PRODUITS COMMERCIAUX SPECIFIQUES, PROCEDES OU SERVICES PAR SON NOM COMMERCIAL, SA MARQUE DE COMMERCE, SON FABRICANT OU AUTRE, NE CONSTITUENT NI N'IMPLIQUENT NECESSAIREMENT LA PROMOTION, LA RECOMMANDATION OU LA PREFERENCE PAR EPRI.

LES ENTREPRISES SUIVANTES, SOUS CONTRAT AVEC EPRI, ONT PREPARE CE RAPPORT :

Dominion Engineering, Inc.

LE CONTENU TECHNIQUE DE CE PRODUIT **N'A PAS ÉTÉ** PRÉPARÉ CONFORMÉMENT AU MANUEL DU PROGRAMME DE QUALITÉ DE L'EPRI QUI REMPLIT LES EXIGENCES DU 10 CFR 50, ANNEXE B. CE PRODUIT **N'EST PAS** SOUMIS AUX EXIGENCES DU 10 CFR PARTIE 21.

REMARQUE

Pour plus informations sur EPRI, appelez le Centre de service clientèle d'EPRI au +1 800.313.3774 ou envoyez un e-mail à askepri@epri.com.

Together…Shaping the Future of Energy®

REMERCIEMENTS

Les entreprises suivantes, sous contrat avec EPRI, a préparé ce rapport :

Dominion Engineering, Inc.
12100 Sunrise Valley Drive, Suite 220
Reston, VA 20191

Chercheurs principaux
K. Fuhr
M. Wolfson
G. White
M. Burkardt

Ce rapport décrit une recherche parrainée par EPRI.

RESUME

La microstructure des matériaux en acier inoxydable austénitique moulé (CASS) remet en question la fiabilité des techniques d'examen par ultrasons. Ainsi, les exigences de qualification pour les procédures, le personnel et l'équipement d'essai aux ultrasons (UT) utilisés pour l'examen de la tuyauterie CASS conformément au Code des chaudières et appareils sous pression de l'American Society of Mechanical Engineers (ASME), section XI, annexe VIII obligatoire, n'ont pas été élaborées. D'après les recherches actuelles, les défis les plus difficiles pour l'examen des composants de tuyauterie CASS sont la détection des fissures axiales et le dimensionnement en profondeur des fissures circonférentielles.

En plus des limites de l'essai UT, le matériau CASS est sujet au vieillissement thermique, ce qui provoque une dégradation de la ténacité à la rupture au fil du temps. L'étendue de la dégradation de la ténacité dépend de la teneur en ferrite delta (δ-*Fe*) du composant particulier. Le mode de défaillance qui préoccupe le matériau CASS est la propagation d'une fissure (par exemple, à partir d'un défaut de fabrication préexistant) à une taille qui pourrait remettre en question l'intégrité du composant, étant donné la taille critique réduite de fissure à la plus faible ténacité à la rupture. Le principal mécanisme de propagation des fissures qui intéresse les matériaux CASS exposés au liquide de refroidissement du réacteur à eau sous pression (REP) est la fissuration par fatigue. L'expérience de l'usine et les essais montrent que l'acier inoxydable austénitique dans l'environnement REP résiste généralement à la fissuration par corrosion sous contrainte, tandis que la teneur en ferrite delta du matériau CASS devrait avoir un effet bénéfique sur la susceptibilité à la fissuration par corrosion sous contrainte.

Le présent rapport décrit l'approche probabiliste de la mécanique de la rupture (PFM) et les résultats obtenus pour relever les défis de qualification des essais UT pour la tuyauterie CASS. Les analyses PFM évaluent l'implication structurelle des défauts axiaux présents dans la tuyauterie CASS et se propageant sous forme de fissures sans créditer l'examen en service. Des analyses PFM supplémentaires évaluent la marge structurelle fournie par une méthode alternative d'évaluation des défauts qui ne nécessite pas d'informations de dimensionnement en profondeur lors de la détection d'une fissuration circonférentielle. Les évaluations PFM ont été réalisées à l'aide d'un code logiciel développé principalement pour ce projet appelé PIPER-CASS (PIPING Integrity Probabilistic Evaluation for Reactors – Cast Austenitic Stainless Steel). PIPER-CASS se concentre sur la modélisation de la propagation des fissures de fatigue et de la stabilité des composants de tuyauterie CASS, y compris les matériaux vieillis thermiquement avec une faible ténacité.

Le présent travail vise à appuyer l'élaboration de l'annexe VIII, supplément 9 obligatoire pour les CASS et des solutions de rechange à l'examen actuel de la section XI et aux exigences d'acceptation des défauts pour les composants de tuyauterie CASS.

Mots-clés

Code des chaudières et appareils sous pression ASME (BPVC)
Acier inoxydable austénitique coulé (CASS)
Propagation des fissures de fatigue
Probabiliste de la mécanique de la rupture (PFM)
Examen non destructif (NDE)

RESUME

Numéro des produits livrables : 3002023893

Type de produits : Rapport technique

Titre produit : Programme de fiabilité des matériaux : Évaluation probabiliste de la mécanique de la rupture des composants de tuyauterie en acier inoxydable austénitique moulé des REP (MRP-479)

Auditoire principal : Développeurs de codes et de normes relatifs aux composants de tuyauterie en acier inoxydable austénitique moulé (CASS)

Auditoire secondaire : Personnel technique des titulaires de permis et des régulateurs de réacteur à eau sous pression (REP)

PRINCIPALE QUESTION DE RECHERCHE

Quelles sont les solutions analytiques disponibles pour compléter les capacités actuelles d'examen non destructif (NDE) pour les composants de tuyauterie CASS, en particulier pour la détection de fissures axiales et le dimensionnement en profondeur de fissures circonférentielles ?

PRÉSENTATION DE LA RECHERCHE

Le présent rapport décrit l'approche de la mécanique probabiliste de la rupture (PFM) et les résultats qui visent à appuyer les exigences d'examen alternatives pour les composantes du CASS. Le présent travail vise à appuyer l'élaboration du Code des chaudières et appareils sous pression ASME, section XI, annexe VIII obligatoire, Supplément 9 pour CASS et à affiner les exigences d'examen de la section XI, paragraphe IWB-2500 (catégories d'examen B-F et B-J)propres à la tuyauterie CASS. Pour la fissuration axiale, l'effet sur la sûreté nucléaire (probabilité de la rupture) et la défense en profondeur (étanchéité) a été étudié en supposant qu'il n'y ait aucun bénéfice d'une NDE périodique. Pour la fissuration circonférentielle, une autre procédure d'évaluation des défauts est proposée pour accepter la fissuration détectée sans compter sur une capacité de calibrage en profondeur qualifiée.

PRINCIPALES CONCLUSIONS

- Pour ce projet, un code PFM basé sur Python appelé PIPER-CASS (PIPING Integrity Probabilistic Evaluation for Reactors – Cast Austenitic Stainless Steel) a été développé. Ce code PFM applique plusieurs des mêmes modèles que le programme xLPR, mais se concentre sur la modélisation de la propagation des fissures de fatigue et de la stabilité des fissures par la mécanique de la rupture élastique-plastique (EPFM).

- Les résultats de la modélisation PFM montrent qu'un examen périodique pour détecter des fissures orientées axialement dans la tuyauterie CASS de la boucle principale (y compris les REP de charge de base et REP fonctionnant en fonctionnement d'alimentation flexible (FPO)) et dans la tuyauterie CASS de ligne de surtension (y compris la charge de base, mais pas FPO) n'est pas nécessaire pour assurer l'intégrité structurelle et étanche des tuyaux. Les lignes de surtension dans les centrales électriques fonctionnant sous FPO présentent un risque accru de propagation de fissures de fatigue en raison de la possibilité qu'un grand nombre de transitoires de surtension soient déclenchés par les changements de puissance de FPO.
- Les résultats de modélisation PFM montrent que, pour une fissure détectée avec une longueur angulaire totale allant jusqu'à 32, la méthode alternative d'évaluation des défauts proposée garantit l'intégrité structurelle des composants de tuyauterie de boucle principale CASS pour un cycle de combustible de fonctionnement continu après la détection d'une fissure orientée de façon circonférentielle.

IMPORTANCE DE CETTE ANALYSE

La microstructure hétérogène des matériaux CASS est un obstacle à la qualification de certains aspects de l'essai aux ultrasons (UT). Une base technique démontrant que la détection de fissurations axiales dans les canalisations CASS est inutile relève le défi posé par les procédures UT qui satisfont de manière fiable aux normes de qualification de démonstration de performance. Le manque de capacité de dimensionnement en profondeur qualifiée pour les fissures circonférentielles ou les défauts de type fissure dans la tuyauterie CASS empêche l'application de procédures d'évaluation des défauts standard, de sorte qu'une procédure alternative est nécessaire pour permettre un fonctionnement continu et limiter les réparations émergentes inutiles.

APPLICATION DES RÉSULTATS

Le présent travail devrait fournir des bases techniques pour les actions du comité du Code ASME visant à traiter l'examen des composantes du CASS. Cela comprend les nouveaux cas du code ASME et le développement de la section XI, l'appendice VIII obligatoire, le supplément 9 pour l'examen CASS qualifié et les alternatives potentielles à la section XI, le sous-article IWB-2500 (catégories d'examen B-F et B-J) les exigences d'examen propres à la tuyauterie CASS.

POSSIBILITÉS D'ENSEIGNEMENTS ET D'ENGAGEMENT

- Le Code de mécanique de la rupture probabiliste à très faible probabilité (xLPR), version 2.2 (EPRI 3002023872) a été publié par l'EPRI en janvier 2023. Plusieurs des modules de code xLPR ont été adaptés pour être utilisés dans PIPER-CASS.
- MRP-362, Rév. 1 (EPRI 3002007383) présente la justification technique de l'évaluation de la tolérance aux défauts des tuyauteries CASS pour soutenir le cas N-838 du code ASME. Un modèle PFM pour la tuyauterie CASS entièrement vieillie a été utilisé pour élaborer des

limites d'acceptation de la taille des défauts répondant à un ensemble de critères d'acceptation de probabilité de défaillance pour chaque niveau de service de chargement.

- L'EPRI 3002010314 documente une étude ronde visant à déterminer la performance des techniques d'EDN sur un ensemble de spécimens de SAAC défectueux qui contenaient des conditions géométriques et de surface réalistes.
- Le MRP-424 (EPRI 3002010517) comprend une ébauche des exigences en matière d'examen pour les soudures de tuyauterie CASS, fournissant un cadre à partir duquel la version finale de la section XI, annexe VIII obligatoire, supplément 9 peut être rédigée.

CONTACTS EPRI : Do Jun Shim, Cadre technique, dshim@epri.com

PROGRAMME : Énergie nucléaire, P41 ; Programme de fiabilité des matériaux REP (PRM), P41.01.04

CATÉGORIE DE MISE EN ŒUVRE : Référence - Base technique

TABLE DES MATIERES

LISTE DES FIGURES

LISTE DES TABLEAUX

材料信頼性プログラム：PWR の鋳造オーステナイト系ステンレス鋼配管コンポーネントの確率破壊力学的評価 (MRP-479)

3002023893

最終報告、2024 年 6 月

EPRI プロジェクトマネージャ
D. Shim

EPRI 原子力品質保証プログラムの条件の全体または一部が本製品に適用されます。	YES NO

EPRI
3420 Hillview Avenue, Palo Alto, California 94304-1338 USA
800.313.3774・650.855.2121・askepri@epri.com・www.epri.com

保証の放棄および責任の制限

本文書は、以下に記載する組織により作成され、それらの組織は、電力研究所 (EPRI) が出資または共同出資した調査の説明責任を明らかにしています。EPRI、EPRI のメンバー、共同スポンサー、および以下に記載する組織のいずれも、またそれらの代理として機能する者の誰も、

(A) 明示的にも黙示的にも、(I) 本文書中で開示される情報、装置、方法、プロセス、または商品性あるいは特定目的への適合性を含むそれらに類似した項目や、 (II) それらの使用が第三者の知的財産権を含む個人の権利を侵害または妨害しないことや、 (III) 本文書が特定ユーザーの状況に適することを、表明または保証しません。また、

(B) お客様が本文書または本文書で開示されている情報、装置、方法、プロセスまたはそれらに類似した項目を選択あるいは使用したことから生じる派生的損害 (EPRI または EPRI の職員がその損害の可能性を知らされていた場合であっても) を含む、いかなる損害やその他の責任の一切を負わないものとします。

本文書において商号、商標、メーカー、またはその他によって固有の市販商品、プロセスまたはサービスが言及されていても、それは必ずしも支持や推奨または EPRI による賛同を表明または示唆するものではありません。

以下の組織が EPRI との契約に従い本レポートを作成しました。

Dominion Engineering, Inc.

本成果物の技術的内容は、10 CFR 50、付録 B の要件を満たす EPRI の品質保証プログラム マニュアルに**準拠していません**。また、本成果物は 10 CFR パート 21 の要件の**対象外です**。

注

EPRI の詳細については、EPRI カスタマーアシスタンスセンター (800.313.3774) にお電話いただくか、 askepri@epri.com までメールでお問い合わせください。

Together…Shaping the Future of Energy®

謝辞

以下の組織が EPRI との契約に従い本レポートを作成しました。

Dominion Engineering, Inc.

12100 Sunrise Valley Drive, Suite 220

Reston, VA 20191

主要調査員

K. Fuhr

M. Wolfson

G. White

M. Burkardt

本報告書は、EPRI がスポンサーとなった調査について説明します。

概要

鋳造オーステナイト系ステンレス鋼 (CASS) 素材の材料微細構造は、超音波検査技法の信頼性に課題を突きつけています。そのため、米国機械学会 (ASME) の沸騰型および加圧型容器コードのセクション XI、必須付録 VIII に従う、CASS 配管の検査のために用いられる超音波試験 (UT) の手順、人員、および装置を認定するための要件は、まだ開発されていません。現時点での研究に基づく、CASS 配管コンポーネント検査における最も困難な課題は、軸方向の亀裂の検出と、円周方向の亀裂の深さ測定となっています。

UT 検査の限界に加えて、CASS 材料は、熱による経年変化の影響を受けやすく、これは時間経過とともに、破壊靭性の低下を招きます。靭性低下の程度は、特定のコンポーネント内のデルタフェライト (δ-*Fe*) 成分量に依存します。CASS 材料の、懸念すべき破壊モードは、破壊靭性の低下で臨界亀裂サイズが小さくなるため、亀裂（例、製造時に存在していた傷）がコンポーネントの健全性に影響を与えるほどに成長することです。加圧水原子炉 (PWR) 冷却水にさらされる CASS 材料の、関心を引く主要な亀裂成長の機構は、疲労亀裂です。原子炉での経験と試験は、PWR 環境に置かれたオーステナイト系ステンレス鋼材料は、一般に応力腐食割れには強く、さらに CASS 材料のデルタフェライト成分は応力腐食割れに対する感受性において良い影響を与えることが期待されることを示しています。

本レポートは、確率破壊力学 (PFM) のアプローチと、CASS 配管の UT 検査の有効性の課題に対処する上で得られた結果について、記述しています。PFM 分析は、CASS 配管に存在し、亀裂として伝搬していく軸方向の傷が、構造に関して示唆していることを、供用中の検査なしで評価します。付加的な PFM 分析は、円周方向の亀裂の検出で深さ情報を必要としない、代替となる傷評価の方法論が提供する構造上のマージンを評価します。PFM による評価は、PIPER-CASS (原子炉配管健全性の確率的評価 - 鋳造オーステナイト系ステンレス鋼) と呼ばれる、このプロジェクトのために特別に開発さ

れたソフトウェアコードを用いて実行されました。PIPER-CASS は、CASS 配管コンポーネントの疲労亀裂の成長と安定性のモデリングに特に焦点を当てています。このようなコンポーネントには、熱的経年変化が進んで靭性が低下した材料も含まれます。

この事業は、CASS を対象とした、必須付録 VIII、補足事項 9 の開発と、現行のセクション XI、CASS 配管コンポーネントの検査と傷の受容可能要件の代替事項の開発をサポートすることを意図しています。

キーワード

ASME 沸騰水および加圧水容器コード (BPVC)
鋳造オーステナイト系ステンレス鋼 (CASS)
疲労亀裂の成長
確率破壊力学 (PFM)
非破壊検査 (NDE)

要旨

提供番号: 3002023893

製品タイプ: 技術報告書

製品タイトル: 材料信頼性プログラム：PWR の鋳造オーステナイト系ステンレス鋼配管コンポーネントの確率破壊力学的評価 (MRP-479)

主要な読者: 鋳造オーステナイト系ステンレス鋼配管コンポーネントに関連したコードと規格の開発者

二次的な読者: 加圧水型原子炉 (PWR) のライセンス取得者と規制当局の技術者たち

研究に関連した主要な質問

CASS 配管コンポーネントに対する現在の非破壊的検査 (NDE) を補うもの、特に軸方向の亀裂の検出と円周方向の亀裂の深さ測定を行うために、どのような分析的ソリューションが利用可能ですか。

研究の概要

本レポートは、CASS コンポーネントの代替検査要件をサポートすることを目指す、確率破壊力学 (PFM) のアプローチと結果について説明しています。この作業は、ASME 沸騰および圧力容器コード、セクション XI、必須付録 VIII 、CASS に関する補足 9 とセクション XI の微調整、副条項 IWB-2500 (検査カテゴリー B-F と B-J) の CASS 配管固有の検査要件の開発をサポートすることを意図しています。軸方向の亀裂については、定期的な NDE からのメリットを仮定しない場合の、原子力の安全性 (破壊確率) と多層防御 (耐漏出性) が調査されました。円周方向の亀裂については、認定された、深さ測定の能力に依存することなく、検出された亀裂を受容することに関しては、代替となる欠陥評価の手順が提案されています。

主要な知見

- 今回の作業では、PIPER-CASE (原子炉配管健全性の確率的評価 - 鋳造オーステナイト系ステンレス鋼) と呼ばれる、Python ベースの PFM コードが開発されました。この PFM コードは、xLPR プログラムと同じモデルの多くに当てはまりますが、特に疲労亀裂成長のモデリングと、弾性-塑性破壊機構 (EPFM) による亀裂に対する安定性に焦点を当てています。
- PFM モデリングの結果は、メインループ CASS 配管 (ベース負荷 PWR と柔軟な出力運転 (FPO) の両方を含む) と、サージライン CASS 配管(ベース負荷 PWR は含むが FPO は含まない) での、軸方向の亀裂を検出するための定期的な点検は、配管の構造および耐漏出性を確保する点では不必要であることを示しています。FPO の下で運転している CE プラントのサージラインは、FPO の出力シフトがトリガーする、多数のサージ過渡の可能性のために、疲労亀裂に対する懸念が大きくなっています。
- PFM モデリングの結果は、最大で 32°の角度の全長にわたる亀裂を検出することができるため、提案された代替の欠陥評価方式により、円周方向の亀裂検出後の 1 燃料サイクルの連続運転の間、CASS のメインループ配管コンポーネントの構造的完全性が確保されることを示しています。

なぜ重要か

CASS 材料の異種微細構造は、超音波検査 (UT) のいくつかの側面を認定する上での障害となっています。CASS 配管の軸方向の亀裂の検出が不要であることを実証する技術的基盤があれば、UT の手順で、性能実証の認定基準が確実に満たされるという課題に対応できます。CASS 配管の円周方向の亀裂、または亀裂のような傷の深さの測定を十分に行う能力が欠けていると、標準的な傷の評価手順の適用が難しくなるため、連続運転を可能にし、不必要な緊急修理を少なくするには、代替の手順が必要とされます。

結果をどのように適用するか

この作業は、ASME コード委員会が、CASS コンポーネントの検査に対して措置を取るための、技術的な基盤を提供するものと期待されています。これには、新しい ASME コードケースと、セクション XI、必須付録 VIII の開発、認定された CASS 検査のための補足とセクション XI の可能な代替案、副条項 IWB-2500 (検査カテゴリー B-F と B-J) の CASS 配管固有の検査要件が含まれます。

学習と関与のための機会

- 2023 年 1 月には、EPRI により、『極めて可能性の小さい破裂 (xLPR) に関する確率破壊力学コード、バージョン 2.2 (EPRI 3002023872)』がリリースされました。xLPR コードモジュールのいくつかは、PIPER-CASS での使用のため、採用されました。
- MRP-362、改訂版 1 (EPRI 3002007383) は、ASME コードケース N-838 をサポートする、CASS 配管の傷の許容度評価を正当化する技術的な理由を示しています。最大年数が経過した CASS 配管の PFM モデルが、傷サイズの許容限界を定めるために用いられました。この限界は、各負荷運転レベルに対応する、一連の確率許容基準を満たすものです。
- EPRI 3002010314 では、NDE 技法のパフォーマンスを決定するために行われた、現実のものに近い表面と形状条件を持つ、傷の付いた CASS 試料のセットに対するラウンドロビン式の研究について記述しています。
- MRP-424 (EPRI 3002010517) には、CASS 配管溶接部に対する検査要件の草稿が含まれています。これは、セクション XI の最終版、必須付録 VIII、補足 9 の下書き作成のための枠組みを提供します。

EPRI の連絡先: Do Jun Shim、技術責任者、dshim@epri.com

プログラム: 原子力、P41; PWR 材料信頼性プログラム (MRP)、P41.01.04

実施カテゴリー: 参照文献 – 技術的基盤

目次

図の一覧

表の一覧

자재 신뢰도 프로그램: PWR 주조 오스테나이트계 스테인리스강 배관 구성요소(MRP-479)의 확률론적 파괴 역학 평가

3002023893

최종 보고서, 2024 년 6 월

EPRI 프로젝트 매니저

D. Shim

EPRI 원자력 품질 보증 프로그램(Nuclear Quality Assurance Program)의 규정 전체 또는 일부가 이 제품에 적용됩니다.	YES NO

EPRI

3420 Hillview Avenue, Palo Alto, California 94304-1338 USA

800.313.3774 • 650.855.2121 • askepri@epri.com • www.epri.com

보증의 부인 및 책임 제한

본 문서는 ELECTRIC POWER RESEARCH INSTITUTE, INC.(EPRI)가 후원 또는 공동 후원한 작업에 대한 설명으로서 아래 이름으로 명명된 조직에서 작성했습니다 . EPRI, EPRI 의 구성원, 공동 후원자, 아래 조직, 이들을 대행하는 개인 중 어느 누구도

(A) 명시적이거나 암시적이든 간에 다음 내용을 보증하거나 주장하지 않습니다: (I) 특정 용도에 대한 상업성과 적합성을 포함하여 정보, 기구, 방법, 절차 또는 본 문서에 공개된 유사한 품목 사용과 관련하여 (II) 그러한 사용이 어느 당사자의 지적 재산을 포함하여 개인적으로 소유한 권한을 침해하거나 방해하지 않음, (III) 본 문서가 특정 사용자의 상황에 적합함, 또는

(B) 본 문서나 정보, 기구, 방법, 절차 또는 본 문서에 공개된 유사한 품목을 선택하거나 사용함으로써 발생한 손해나 기타 책임(EPRI 또는 어느 EPRI 담당자가 그러한 손해의 가능성을 사전에 알고 있는 경우라도 모든 결과적 손해 포함)에 대해 책임을 지지 않습니다.

상품명, 상표, 제조업체 등 특정 상업용 제품, 절차 또는 서비스에 대한 본 문서의 참조는 반드시 EPRI 의 보증, 추천, 선호로 해석되거나 그러한 의미를 내포하지 않습니다.

EPRI 의 계약에 따라 다음 조직이 본 보고서를 작성했습니다.

Dominion Engineering, Inc.

본 제품의 기술 콘텐츠는 부록 B, 10 CFR 50 의 요건을 충족하는 EPRI 품질 프로그램 설명서에 따라 작성되지 **않았습니다**. 본 제품에는 10 CFR PART 21 의 요건이 적용되지 **않습니다**.

본 발행물은 다음과 같이 문헌에 인용해야 하는 기업 문서입니다. [Title]. EPRI, Palo Alto, CA: 2024. [Subject].

승인

EPRI 의 계약에 따라 다음 조직이 본 보고서를 작성했습니다.

Dominion Engineering, Inc.
12100 Sunrise Valley Drive, Suite 220
Reston, VA 20191

책임 연구원
K. Fuhr
M. Wolfson
G. White
M. Burkardt

본 보고서에는 EPRI 에서 후원하는 연구에 대한 설명이 나와 있습니다.

초록

CASS(주조 오스테나이트계 스테인리스강)의 재료 미세구조는 초음파 검사 기술의 신뢰성에 과제를 안깁니다. 이와 같이 미국기계공학회(ASME) 보일러 및 압력 용기 코드, 섹션 XI, 필수 부록 VIII 에 따라 CASS 배관 검사에 사용되는 초음파 검사(UT) 절차, 인력 및 장비에 대한 자격 요구 사항은 개발되지 않았습니다. 현재 연구에 따르면 CASS 배관 구성요소를 검사할 때 가장 어려운 과제는 축방향 균열 감지 그리고 원주방향 균열 깊이 측정입니다.

UT 검사의 한계 외에도 CASS 재료는 열적 노화가 발생하여 시간이 지남에 따라 파괴 인성이 저하됩니다. 인성의 저하 정도는 특정 구성요소의 델타 페라이트(δ-*Fe*) 함량에 따라 달라집니다. CASS 재료의 우려되는 장애 모드는 낮은 파괴 인성에서 감소된 임계 균열 크기를 고려할 때 구성요소의 무결성을 해칠 수 있는 크기로 균열(예: 기존 제조 결함으로 인해)이 성장하는 것입니다. 가압경수로(PWR) 냉각수에 노출된 CASS 재료에서 관심을 끄는 주요 균열 성장 메커니즘은 피로 균열입니다. 플랜트 경험 및 테스트에 따르면 PWR 환경의 오스테나이트계 스테인리스강 재료는 일반적으로 응력 부식 균열에 저항력이 있는 반면, CASS 재료의 델타 페라이트 함량은 응력 부식 균열에 대한 민감도에 유익한 효과가 있을 것으로 예상됩니다.

이 보고서에서는 CASS 배관에 대한 UT 검사의 자격 문제를 해결하기 위해 확보한 확률론적 파괴 역학(PFM) 접근법과 결과를 설명합니다. PFM 분석은 가동 중 검사를 고려하지 않은 상태에서 CASS 배관에 존재하고 균열로 전파되는 축 결함의 구조적 영향을 평가합니다. 추가 PFM 분석은 원주방향 균열 감지 시 깊이 측정 정보가 필요하지 않은 대체 결함 평가 방법으로 제공되는 구조적 마진을 평가합니다. PFM 평가는 PIPER-CASS(원자로에 대한 배관 건전성 확률 평가 - 주조 오스테나이트 스테인리스강)라는 이 프로젝트를 위해 특별히 개발된 소프트웨어 코드를 사용하여 수행했습니다. PIPER-CASS 는 인성이 낮은 열적 노화 재료를 포함하여 CASS 배관 구성요소의 피로 균열 성장과 안정성의 모델링에 중점을 둡니다.

이 작업은 CASS 에 대한 필수 부록 VIII, 보충 자료 9 의 개발을 지원하고 CASS 배관 구성요소에 대한 현재 섹션 XI 검사와 결함 허용 요구 사항의 대안을 지원하기 위한 것입니다.

키워드

ASME 보일러 및 압력 용기 코드(BPVC)

주조 오스테나이트계 스테인리스강(CASS)

피로 균열 성장

확률론적 파괴 역학(PFM)

비파괴 검사(NDE)

개요

산출물 번호: 3002023893

제품 유형: 기술 보고서

제품 제목: 자재 신뢰도 프로그램: PWR 주조 오스테나이트계 스테인리스강 배관 구성요소(MRP-479)의 확률론적 파괴 역학 평가

일차 대상: CASS(주조 오스테나이트 스테인리스강) 배관 구성요소와 관련된 코드 및 표준 개발자

이차 대상: 가압경수로(PWR) 사업자 및 규제기관의 기술진

연구에 대한 주요 질문

CASS 배관 구성요소에 대한 현재 비파괴 검사(NDE) 기능을 보완하기 위해, 특히 축 균열 감지 및 원주방향 균열의 깊이 측정을 위해 어떤 분석 솔루션을 사용할 수 있습니까?

연구 개요

이 보고서에서는 이 보고서에서는 CASS 구성요소에 대한 대체 검사 요구 사항을 지원하기 위한 확률론적 파괴 역학(PFM) 접근법과 결과를 설명합니다. 이 작업은 CASS 를 위한 ASME 보일러 및 압력 용기 코드, 섹션 XI, 필수 부록 VIII, 보충 자료 9 의 개발 그리고 CASS 배관과 관련된 섹션 XI, 하위 조항 IWB-2500(검사 범주 B-F 및 B-J) 검사 요구 사항의 개선을 지원하기 위한 것입니다. 축방향 균열의 경우, 주기적인 NDE 의 이점이 없다는 가정하에 원자력 안전(파열 확률)과 심층 방어(누출 방지)에 미치는 영향을 조사했습니다. 원주방향 균열의 경우에는 적격한 깊이 측정 기능에 의존하지 않고 감지된 균열을 허용하기 위한 대체 결함 평가 절차를 제안했습니다.

주요 연구 결과

- 이 활동을 위해 PIPER-CASS(원자로에 대한 배관 건전성 확률 평가 - 주조 오스테나이트 스테인리스강)라는 Python 기반 PFM 코드를 개발했습니다. 이 PFM

코드는 xLPR 프로그램과 동일한 모델을 다수 적용하지만 피로 균열 성장 및 EPFM(탄성 소성 파괴 역학) 균열 안정성 모델링에 중점을 둡니다.

- PFM 모델링 결과는 메인 루프 CASS 배관(FPO(Flexible Power Operation)에서 작동하는 기본 하중 PWR 및 PWR 모두 포함) 및 서지 라인 CASS 배관(FPO 가 아닌 기본 하중 포함)에서 축방향 균열을 감지하기 위한 주기적인 검사가 파이프 구조 및 누출 방지 무결성을 보장하는 데 필요하지 않음을 보여줍니다. FPO 하에서 운영되는 CE 플랜트의 서지 라인에서는 FPO 전력 이동으로 인해 트리거될 수 있는 많은 수의 서지 과도현상 가능성으로 인해 피로 균열 성장에 대한 우려가 증가하고 있습니다.
- PFM 모델링 결과는 최대 32° 각도 전체 길이의 감지된 균열에 대해 제안된 대체 결함 평가 방법이 원주방향 균열이 감지된 후 계속 작동한 하나의 연료 주기 동안 CASS 메인 루프 배관 구성요소의 구조적 무결성을 보장함을 보여줍니다.

이 사안이 중요한 이유

CASS 재료의 이질적인 미세구조는 초음파 검사(UT)의 특정 측면을 검증하는 데 장애가 됩니다. CASS 배관의 축 균열 감지가 불필요함을 보여주는 기술적 근거는 성능 입증 자격 표준을 안정적으로 충족하는 UT 절차의 과제를 해결합니다. CASS 배관의 원주방향 균열 또는 균열 같은 결함에 대한 적격한 깊이 측정 기능이 부족하면 표준 결함 평가 절차를 적용할 수 없으므로 지속적인 작동을 허용하고 불필요한 응급 수리를 제한하기 위한 대체 절차가 필요합니다.

결과를 적용하는 방법

이 작업은 CASS 구성요소의 검사를 다루기 위한 ASME 코드위원회 조치의 기술적 근거를 제공할 것으로 예상됩니다. 여기에는 적격한 CASS 검사를 위한 새로운 ASME 코드 사례 및 섹션 XI, 필수 부록 VIII, 보충 자료 9 의 개발 그리고 CASS 배관과 관련된 섹션 XI, 하위 조항 IWB-2500(검사 범주 B-F 및 B-J) 검사 요구 사항에 대한 잠재적 대안이 포함됩니다.

학습 및 참여 기회

- xLPR(Extremely Low Probability of Rupture) 확률론적 파괴 역학 코드, 버전 2.2(EPRI 3002023872)이 2023 년 1 월에 EPRI 에서 출시되었습니다. 몇몇 xLPR 코드 모듈은 PIPER-CASS 에 사용하도록 조정되었습니다.

- MRP-362, Rev. 1(EPRI 3002007383)은 ASME 코드 사례 N-838 을 지원하기 위한 CASS 배관의 내결함성 평가에 대한 기술적 정당성을 제시합니다. 완전히 노화된 CASS 배관에 대한 PFM 모델을 사용하여 각 하중 서비스 수준을 다루는 일련의 고장 확률 허용 기준을 충족하는 결함 크기 허용 한계를 개발했습니다.
- EPRI 3002010314 는 실제적인 표면 및 형상 조건을 포함하는 결함 있는 일련의 CASS 표본에 대한 NDE 기술의 성능을 결정하기 위해 라운드 로빈 연구를 문서화합니다.
- MRP-424(EPRI 3002010517)에는 CASS 배관 용접에 대한 검사 요구 사항의 초안이 포함되어 있어 섹션 XI, 필수 부록 VIII, 보충 자료 9 의 최종 버전을 작성할 수 있는 프레임워크를 제공합니다.

EPRI 연락처: 심도준, 기술 책임자, dshim@epri.com

프로그램: Nuclear Power, P41; PWR Materials Reliability Program (MRP), P41.01.04

실행 범주: 참고 – 기술적 근거

목차

그림 목록

표 목록

Programa de fiabilidad de materiales (MRP): Evaluación de la mecánica de fractura probabilística de componentes de tuberías de acero inoxidable austenítico fundido en PWR (MRP-479)

3002023893

Informe final, junio de 2024

Gestor de proyectos de EPRI
D. Shim

A este producto le son aplicables, total o parcialmente, los requisitos del Programa de Garantía de Calidad Nuclear de EPRI.	YES NO

EPRI
3420 Hillview Avenue, Palo Alto, California 94304-1338 (EE. UU.)
800.313.3774 ▪ 650.855.2121 ▪ askepri@epri.com ▪ www.epri.com

EXENCIÓN DE GARANTÍAS Y LIMITACIÓN DE RESPONSABILIDAD

ESTE DOCUMENTO HA SIDO ELABORADO POR LAS ORGANIZACIONES INDICADAS A CONTINUACIÓN COMO DESCRIPCIÓN DE LOS TRABAJOS PATROCINADOS O COPATROCINADOS POR ELECTRIC POWER RESEARCH INSTITUTE, INC. (EPRI). NI EPRI, NI NINGUNO DE SUS MIEMBROS, COPATROCINADORES U ORGANIZACIONES QUE SE INDICAN A CONTINUACIÓN, ASÍ COMO NINGUNA OTRA PERSONA QUE LOS REPRESENTE:

(A) OFRECERÁN GARANTÍA ALGUNA NI REALIZARÁN NINGUNA DECLARACIÓN DE HECHO DE NINGÚN TIPO, EXPLÍCITA O IMPLÍCITA, (I) CON RESPECTO AL USO DE CUALQUIER INFORMACIÓN, APARATO, MÉTODO, PROCESO O SIMILARES DESCRITOS EN ESTE DOCUMENTO, INCLUYENDO SU COMERCIABILIDAD E IDONEIDAD PARA UNA FINALIDAD DETERMINADA, (II) DE QUE DICHO USO NO INFRINJA NI INTERFIERA CON DERECHOS DE PROPIEDAD PRIVADOS, INCLUYENDO LA PROPIEDAD INTELECTUAL DE CUALQUIERA DE LAS PARTES, (III) DE QUE ESTE DOCUMENTO SEA ADECUADO PARA SU USO EN CUALQUIER CIRCUNSTANCIA ESPECÍFICA DEL USUARIO;

(B) ASUMIRÁ LA RESPONSABILIDAD POR POSIBLES DAÑOS, ASÍ COMO CUALQUIER OTRO TIPO DE RESPONSABILIDAD (INCLUYENDO DAÑOS INDIRECTOS, INCLUSO SI SE HA ADVERTIDO A EPRI O A CUALQUIERA DE SUS REPRESENTANTES DE LA POSIBILIDAD DE LOS MISMOS) DERIVADOS DE LA ELECCIÓN O UTILIZACIÓN POR SU PARTE DE ESTE DOCUMENTO O DE CUALQUIER INFORMACIÓN, APARATO, MÉTODO, PROCESO O SIMILARES DESCRITOS EN ESTE DOCUMENTO.

LA ALUSIÓN A CUALQUIER SERVICIO, PROCESO O PRODUCTO COMERCIAL CONCRETO INCLUIDO EN EL PRESENTE DOCUMENTO MEDIANTE SU NOMBRE, MARCA COMERCIAL, FABRICANTE O DE CUALQUIER OTRO MODO NO CONSTITUYE NI IMPLICA NECESARIAMENTE LA APROBACIÓN, RECOMENDACIÓN NI ACEPTACIÓN POR PARTE DE EPRI.

LAS SIGUIENTES ORGANIZACIONES HAN SIDO CONTRATADAS POR EPRI PARA LA PREPARACIÓN DE ESTE INFORME:

Dominion Engineering, Inc.

EL CONTENIDO TÉCNICO DE ESTE PRODUCTO **NO** SE HA ELABORADO DE ACUERDO CON EL MANUAL DEL PROGRAMA DE CALIDAD DE EPRI, QUE CUMPLE CON LOS REQUISITOS DEL APÉNDICE B DE 10 CFR 50. ESTE PRODUCTO **NO** ESTÁ SUJETO A LOS REQUISITOS DEL APARTADO 21 DE 10 CFR.

NOTA

Si desea obtener más información acerca de EPRI, póngase en contacto con el Centro de atención al cliente de EPRI en el teléfono (+1) 800 313 3774 o en la dirección askepri@epri.com.

Together…Shaping the Future of Energy®

RECONOCIMIENTOS

Este informe ha sido elaborado por la siguiente organización contratada por EPRI:

Dominion Engineering, Inc.
12100 Sunrise Valley Drive, Suite 220
Reston, VA 20191

Investigadores principales
K. Fuhr
M. Wolfson
G. White
M. Burkardt

En este informe se describe una investigación patrocinada por EPRI.

RESUMEN

La microestructura de los materiales de acero inoxidable austenítico fundido (CASS, por sus siglas en inglés) pone a prueba la fiabilidad de las técnicas de inspección por ultrasonidos. Por este motivo, no se han establecido los requisitos de cualificación relativos a los procedimientos, el personal y los equipos correspondientes a las pruebas de ultrasonidos (UT, por sus siglas en inglés) utilizadas para el estudio de las tuberías fabricadas con CASS de acuerdo con la Sección XI, Apéndice VIII del Código de calderas y recipientes a presión de la ASME (Sociedad estadounidense de ingenieros mecánicos). De acuerdo con las investigaciones actuales, los problemas más importantes a la hora de examinar los componentes de las tuberías de CASS son la detección de grietas axiales y el dimensionamiento en profundidad de las grietas circunferenciales.

Además de las limitaciones de las pruebas de ultrasonidos, el material CASS es vulnerable al envejecimiento térmico, lo que provoca una degradación de la tenacidad a la fractura con el paso del tiempo. El grado de degradación de la tenacidad de este componente depende de su contenido de hierro delta (*Fe* δ). El principal modo de fallo del material CASS es el crecimiento de grietas (por ejemplo, originadas por defectos de fabricación) hasta alcanzar un tamaño que podría poner en peligro la integridad del componente, dado el reducido tamaño crítico de la grieta con una menor tenacidad a la fractura. El principal mecanismo de interés para el crecimiento de grietas en el material CASS expuesto al refrigerante de reactores de agua a presión (PWR, por sus siglas en inglés) es el agrietamiento por fatiga. La experiencia y las pruebas realizadas en las centrales demuestran que el acero inoxidable austenítico en el entorno de los PWR es, por lo general, resistente al agrietamiento por corrosión bajo tensión, mientras que se espera que el contenido de hierro delta del material CASS mejore la susceptibilidad al agrietamiento por corrosión bajo tensión.

En este informe se describe el método de mecánica de fractura probabilística (PFM, por sus siglas en inglés) aplicado y los resultados obtenidos para responder a los problemas de cualificación de las pruebas de ultrasonidos para tuberías de CASS. Los análisis de PFM evalúan la implicación estructural de la presencia de defectos axiales en las tuberías de CASS y su propagación en forma de grietas sin tener en cuenta las pruebas en servicio. Otros análisis de PFM evalúan el margen estructural proporcionado por una metodología alternativa de evaluación de defectos que no requiere información sobre el dimensionamiento en profundidad tras la detección de grietas circunferenciales. Las evaluaciones de PFM se realizaron utilizando un software desarrollado específicamente para este proyecto denominado PIPER-CASS (Piping Integrity Probabilistic Evaluation for Reactors – Cast Austenitic Stainless Steel). PIPER-CASS se centra en la elaboración de modelos del crecimiento de las grietas por fatiga y la estabilidad de los componentes de las tuberías de CASS, incluido el material envejecido térmicamente con baja tenacidad.

Con este trabajo se pretende contribuir al desarrollo del Apéndice VIII, Suplemento 9 para CASS, así como de alternativas a los requisitos actuales de inspección y aceptación de defectos de la Sección XI para componentes de tuberías de CASS.

Palabras clave

Código de calderas y recipientes a presión (BPVC) de la ASME
Acero inoxidable austenítico fundido (CASS)
Crecimiento de grietas por fatiga
Mecánica de fractura probabilística (PFM)
Inspección no destructiva (NDE)

RESUMEN EJECUTIVO

Número de entregable: 3002023893

Tipo de producto: informe técnico

Título del producto: Programa de fiabilidad de materiales (MRP): Evaluación de la mecánica de fractura probabilística de componentes de tuberías de acero inoxidable austenítico fundido en PWR (MRP-479)

Público principal: Redactores de códigos y normas relacionados con los componentes de tuberías de acero inoxidable austenítico fundido (CASS).

Audiencia secundaria: Personal técnico de los licenciatarios y reguladores de reactores de agua a presión (PWR)

ASPECTO PRINCIPAL A INVESTIGAR

¿De qué soluciones analíticas se dispone para complementar las técnicas actuales de inspección no destructiva (NDE) de los componentes de tuberías de CASS, específicamente para la detección de grietas axiales y el dimensionamiento en profundidad de las grietas circunferenciales?

RESUMEN DE LA INVESTIGACIÓN

En este informe se describen el método de mecánica de fractura probabilística (PFM) y sus resultados para determinar los requisitos de inspección alternativos para los componentes de CASS. Este trabajo tiene por objeto contribuir a la elaboración del Código de calderas y recipientes a presión de la ASME, Sección XI, Apéndice VIII, Suplemento 9 para CASS, así como al perfeccionamiento de los requisitos de inspección de la Sección XI, Subartículo IWB-2500 (Categorías de inspección B-F y B-J) específicos para las tuberías de CASS. Para las grietas axiales, se investigó el efecto en la seguridad nuclear (probabilidad de ruptura) y en la defensa en profundidad (estanqueidad), asumiendo la ausencia de beneficios de una NDE periódica. Para las grietas circunferenciales, se propone un procedimiento alternativo de evaluación de defectos para la aceptación de las grietas detectadas sin depender de una capacidad cualificada de dimensionamiento en profundidad.

RESULTADOS CLAVE

- Con este objetivo, se ha desarrollado un código de PFM basado en Python denominado PIPER-CASS (Piping Integrity Probabilistic Evaluation for Reactors - Cast Austenitic Stainless Steel). Este código de PFM aplica muchos de los mismos modelos que el programa xLPR, pero se centra en elaborar modelos tanto del crecimiento de las grietas por fatiga como de la estabilidad de las grietas de mecánica de fractura elástico-plástica (EPFM).

- Los modelos de PFM elaborados demuestran que no es necesario realizar inspecciones periódicas para detectar grietas orientadas axialmente en las tuberías de CASS del circuito principal (incluidos los PWR de carga base y los PWR de operación flexible[FPO]) ni en las tuberías de CASS del sistema de compensación (incluidos los PWR de carga base, pero no los de operación flexible) para garantizar la integridad estructural y la estanqueidad de las tuberías. Las tuberías de compensación de las centrales de CE que funcionan con FPO están más expuestas a la aparición de grietas por fatiga debido a la posibilidad de que se desencadene un gran número de transitorios de compensación por los cambios de potencia del modelo FPO.
- Los resultados de la elaboración de modelos de PFM demuestran que, para una grieta detectada con una longitud angular completa de hasta 32°, el método alternativo de evaluación de defectos propuesto garantiza la integridad estructural de los componentes de las tuberías de CASS del circuito principal durante un ciclo de combustible de funcionamiento continuado tras la detección de una grieta orientada circunferencialmente.

POR QUÉ ES IMPORTANTE

La microestructura heterogénea de los materiales de CASS es un impedimento para la cualificación de ciertos aspectos de las pruebas de ultrasonidos (UT). Una base técnica que demuestre que no es necesario detectar las grietas axiales en las tuberías de CASS soluciona el problema de que los procedimientos de UT deben cumplir de forma fiable las normas de cualificación para la demostración del rendimiento. La falta de capacidad cualificada de dimensionamiento en profundidad de las grietas circunferenciales u otros defectos similares a las grietas en las tuberías de CASS impide la aplicación de los procedimientos de evaluación de defectos estándar, por lo que es necesario un procedimiento alternativo que permita el funcionamiento continuado y limite las reparaciones innecesarias.

CÓMO APLICAR LOS RESULTADOS

Se espera que este trabajo proporcione las bases técnicas para que el comité del Código de la ASME pueda tomar medidas en relación con la inspección de los componentes de CASS. Esto incluye nuevos casos del Código de la ASME y el desarrollo de la Sección XI, Apéndice VIII, Suplemento 9 para la inspección cualificada de CASS y posibles alternativas a los requisitos de inspección de la Sección XI, Subartículo IWB-2500 (Categorías de inspección B-F y B-J) específicos para las tuberías de CASS.

OPORTUNIDADES DE APRENDIZAJE Y DE PARTICIPACIÓN

- El Código de mecánica de fractura probabilística xLPR (Extremely Low Probability of Rupture), versión 2.2 (EPRI 3002023872) fue publicado por EPRI en enero de 2023. Varios de los módulos del código xLPR se adaptaron para su uso en PIPER-CASS.
- MRP-362, Rev. 1 (EPRI 3002007383) presenta la justificación técnica de la evaluación de la tolerancia a los defectos de las tuberías de CASS para avalar el caso N-838 del Código de la ASME. Se utilizó un modelo PFM para tuberías de CASS totalmente desgastadas con el

objetivo de desarrollar límites de aceptación del tamaño de los defectos que cumplieran una serie de criterios de aceptación de la probabilidad de fallo para cada nivel de servicio de carga.

- EPRI 3002010314 documenta un estudio round-robin para determinar el rendimiento de las técnicas NDE en un conjunto de especímenes CASS defectuosos que contenían condiciones superficiales y geométricas realistas.
- MRP-424 (EPRI 3002010517) incluye un borrador de los requisitos de inspección para las soldaduras de tuberías de CASS, lo que proporciona un marco a partir del cual se puede redactar la versión final de la Sección XI, Apéndice VIII, Suplemento 9.

PERSONAS DE CONTACTO EN EPRI: Do Jun Shim, Ejecutivo Técnico, dshim@epri.com

PROGRAMA: Nuclear Power, P41; PWR Materials Reliability Program (MRP), P41.01.04

CATEGORÍA DE IMPLEMENTACIÓN: Referencia – Base técnica

ÍNDICE

LISTA DE FIGURAS

LISTA DE TABLAS

Tillförlitlighetsprogram för material: Probabilistic Fracture Mechanics Evaluation of PWR Cast Austenitic Stainless Steel Piping Components (MRP-479)

3002023893

Slutrapport, juni 2024

EPRI-projektledare
D. Shim

Alla eller en del av kraven i EPRI Nuclear Quality Assurance Program (Kvalitetssäkringsprogram för kärnkraftsanläggningar) gäller för denna produkt.	YES NO

EPRI

3420 Hillview Avenue, Palo Alto, California 94304-1338 USA

+1-800-313-3774 ▪ +1-650-855-2121 ▪ askepri@epri.com ▪ www.epri.com

FRISKRIVNING AV GARANTIER OCH ANSVARSBEGRÄNSNING

DETTA DOKUMENT HAR UTFÄRDATS AV DEN ELLER DE ORGANISATIONER SOM ANGES NEDAN SOM EN REDOVISNING AV ARBETE SOM SPONSRAS ELLER SAMSPONSRAS AV ELECTRIC POWER RESEARCH INSTITUTE, INC. (EPRI). VARKEN EPRI, MEDLEMMAR AV EPRI, SAMSPONSOR, ORGANISATION ELLER ORGANISATIONER NEDAN, ELLER NÅGON SOM HELST PERSON SOM AGERAR Å DERAS VÄGNAR:

(A) UTFÄRDAR NÅGON SOM HELST GARANTI ELLER UTFÄSTELSE, UTTRYCKLIG ELLER UNDERFÖRSTÅDD, (I) MED AVSEENDE PÅ ANVÄNDNING AV NÅGON SOM HELST INFORMATION, APPARAT, METOD, PROCESS ELLER LIKNANDE OBJEKT SOM BESKRIVS I DETTA DOKUMENT, INKLUSIVE SÄLJBARHET OCH LÄMPLIGHET FÖR ETT VISST SYFTE, ELLER (II) ATT SÅDAN ANVÄNDNING INTE GÖR INTRÅNG PÅ ELLER UTGÖR STÖRNING I PRIVATÄGDA RÄTTIGHETER, INKLUSIVE NÅGON PARTS IMMATERIELLA EGENDOM, ELLER (III) ATT DETTA DOKUMENT PASSAR FÖR NÅGON VISS ANVÄNDARES OMSTÄNDIGHETER; ELLER

(B) ANTAR ANSVAR FÖR NÅGRA SOM HELST SKADOR ELLER ANNAT SOM HELST ANSVAR (INKLUSIVE ALLA FÖLJDSKADOR, ÄVEN OM EPRI ELLER NÅGON EPRI-REPRESENTANT HAR INFORMERATS OM RISKEN FÖR SÅDANA SKADOR) SOM RESULTAT AV DITT VAL ELLER DIN ANVÄNDNING AV DETTA DOKUMENT ELLER NÅGON INFORMATION, APPARAT, METOD, PROCESS ELLER LIKNANDE OBJEKT SOM BESKRIVS I DETTA DOKUMENT.

HÄNVISNING HÄRI TILL NÅGON SPECIFIK KOMMERSIELL PRODUKT, PROCESS ELLER SERVICE MED DESS HANDELSNAMN, VARUMÄRKE, TILLVERKARE ELLER PÅ ANNAT SÄTT, INNEBÄR ELLER ANTYDER INTE NÖDVÄNDIGTVIS ATT DE GODKÄNNS, REKOMMENDERAS ELLER FAVORISERAS AV EPRI.

FÖLJANDE ORGANISATION(ER), UNDER KONTRAKT MED EPRI, SKAPADE DENNA RAPPORT:

Dominion Engineering, Inc.

DET TEKNISKA INNEHÅLLET I DEN HÄR PRODUKTEN HAR **INTE** FÖRBERETTS I ENLIGHET MED EPRI:S HANDBOK FÖR KVALITETSPROGRAMMET SOM UPPFYLLER KRAVEN I 10 CFR 50, BILAGA B. DENNA PRODUKT LYDER **INTE** UNDER KRAVEN I LAGEN 10 CFR DEL 21.

ANM.

För ytterligare information om EPRI, ring EPRI:s kundsupportcenter på 800.313.3774 eller skicka e-post till askepri@epri.com.

Together … Shaping the Future of Energy®

ERKÄNNANDEN

Följande organisation, under kontrakt med EPRI, skapade denna rapport:

Dominion Engineering, Inc.
12100 Sunrise Valley Drive, Suite 220
Reston, VA 20191, USA

Huvudutredare
K. Fuhr
M. Wolfson
G. White
M. Burkardt

Den här rapporten beskriver forskning som sponsras av EPRI.

SAMMANDRAG

Den materiella mikrostrukturen i gjutet austenitiskt rostfritt stål (CASS) försvårar tillförlitligheten för ultraljudundersökningstekniker. Som sådan har kvalificeringskraven för förfaranden, personal och utrustning vid ultraljudsprovning (UT) som används för undersökning av CASS-rör i enlighet med American Society of Mechanical Engineers (ASME) Boiler and Pressure Vessel Code, Section XI, Mandatory Appendix VIII inte utvecklats. Baserat på aktuell forskning är de svåraste utmaningarna för undersökning av CASS-rörkomponenter upptäckten av axiella sprickor och djupdimensionering av omkretssprickor.

Förutom begränsningarna i ultraljudsprovning utsätts CASS-material för termisk åldring, vilket orsakar nedbrytning av brottseghet över tid. Graden av brottseghet beror på innehållet av delta ferrit (δ-*Fe*) i den specifika komponenten. Felläget i fråga för CASS-material är en sprickas tillväxt (t.ex. från ett befintligt tillverkningsfel) till en storlek som kan utmana komponentens integritet, med tanke på den minskade kritiska sprickstorleken vid den lägre spricksegheten. Den viktigaste spricktillväxtmekanismen av intresse för CASS-material som utsätts för tryckvattenreaktorers (PWR) kylvätska är utmattningssprickbildning. Anläggningens erfarenhet och testning visar att austenitiskt rostfritt stål i PWR-miljön i allmänhet är resistent mot sprickor från spänningskorrosion, medan delta ferritinnehållet i CASS-material förväntas ha en fördelaktig inverkan på sprickbildningens mottaglighet för spänningskorrosion.

Den här rapporten beskriver metoden för probabilitstisk brottsmekanik (PFM) och resultaten som erhållits för att ta itu med utmaningarna i kvalifikationen av ultraljudsprovning av CASS-rör. PFM-analyser bedömer de strukturella implikationerna av att axiella brister förekommer i CASS-rör och sprider sig som sprickor utan att kreditera en undersökning under drift. Ytterligare PFM-analyser bedömer den strukturella marginal som tillhandahålls av en alternativ felutvärderingsmetod som inte kräver information om djupstorlek vid upptäckten av omkretssprickor. PFM-utvärderingarna utfördes med hjälp av en programkod som har utvecklats speciellt för detta projekt som kallas PIPER-CASS (Piping Integrity Probabilistic Evaluation for Reactors - Cast austenitic Stainless Steel). PIPER-CASS fokuserar på modellering av tillväxten av utmattningssprickor och stabiliteten hos CASS rörkomponenter, inklusive termiskt åldrat material med låg seghet.

Detta arbete är avsett att stödja utvecklingen av Mandatory Appendix VIII, tillägg 9 för CASS och alternativ till den nuvarande avsnitt XI-undersökningen och kraven på godkännande av brister för CASS-rörkomponenter.

Nyckelord

ASME Boiler and Pressure Vessel Code (BPVC)
Gjutet austenitiskt rostfritt stål (CASS)
Tillväxt av utmattningssprickor
Probabilitsisk brottsmekanik (PFM)
Icke-destruktiv undersökning (NDE)

EXEKUTIV SAMMANFATTNING

Leveransnummer: 3002023893

Produkttyp: Teknisk rapport|

Produkttitel: Tillförlitlighetsprogram för material: Probabilistic Fracture Mechanics Evaluation of PWR Cast Austenitic Stainless Steel Piping Components (MRP-479)

Huvudmålgrupp: Utvecklare av koder och standarder relaterade till rörledningar av gjutet autentistiskt rostfritt stål (CASS)

Sekundär målgrupp: Teknisk personal hos licenstagare och regulatorer för tryckvattenreaktorer (PWR)

NYCKELFORSKNINGSFRÅGOR

Vilka analytiska lösningar som finns tillgängliga för att komplettera den nuvarande icke-destruktiva undersökningens (NDU) kapacitet för CASS rördelar, särskilt för detektering av axiell sprickbildning och djupdimensionering av omkretssprickor?

FORSKNINGSÖVERSIKT

Den här rapporten beskriver metoden för probabilitstisk brottsmekanik (PFM) och resultaten som är avsedda att stödja alternativa undersökningskrav för CASS-komponenter. Detta arbete är avsett att stödja utvecklingen av undersökningskraven för ASME Boiler and Pressure Vessel Code, Section XI, Mandatory Appendix VIII, Supplement 9 for CASS and refinement of Section XI, Subarticle IWB-2500 (Examination Categories B-F and B-J) som är specifika för CASS-rörledningar. För axiell sprickbildning undersöktes effekten på kärnsäkerheten (spricksannolikhet) och djupt försvar (läckagetäthet), förutsatt att ingen periodisk icke-destruktiv undersökning var till nytta. För omkretssprickor föreslås ett alternativt felbedömningsförfarande för godkännande av upptäckt sprickbildning utan att förlita sig på en kvalificerad djupdimensioneringsförmåga.

NYCKELRESULTAT

- För detta arbete utvecklades en Python-baserad PFM-kod som heter PIPER-CASS (Piping Integrity Probabilistic Evaluation for Reactors - Cast austenitic Stainless Steel). Denna PFM-kod tillämpar många av de samma modeller som xLPR-programmet men fokuserar på modellering av tillväxten av utmattningssprickor och sprickstabiliteten för elastisk-plastbrottmekanik (EPFM).
- Resultaten från PFM-modelleringen visar att periodisk undersökning för att upptäcka axiellt orienterad sprickbildning i huvudslingan av CASS-rör(inklusive både PWR:er och PWR:er under flexibel kraftdrift (FPO)) och i CASS-rörsystem med överspänningsledning (inklusive

grundbelastning men inte FPO) är onödigt för att säkerställa integriteten hos rörstruktur och läckagetäthet. Överspänningsledningar i CE-anläggningar som är verksamma under flexibel kraftdrift (FPO) har en ökad risk för tillväxten av utmattningssprickor på grund av risken för ett stort antal överspänningstransienter som utlöses av effektförskjutningar under flexibel kraftdrift.

- Resultaten av PFM-modellering visar att för att upptäcka en spricka med en vinklad full längd på upp till 32 grader, säkerställer den föreslagna alternativa felutvärderingsmetoden strukturell integritet hos CASS-huvudslingans rördelar för en bränslecykel med fortsatt drift efter detektering av en omkretsspricka.

VARFÖR DETTA ÄR VIKTIGT

Den heterogena mikrostrukturen hos CASS-material är ett hinder för kvalificering av vissa aspekter av ultraljudsundersökningar (UT). En teknisk grund som visar att detektering av axiell sprickbildning i CASS-rörsystem inte är nödvändig tar itu med utmaningen hos UT-procedurer som på ett tillförlitligt sätt uppfyller kvalificeringsstandarder för prestandademonstration. Bristen på kvalificerad djupdimensioneringsförmåga för omkretssprickor eller sprickliknande brister i CASS-rörledningar förhindrar tillämpningen av standardförfaranden för utvärdering av fel, så ett alternativt förfarande behövs för att tillåta fortsatt drift och begränsa onödiga akuta reparationer.

HUR RESULTATEN SKA TILLÄMPAS

Detta arbete förväntas ge tekniska underlag för ASME kodkommitténs åtgärder för att ta itu med granskningen av CASS-komponenter. Detta inkluderar nya ASME kodfall och utvecklingen av utredningskraven i Section XI, Mandatory Appendix VIII, Supplement 9, för kvalificerad CASS-undersökning och potentiella alternativ till Section XI, Subarticle IWB-2500 (Examination Categories B-F and B-J), specifika för CASS-rörledningar.

MÖJLIGHETER ATT LÄRA SIG OCH BLI ENGAGERAD

- Extremely Low Probability of Rupture (xLPR) Probabilistic Fracture Mechanics Code, Version 2.2 (EPRI 3002023872) utgavs av EPRI i januari 2023. Flera av xLPR-kodmodulerna anpassades för användning i PIPER-CASS.
- MRP-362, Rev. 1 (EPRI 3002007383) presenterar den tekniska motiveringen för feltoleransutvärderingen av CASS-rörledningar för att stödja ASME Code Case N-838. En PFM-modell för fullt åldrade CASS-rörledningar användes för att utveckla gränsvärden som uppfyller en uppsättning kriterier för acceptans av felsannolikhet för varje belastningsnivå.
- EPRI 3002010314 dokumenterar en round-robin-studie för att fastställa prestandan hos NDU-tekniker på en uppsättning felaktiga CASS-prover som innehöll realistiska förhållanden för ytor och geometri.

- MRP-424 (EPRI 3002010517) innehåller ett utkast till undersökningskrav för CASS-rörsvetsar, vilket ger ett ramverk från vilket den slutliga versionen av Section XI, Mandatory Appendix VIII, Supplement 9 kan skapas.

EPRI-KONTAKTER: Jan Shim, teknisk chef, dshim@epri.com

PROGRAM: Nuclear Power, P41; PWR Materials Reliability Program (MRP), P41.01.04

IMPLEMENTERINGSKATEGORI: Referens – teknisk grund

INNEHÅLL

FÖRTECKNING ÖVER FIGURER

TABELLFÖRTECKNING

Programa de confiabilidade de materiais: Análise da mecânica da fratura probabilística de componentes de tubulação de aço inoxidável austenítico fundido de PWRs (MRP-479)

3002023893

Relatório final, junho de 2024

Gerente de projeto do EPRI
D. Shim

Todos ou parte dos requisitos do Programa de garantia de qualidade nuclear do EPRI se aplicam a este produto.	YES NO

EPRI
3420 Hillview Avenue, Palo Alto, California 94304-1338 EUA
800.313.3774 ▪ 650.855.2121 ▪ askepri@epri.com ▪ www.epri.com

ISENÇÃO DE GARANTIAS E LIMITAÇÃO DE RESPONSABILIDADES

ESTE DOCUMENTO FOI ELABORADO PELAS ORGANIZAÇÕES INDICADAS A SEGUIR COMO UMA PRESTAÇÃO DE CONTAS DO TRABALHO PATROCINADO OU COPATROCINADO PELO EPRI (ELECTRIC POWER RESEARCH INSTITUTE, INC.). O EPRI, QUAISQUER MEMBROS DO EPRI, COPATROCINADORES, ORGANIZAÇÕES A SEGUIR OU QUALQUER PESSOA QUE ATUE EM NOME DE QUALQUER UM DELES NÃO:

(A) OFERECEM QUALQUER GARANTIA OU FAZEM QUAISQUER DECLARAÇÕES, EXPRESSAS OU IMPLÍCITAS, (I) COM RELAÇÃO AO USO DE QUALQUER INFORMAÇÃO, EQUIPAMENTO, MÉTODO, PROCESSO OU ITEM SIMILARES DIVULGADOS NESTE DOCUMENTO, INCLUINDO GARANTIAS DE COMERCIALIZAÇÃO E ADEQUAÇÃO A UMA FINALIDADE ESPECÍFICA; OU (II) QUE TAL USO NÃO VIOLE NEM INTERFIRA COM DIREITOS DE PROPRIEDADE PRIVADOS, INCLUINDO PROPRIEDADES INTELECTUAIS DE QUAISQUER PARTES; OU (III) QUE ESTE DOCUMENTO SEJA ADEQUADO A QUALQUER CIRCUNSTÂNCIA ESPECÍFICA DE UM USUÁRIO ESPECÍFICO; NEM

(B) ASSUMEM RESPONSABILIDADE POR QUAISQUER DANOS OU OUTRAS OBRIGAÇÕES (INCLUINDO DANOS CONSEQUENCIAIS, MESMO QUE O EPRI OU ALGUM REPRESENTANTE DO EPRI TENHA SIDO NOTIFICADO DA POSSIBILIDADE DE TAIS DANOS) DECORRENTES DE SUA SELEÇÃO OU UTILIZAÇÃO DESTE DOCUMENTO OU DE QUAISQUER INFORMAÇÕES, EQUIPAMENTOS, MÉTODOS, PROCESSOS OU ITENS SEMELHANTES DIVULGADOS NESTE DOCUMENTO.

A REFERÊNCIA A QUALQUER PRODUTO COMERCIAL, PROCESSO OU SERVIÇO ESPECÍFICO ATRAVÉS DE SEU NOME COMERCIAL, MARCA COMERCIAL, FABRICANTE OU QUALQUER OUTRA FORMA, NÃO IMPLICA NECESSARIAMENTE QUE A EPRI O ENDOSSE, RECOMENDE OU FAVOREÇA.

A(S) SEGUINTE(S) ORGANIZAÇÃO(ÕES), MEDIANTE CONTRATO COM O EPRI, ELABOROU(ARAM) ESTE RELATÓRIO:

Dominion Engineering, Inc.

O CONTEÚDO TÉCNICO DESTE PRODUTO **NÃO** FOI PREPARADO DE ACORDO COM O MANUAL DO PROGRAMA DE QUALIDADE DO EPRI QUE CUMPRE OS REQUISITOS DA NORMA 10 CFR 50, APÊNDICE B. ESTE PRODUTO **NÃO** ESTÁ SUJEITO AOS REQUISITOS DA NORMA 10 CFR PARTE 21.

NOTA

Para obter informações adicionais sobre o EPRI, entre em contato com o Centro de assistência ao consumidor do EPRI pelo telefone 800.313.3774 (EUA) ou pelo e-mail askepri@epri.com.

Together…Shaping the Future of Energy®

RECONHECIMENTOS

As seguintes organizações, mediante contrato com o EPRI, elaboraram este relatório:

Dominion Engineering, Inc.
12100 Sunrise Valley Drive, Suite 220
Reston, VA 20191, EUA

Pesquisadores principais
K. Fuhr
M. Wolfson
G. White
M. Burkardt

Este relatório descreve a pesquisa patrocinada pelo EPRI.

RESUMO

A microestrutura material dos materiais de CASS (aço inoxidável austenítico fundido) desafia a confiabilidade de técnicas de ensaio por ultrassom. Assim sendo, os requisitos de qualificação para procedimentos, pessoal e equipamentos de UT (ensaio por ultrassom) utilizados na inspeção de tubulações de CASS de acordo com o Código de Caldeiras e Vasos de Pressão da ASME (Sociedade Americana de Engenheiros Mecânicos), Seção XI, Anexo VIII obrigatório, não foram desenvolvidos. Com base em pesquisas atuais, os desafios mais difíceis para a inspeção de componentes de tubulação de CASS são a detecção de trincas axiais e o dimensionamento da profundidade de trincas circunferenciais.

Além das limitações da inspeção por UT, o material de CASS está sujeito ao envelhecimento térmico, o que causa degradação da tenacidade à fratura ao longo do tempo. A extensão da degradação da tenacidade depende do teor de ferrita delta (δ-Fe) do componente específico. O modo de falha preocupante em material de CASS é o aumento de uma trinca (por exemplo, de uma falha de fabricação preexistente) até um tamanho que possa desafiar a integridade do componente, considerando o tamanho crítico reduzido da trinca devido à menor tenacidade à fratura. O principal mecanismo de crescimento de trinca no material de CASS exposto a líquido refrigerante de PWR (reator de água pressurizada) é a trinca por fadiga. A experiência e os ensaios em usinas mostram que material de aço inoxidável austenítico no ambiente de PWR geralmente é resistente a trincas por corrosão sob tensão, enquanto espera-se que o teor de ferrita delta no material de CASS tenha um efeito benéfico para a suscetibilidade a trincas por corrosão sob tensão.

Este relatório descreve a abordagem PFM (mecânica da fratura probabilística) e os resultados obtidos para lidar com os desafios na qualificação de inspeções por UT para tubulações de CASS. As análises de PFM avaliam a implicação estrutural de falhas axiais presentes em tubulações de CASS que se propagam como trincas sem considerar as inspeções de manutenção realizadas. Análises adicionais de PFM avaliam a margem estrutural fornecida por uma metodologia alternativa de análise de falhas que não requer informações de tamanho de profundidade após a detecção de trincas circunferenciais. As análises de PFM foram realizadas usando um código de software desenvolvido especificamente para este projeto chamado PIPER-CASS (Análise probabilística da integridade de tubulações para reatores — Aço inoxidável austenítico fundido). O PIPER-CASS concentra-se na modelagem do crescimento de trincas por fadiga e na estabilidade de componentes de tubulações de CASS, incluindo material envelhecido termicamente com baixa tenacidade.

Este trabalho tem como objetivo apoiar o desenvolvimento do Apêndice VIII Obrigatório, Suplemento 9 para CASS e alternativas aos atuais requisitos de inspeção e aceitação de falhas da Seção XI para componentes de tubulações de CASS.

Palavras-chave

BPVC (Código de Caldeiras e Vasos de Pressão) da ASME
CASS (Aço inoxidável austenítico fundido)
Crescimento de trincas por fadiga
PFM (Mecânica da fratura probabilística)
NDE (Ensaios não destrutivos)

RESUMO EXECUTIVO

Número do documento: 3002023893

Tipo de produto: Relatório técnico

Título do produto: Programa de confiabilidade de materiais: Análise da mecânica da fratura probabilística de componentes de tubulação de aço inoxidável austenítico fundido de PWRs (MRP-479)

Público principal: desenvolvedores de Códigos e Normas relacionados a componentes de tubulações de CASS (aço inoxidável austenítico fundido)

Público secundário: equipe técnica de licenciados e reguladores de PWRs (reatores de água pressurizada)

PRINCIPAL PERGUNTA DA PESQUISA

Quais soluções analíticas estão disponíveis para complementar as atuais capacidades de NDE (ensaio não destrutivo) para componentes de tubulações de CASS, especificamente para a detecção de trincas axiais e dimensionamento da profundidade de trincas circunferenciais?

VISÃO GERAL DA PESQUISA

Este relatório descreve a abordagem de PFM (mecânica da fratura probabilística) e os resultados com o intuito de apoiar requisitos alternativos de inspeção para componentes de CASS. Este trabalho tem como objetivo apoiar o desenvolvimento do Código de Caldeiras e Vasos de Pressão da ASME, Seção XI, Apêncice VIII Obrigatório, Suplemento 9 para CASS e o refinamento dos requisitos de inspeção da Seção XI, Subartigo IWB-2500 (Categorias de inspeção B-F e B-J) para tubulações de CASS. Para trincas axiais, os efeitos na segurança nuclear (probabilidade de rutura) e na defesa em profundidade (estanqueidade de vazamentos) foram analisados desconsiderando quaisquer benefícios dos NDEs periódicos. Para trincas circunferenciais, um procedimento alternativo de análise de falhas é proposto para aceitação de trincas detectadas sem depender de uma capacidade de dimensionamento de profundidade qualificada.

PRINCIPAIS DESCOBERTAS

- Para este esforço, foi desenvolvido um código de PFM com base em Python chamado PIPER-CASS (Avaliação probabilística da integridade de tubulações para reatores — Aço inoxidável austenítico fundido). Esse código de PFM aplica muitos dos mesmos modelos do programa xLPR, mas concentra-se na modelagem do crescimento de trincas por fadiga e na estabilidade de trincas na EPFM (mecânica da fratura elasto-plástica).

- Os resultados de modelagem de PFM mostram que a inspeção periódica para detectar trincas de orientação axial na tubulação de CASS do circuito principal (incluindo PWRs de carga base e PWRs que operam sob FPO [operação de alimentação flexível]) e na tubulação de CASS de linha de surto (incluindo carga base, mas não FPO) é desnecessária para garantir a integridade estrutural e estanqueidade de vazamentos das tubulações. As linhas de surto em usinas CE que operam sob FPO possuem uma preocupação maior com o crescimento de trincas por fadiga devido ao potencial de um grande número de transientes de surto serem acionados por mudanças de alimentação da FPO.
- Os resultados da modelagem de PFM mostram que, para uma trinca detectada com um comprimento angular total de até 32°, o método alternativo de análise de falhas proposto garante a integridade estrutural dos componentes da tubulação de CASS do circuito principal por um ciclo de combustível de operação contínua após a detecção de uma trinca com orientação circunferencial.

PORQUE QUE ISSO IMPORTA

A microestrutura heterogênea de materiais de CASS é um impedimento para a qualificação de determinados aspetos do UT (ensaio por ultrassom). Uma base técnica que demonstra que a detecção de trincas axiais em tubulações de CASS é desnecessária lida com o desafio de garantir que os procedimentos de UT atendam aos padrões de qualificação de demonstração de desempenho. A falta de capacidade qualificada de dimensionamento de profundidade para trincas circunferenciais ou falhas semelhantes a trincas em tubulações de CASS impede a aplicação de procedimentos padrão de avaliação de falhas, portanto, é necessário um procedimento alternativo para permitir a operação contínua e limitar reparos emergentes desnecessários.

COMO APLICAR OS RESULTADOS

Espera-se que este trabalho forneça bases técnicas para ações do comitê do Código ASME que abordem a inspeção de componentes de CASS. Isso inclui novos Casos do Código ASME e o desenvolvimento da Seção XI, Apêndice VIII obrigatório, Suplemento 9 para inspeção qualificada de CASS e alternativas em potencial à Seção XI, Subartigo IWB-2500 (Categorias de inspeção B-F e B-J) para tubulações de CASS.

OPORTUNIDADES DE APRENDIZAGEM E ENVOLVIMENTO

- O Código de Mecânica da Fratura Probabilística de xLPR (Probabilidade Extremamente Baixa de Ruptura), Versão 2.2 (EPRI 3002023872), foi lançado pelo EPRI em janeiro de 2023. Diversos dos módulos de código de xLPR foram adaptados para uso com o PIPER-CASS.
- O MRP-362, Rev. 1 (EPRI 3002007383) apresenta a justificativa técnica para a avaliação de tolerância a falhas de tubulações de CASS para suporte ao Caso N-838 do Código ASME. Foi utilizado um modelo de PFM para tubulações de CASS totalmente envelhecidas para desenvolver limites de aceitação de tamanho de falhas que atendem a um conjunto de critérios de aceitação de probabilidade de falha para cada nível de serviço de carregamento.

- O EPRI 3002010314 documenta um estudo interlaboratorial para determinar o desempenho das técnicas de NDE em um conjunto de espécimes de CASS com falhas que continha condições geométricas e superficiais realistas.
- O MRP-424 (EPRI 3002010517) inclui um esboço dos requisitos de inspeção para soldas de tubulações de CASS, fornecendo uma estrutura a partir da qual pode ser redigida a versão final da Seção XI, Apêndice VIII Obrigatório, Suplemento 9.

CONTATOS DO EPRI: Do Jaun Shim, executivo técnico, dshim@epri.com

PROGRAMA: Energia nuclear, P41; MRP (Programa de confiabilidade de materiais) de PWRs, P41.01.04

CATEGORIA DE IMPLEMENTAÇÃO: Referência — Base técnica

SUMÁRIO

LISTA DE FIGURAS

LISTA DE TABELAS

About EPRI

Founded in 1972, EPRI is the world's preeminent independent, non-profit energy research and development organization, with offices around the world. EPRI's trusted experts collaborate with more than 450 companies in 45 countries, driving innovation to ensure the public has clean, safe, reliable, affordable, and equitable access to electricity across the globe. Together, we are shaping the future of energy.

PROGRAM

Pressurized Water Reactor Materials Reliability Program (MRP), P41.01.04

For more information, contact:

EPRI Customer Assistance Center
800.313.3774 • askepri@epri.com

3002023893 **June 2024**

EPRI

3420 Hillview Avenue, Palo Alto, California 94304-1338 USA • 650.855.2121 • **www.epri.com**